# THRESHOLDS OF STRETCH-INDUCED INJURY

# IN CEREBRAL ARTERIES

by

Edward David Bell

A dissertation submitted to the faculty of
The University of Utah
in partial fulfillment of the requirements for the degree of

Doctor of Philosophy

Department of Bioengineering

The University of Utah

May 2016

**The University of Utah Graduate School**

**STATEMENT OF DISSERTATION APPROVAL**

The dissertation of **Edward David Bell**

has been approved by the following supervisory committee members:

| | | |
|---|---|---|
| **Kenneth L. Monson** | , Chair | **12/18/2015** Date Approved |
| **Patrick A. Tresco** | , Member | **12/18/2015** Date Approved |
| **Richard D. Rabbitt** | , Member | **12/18/2015** Date Approved |
| **Robert Hitchcock** | , Member | **12/18/2015** Date Approved |
| **Anthony J. Donato** | , Member | **12/18/2015** Date Approved |

and by **Patrick A. Tresco** , Chair/Dean of

the Department/College/School of **Bioengineering**

and by David B. Kieda, Dean of The Graduate School.

# ABSTRACT

The cerebrovasculature is vital in maintaining health in the brain, but can be damaged by traumatic brain injury (TBI). Even in cases without hemorrhage, vessels are deformed with the surrounding tissue. Subfailure deformation could result in altered mechanical properties and dysfunction of these vessels. This dissertation aims to provide a better understanding of the biaxial mechanical properties of cerebral arteries, as well as determine mechanical stretch thresholds which produce ultimate failure and subfailure alteration of mechanical properties or vessel function. Three in vitro studies were undertaken. Passive biaxial mechanical properties under physiological loading, as well as failure properties of rat middle cerebral arteries (MCAs), were measured and compared to those of human pial arteries. Best fit parameters for a Fung type strain energy function are provided for the biaxial mechanical properties. Rat MCAs are stiffer in the axial direction than the circumferential, but less stiff in both directions than human arteries. Rat MCAs also exhibit a lower ultimate failure stress but higher failure stretch. The effect of subfailure axial overstretch on the contractile behavior of smooth muscle cells (SMCs) in rat MCAs was investigated. Potassium dose response tests were conducted before and after a single axial overstretch, with varying magnitude and strain rate. Overstretches beyond a threshold of both magnitude and strain rate significantly reduced SMC contraction relative to time-matched controls, mirrored by an increase in potassium concentration required to evoke the half maximal contraction. The effect of subfailure

axial overstretch on passive mechanical properties in sheep MCAs was investigated. Axial response was measured before and after a single quasi-static overstretch of various magnitudes. Post-overstretch, samples showed persistent softening (lower stress values at a given level of stretch). Softening was only observed above an overstretch threshold, and then increased with overstretch severity until a second threshold was reached, above which softening did not increase until failure. This dissertation provides improved understanding of cerebrovascular mechanics and relationships between such data acquired from animals and humans. It also provides insight into the potential role of subfailure cerebrovascular damage in disease states associated with TBI, such as second impact syndrome and stroke.

To my lovely (and exceptionally patient) wife Cathy, without whom this never would have been possible.

TABLE OF CONTENTS

LIST OF FIGURES

LIST OF TABLES

# ACKNOWLEDGMENTS

I have consulted with a large number of people during the course of this work, and I would like to gratefully express my thanks to all of them, not the least of whom being the members of my research advisory committee. I would like to particularly thank the following people for their important contributions:

- Dr. Ken Monson, my PhD advisor. Dr. Monson has provided me with kind and reliable guidance throughout this research. Also, his willingness to be a sounding board for my ideas (some good and some not as good) has been invaluable. In addition, I consider myself very fortunate to call this kind and patient man my friend.
- Dr. Patrick Tresco, for allowing the use of his lab space for the execution of this research.
- Dr. Anthony Donato, for both the use of his lab space from time to time as well as for providing me with dissection instruction and preliminary protocols upon which the study in Chapter 3 was developed.
- Dr. Kurt Albertine and Mar Janna Dahl, for their help with tissue acquisition for the study in Chapter 4.
- Stewart Yeoh, a fellow graduate student. Having starting work in Dr. Monson's lab the same week, Stewart and I have consulted and/or worked together on almost every project he or I have done since. His counsel, perspective, and friendship have been extremely valued.

- Several other fellow graduate students have also been valuable contributors to this work, including Rahul Kunjir (MS, graduated), Jacob Sullivan (MS, graduated), and Matthew Converse (current doctoral student).
- My parents for their love and support (emotional and financial) throughout my time in graduate school.
- My lovely and wonderful wife, Cathy, to whom this dissertation is dedicated, for being willing to sacrifice many comforts of life, and for providing constant emotional support.
- My children, Blake, Jacob, and Kara, who do not have any memory of what life was like when I was not in college. They, along with my wife, Cathy, are my motivation to succeed.

The work in this dissertation was funded in part by grants from the National Institutes of Health (5K25HD048643), the Department of Defense (W81XWH-08-1-0295), and Primary Children's Medical Center Foundation (PCMCF-ISA-KM-01-2012-02).

I also gratefully acknowledge the permissions granted for the reprinting of the various previously published materials in this dissertation.

# CHAPTER 1

# INTRODUCTION

## 1.1 Motivation and Objective

Traumatic Brain Injury (TBI) is a devastating health issue with a huge societal burden. Each year in the United States alone there are 2.4 million TBI cases (CDC, 2013) resulting in 53,000 deaths (Coronado et al., 2011) and incidences of TBI are increasing across the globe (Maas et al., 2008). The economic impact of TBI in the United States has been estimated to be $60 billion per year (Finkelstein et al., 2006)

TBI is extremely complex, including injury to both nervous tissues as well as cerebrovasculature. The final clinical impact of a TBI event is a combination of both the initial mechanical injury and secondary complications caused by pathological processes set in motion by the initial injury. The health of nervous tissue in the brain is of primary importance. Damage to nervous tissue caused by the initial injury includes stretch-induced diffuse axonal injury (Siedler et al., 2014) and concussion (McAllister et al., 2012). However, mechanically-induced damage to cerebral blood vessels results in both hemorrhage and cerebrovascular dysfunction, both of which can lead to devastating secondary complications (Adelson et al., 1997; Bassan et al., 2007; Black, 1986; Burke et al., 2013; Golding, 2002; Golding et al., 1999a). Hemorrhage leads to exposure of nervous tissue to toxic blood products normally segregated from the nervous tissue by the

blood brain barrier, potentially resulting in neuronal death (Bell et al., 2014). Dysfunction of the cerebrovasculature's ability to regulate cerebral blood flow can result in vasogenic edema (Marmarou, 2007; Unterberg et al., 2004), and a myriad devastating complications associated with inadequate circulation. Therefore, it is clear that damage to blood vessels, resulting in structural or functional failure, leads to damage of nervous tissue.

The cerebrovasculature plays a vital role in the health and maintenance of the brain. In order to maintain the appropriate level of cerebral blood flow to meet metabolic needs, smooth muscle cells (SMCs) in the vessel wall modulate their level of contraction, or tone, thus controlling the vessel internal diameter (Lassen, 1974; Ursino, 1994). This process, known as autoregulation, has been shown to be disrupted following TBI (Golding, 2002; Golding et al., 1999a; Kenney et al., 2016), resulting in unfavorable clinical outcomes (Czosnyka et al., 1996; Robertson et al., 1992). Examples of disrupted autoregulation following TBI include vasospasm (Compton and Teddy, 1987; Kramer et al., 2013; Martin et al., 1992; Martin et al., 1997), secondary hypoxia or hypoperfusion (Bramlett et al., 1999; Cherian et al., 1996; Chesnut et al., 1993), and decreased vascular reactivity to hypercapnia in the surrounding brain tissue (Saunders et al., 1979). It is important to note that cerebral autoregulation is dependent on both properly functioning dynamic control mechanisms as well as the proper steady state mechanical properties (Zhang et al., 2009).

Many experimental models have been used to investigate the trauma associated with impact TBI ranging from rodents to primates and humans, including cadavers and live volunteers (Goldsmith, 2001; Goldsmith and Monson, 2005). While the goal is always to gain information about human trauma, only sub-injury level loading can be

ethically inflicted on a living human being. Cadavers are very expensive and their use can result in inaccurate conclusions due to lack of vascular pressurization (Alem et al., 1977; Stalnaker et al., 1977) or difficulty identifying vascular injury (Stalnaker et al., 1973), as well as altered head-neck kinematics due to the lack of cadaveric muscle tone at the time of impact (Bendjellal et al., 1987). Primates are the closest animal model to humans, but cost and recent public opinion makes use of primate models prohibitive. Additionally, a huge variety of potential loading conditions makes experimental definition of all possible injury thresholds nearly impossible. Some examples of these various loading conditions upon which the resulting injury is dependent include direction of loading (Gennarelli et al., 1987; Post et al., 2015), head and neck orientation at the time of impact (Nusholtz et al., 1986), and subject-specific anatomical differences such as thickness of skull (Melvin et al., 1969). It has also been shown in surrogate models that strain distributions within the brain are dependent on both peak acceleration a well as changes in acceleration with time (Thibault et al., 1987). Further, it has been argued that injury thresholds should be determined based on response of tissue rather than applied loading (King et al., 2003). However, it is difficult to quantify the TBI-imposed strain field throughout the brain during experimental closed head injury (Melvin et al., 1993), so computational models have become a common tool for investigating head injury.

Computational models of head injury have advanced substantially in recent years, but still have significant limitations. Models have grown in complexity to include many of the specific tissue structures of the head such as skin, bone, cerebral spinal fluid (CSF), distinct white vs. gray matter regions, and ventricles (Ji et al., 2014; Kleiven, 2007; Yang et al., 2014). Some models also use increasingly accurate geometry such as the internal

features of the skull (Asgharpour et al., 2014; Tse et al., 2015). Results from various independently validated complex computational head injury models often do not agree with each other which is attributed in part to variations in the material parameters utilized (Ji et al., 2014).

Inclusion of vasculature in computational models has produced mixed results. Inclusion of simplified blood vessel geometries in one computational TBI model showed dramatically different strain distributions and peak stress levels within the brain as compared to a similar model without any vasculature (Omori et al., 2000; Zhang et al., 2002). Inclusion of more complex vascular structure in another model produced minimal difference from a similar model without vasculature (Ho and Kleiven, 2007). However, it should be noted that the model containing more complex vasculature did not account for internal pressurization of vessels, and this model does not correlate well with injury distributions within the brain (Fahlstedt et al., 2015).

Despite this apparent conflict, there is evidence that inclusion of vasculature in computational models is necessary. Two-dimensional physical surrogate models with vasculature have significantly different strain distributions than without (Parnaik et al., 2004). Additionally, cadaver head impact studies show better correlation of loading to injury when the vasculature is repressurized (Alem et al., 1977; Nahum and Smith, 1976; Stalnaker et al., 1977). It is therefore plane to see that the vasculature plays a very important role in stress concentrations when the brain is loaded (Omori et al., 2000), and should be included in computational models of TBI.

A previous attempt to mathematically model vascular function and vasospasm shows the potential of computational models incorporating vasculature to investigate both

mechanics and vascular function (Baek et al., 2007b). An equation was presented which represented the mechanical behavior of cerebral arteries including underlying passive mechanics and mechanical contributions from SMC contraction. The intention was that the contribution from the portion of the equation representing SMC contraction would be optimized such that the overall solution would model vascular mechanical behavior under healthy and mechanically damaged conditions. However, by the authors' own admission, their model better serves to highlight the current lack of experimental data showing what types of vascular dysfunction are associated with mechanical injury.

In order to provide the highest accuracy and/or utility of future computational models which incorporate the cerebrovasculature, a better understanding is needed of the vessel specific material properties, including failure and subfailure properties, as well as defined strain thresholds resulting in vascular injury. Additionally, low availability of mechanical data measured from human tissue often necessitates translation of experimental results acquired from animals to the human case, but these relationships are often not well understood.

The objective of this dissertation is to better define the effect subfailure mechanical loading has on the cerebrovasculature along with defining strain thresholds that result in pathological changes. This information will both provide a better understanding of the mechanically related mechanisms of vascular injury post-TBI as well as allow future computational models to potentially predict subfailure vascular damage based on the stains resulting from applied traumatic loading. This will improve the correlation of TBI-related region specific strains within the brain with clinically observed pathologies (Vossoughi and Bandak, 1995). When possible, these results are

compared to data acquired from human tissue to provide a better understanding for the translation of animal vascular data to humans (Chapter 2). In order to provide context for the current research, brief discussions are here provided for cerebral vessel anatomy and structure, mechanics of cerebral arteries, as well as cerebrovascular autoregulation and TBI-induced dysfunction.

## 1.2 Cerebral Vessel Anatomy and Structure

The organization and structure of the cerebral vascular system is unique compared to other organs (Wolff, 1936). Tissues outside the arachnoid membrane are perfused with vasculature that does not penetrate the arachnoid. Inside the arachnoid membrane, perfusion is provided by the internal carotid and vertebral arteries, which enter at the base of the skull and anastomose together to form the Circle of Willis. Six main cerebral arteries (posterior, middle, and anterior cerebral arteries) branch off from this Circle and run along the cortical surface of the brain, continuing to subdivide to form a network along the surface. Along the length of these surface vessels, small arteries branch off and penetrate the cortex at right angles. These further subdivide until they reach the capillary level (Akima et al., 1986; Cassot et al., 2006; Cassot et al., 2010; Reina-De La Torre et al., 1998).

There are several differences in the cerebral vasculature compared to peripheral vessels. Once inside the arachnoid membrane, the vasculature is bathed in CSF, and is enwrapped in an additional layer of pial-arachnoid tissue (Alcolado et al., 1988). This extra layer of tissue continues along the length of the arterial branching until it nears the capillary level; however, cerebral veins do not have this extra tissue layer within the

cortex of the brain (Yamashima and Friede, 1984). Additionally, capillaries in the brain are lined with astrocyte end feet and pericytes which maintain the tight control of the blood brain barrier, while still providing for the metabolic needs of the surrounding tissue (Ballabh et al., 2004). The venous structure is also unique in that blood from the deep brain regions drains via Galen's vein (Meder et al., 1994), while cortical veins merge together to form large bridging veins which exit the subarachnoid space (Andrews et al., 1989; Han et al., 2007; Oka et al., 1985). Blood then collects in the dural venous sinuses and eventually drains through the jugular veins. There is also a great deal of redundancy in the cerebral vasculature, ranging from the Circle of Willis itself, to numerous anastomoses between adjacent vessels, without arteriovenous anastomoses (Duvernoy et al., 1981). These anastomoses have been observed to be as large as 1 mm in diameter in humans (Brozici et al., 2003; Duvernoy et al., 1981).

While sharing some common characteristics with peripheral arteries, cerebral arteries also have distinct differences. An excellent review of the morphological differences between peripheral and cerebral arteries is available (Lee, 1995). Briefly however, cerebral arteries are muscular arteries where the primary mechanical constituents are collagen and elastin fibers along with SMCs (Hayashi et al., 1980; Holzapfel et al., 2000; Humphrey, 1995; Humphrey, 2002). The wall structure can be divided into three main layers (Holzapfel et al., 2000; Humphrey, 2002), the intima, media, and adventitia. The intima, the innermost layer, is composed primarily of endothelial cells attached to the internal elastic lamina (IEL). The media is dominated by helically oriented smooth muscle cells embedded in a network of collagen and elastin fibers (Holzapfel et al., 2000). While primarily in the circumferential direction, the pitch

of this helix varies depending on the location within the vascular tree (Takahashi et al., 1994). The adventitia, the outermost layer, is primarily composed of collagen fibers embedded with fibroblasts and fibrocytes and is much less organized than the other two layers (Holzapfel et al., 2000). The IEL is thicker in cerebral arteries than in peripheral arteries, but the elastin content in the media and adventitia is much lower (Stehbens, 1972; Stephens and Stilwell, 1969). Also, in peripheral arteries, the media and adventitia are separated by the external elastic lamina. While the external elastic lamina is present in cerebral arteries in infancy, it disappears in adults (Hassler and Larsson, 1962).

## 1.3 Mechanics of Cerebral Arteries

As mentioned above, efforts to better prevent and treat cerebrovascular injury and disease are, in part, dependent upon a more complete understanding of vessel mechanics. This includes the definition of blood vessel injury thresholds for failure and subfailure damage, as well as characterization of the relationship between applied forces and vessel function. Reviews of overall head injury mechanics and material properties for cranial tissues are available elsewhere (Goldsmith, 2001; Goldsmith and Monson, 2005; Meaney et al., 2014). Additionally, a comprehensive discussion of the loading to the head during TBI and the clinical manifestations of gross vascular injury are outside the scope of this summary, but a good review of such is provided by Crooks (Crooks, 1991).

The scope of this section is limited to the mechanics of cerebral arteries. More complete reviews of vascular mechanics in general can be found elsewhere (Holzapfel et al., 2000; Humphrey, 1995; Humphrey, 2002). One of the reasons for this specific focus is that cerebral arteries are stiffer than veins and fail at a lower level of stretch (Monson

et al., 2003). This indicates that they would have a greater impact on the traumatic deformation of surrounding brain tissue, and would sustain injury at a lower regional strain level. Cerebral arteries are several orders of magnitude stiffer than surrounding brain tissue. For example, experimental measurements of rat cranial tissues show the instantaneous elastic modulus of gray and white matter to be 0.29 kPa and 0.45 kPa, respectively (Christ et al., 2010). However, the middle cerebral artery has an instantaneous elastic modulus of 1.1 MPa and 0.7 MPa for the axial and circumferential directions, respectively (Bell et al., 2013) (also Chapter 2). This has led some to compare the mechanical contribution of cerebral arteries in brain tissue to that of rebar in concrete (Zhang et al., 2002).

The mechanical behavior of cerebral arteries has common traits with other biological soft tissues, with some additional considerations. In general, cerebral artery mechanical response is nonlinear and anisotropic. The arterial wall is also considered to be incompressible within the physiological loading range (Carew et al., 1968). Like other biological soft tissues, cerebral arteries maintain a certain level of stretch in the in vivo configuration. Finally, due to the presence and action of SMCs in the arterial wall, the mechanical behavior is dependent on both the passive mechanics of the wall constituents as well as SMC contraction.

Like many biological soft tissues, cerebral arteries exhibit nonlinear mechanical behavior due to the proportion and organization of the various arterial wall constituents (Fung, 1993). See **Figure 1.1** for an example of this nonlinear behavior as measured from a stretch test on a pressurized ewe middle cerebral artery (MCA) pulled axially to failure. The shape of the lower portion of this curve, known as the toe region, is determined by

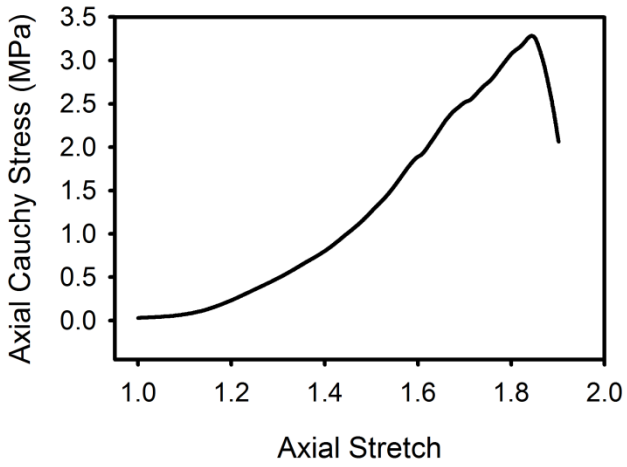


**Figure 1.1: Axial mechanical response of ewe middle cerebral artery pulled to failure at internal pressure of 13.3 kPa (100 mmHg).**

both elastin and collagen fibers in the wall (Chow et al., 2014; Weisbecker et al., 2013). While the contribution of elastin is linear in nature, the slope increases as initially crimped collagen fibers within the wall straighten out and become load bearing, a process known as fiber recruitment (Chow et al., 2014; Schrauwen et al., 2012; Zeinali-Davarani et al., 2015). The subsequent nearly linear portion of the curve reflects the elongation of a majority of the collagen fibers in the artery (Chow et al., 2014; Zeinali-Davarani et al., 2015). It is postulated that the somewhat discontinuous changes in slope in the upper portion of the curve are due to failure of certain microstructural component prior to ultimate failure (Bell et al., 2015; Converse and Monson, 2014), which will be discussed in greater detail near the end of this section.

In addition to the conformation of microstructural components, like the initial crimping of collagen, the orientation of these components also plays an important role in the resultant anisotropy of cerebral arteries. For example, the unloaded orientation of collagen fibers in the adventitia is somewhat random, while the collagen in the media is

oriented in a primarily circumferential helical manner (Chow et al., 2014; Schrauwen et al., 2012). In both human and rat cerebral arteries, the axial direction has been shown to be stiffer than in the circumferential direction at in vivo stretch levels (Bell et al., 2013; Monson et al., 2008). While cerebral arteries are stiffer in humans than rats, the ratio of axial to circumferential stiffness is similar (Bell et al., 2013) (also Chapter 2). This anisotropy results in the mechanical behavior in either direction being dependent on the loading in the other. As a result, biaxial mechanical testing is required for the characterization of cerebral arteries (Bell et al., 2013; Monson et al., 2008).

Arteries in vivo are under a certain amount of stretch. This is easy to see as arteries removed from the body retract axially (Fuchs, 1900). This is an example of residual strain. The parallel concept of residual stress is simply stresses in a material or object that is free from external loading. Residual stress in arteries was first taken into consideration for mechanical analysis by Bergel (Bergel, 1961). However, residual stress is not limited to the axial direction. Circumferential residual stress is shown by cutting a ring cross section of an artery radially (Chuong and Fung, 1986). The cross section then opens into a mostly circular arch with a greater diameter than the original cross section. Circumferential residual strain is quantified by measuring the resultant opening angle ($\alpha$) (**Figure 1.2**). It is important to note, however, that this opening angle can vary significantly along the length of the artery (Liu and Fung, 1988; Monson et al., 2008). Additionally, residual shear strain has been observed and quantified in coronary arteries (Wang and Gleason, 2010, 2014). Residual shear strain causes a resected thin longitudinal strip of the arterial wall to coil into a helical configuration. Finally, the different layers of arteries have been shown to have different amounts of residual stress in

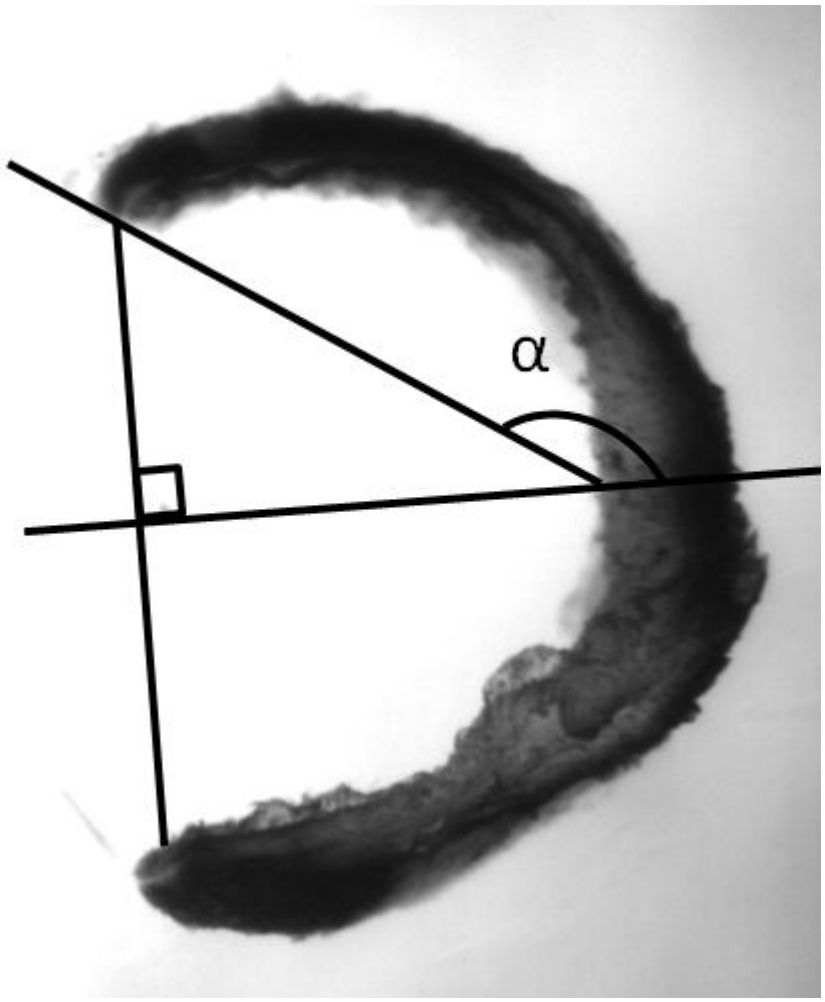


**Figure 1.2: Illustration of the measurement of circumferential residual strain opening angle (α) from a cross section of a human pial artery sliced open radially. Opening angle is in radians and measured from the midpoint of the arc to the end.**

both the axial and circumferential directions (Holzapfel et al., 2007). For example, the circumferential opening angle of the media could be much higher than that of the endothelium. While this layer specific residual strain has been quantified in larger peripheral arteries (Holzapfel et al., 2007), the small size of cerebral arteries make such an attempt difficult. To account for residual stress and strain for stress analysis, one must use the stress relieved configuration as the reference state as described in detail by Holzapfel et al. (Holzapfel et al., 2000).

An important testing consideration related to residual strain is the experimental determination of the in vivo length during in vitro vessel tests. In this regard, a discovery by Van Loon (Van Loon, 1977) is particularly helpful. Van Loon found that when dog arteries are stretched axially at varying levels of constant internal pressure, all the force length plots overlap at a single vessel length. He further confirmed this by showing that at this same length, corresponding to the sample's measured in vivo length, the axial force stayed constant as the pressure was oscillated within the physiological pressure range. Above the in vivo length, the axial force will rise with increasing internal pressure, while the axial force will fall with increasing internal pressure below the in vivo length. This phenomenon has since been confirmed experimentally in rats (Weizsacker et al., 1983) and again in dogs (Brossollet and Vito, 1995).

The contribution of SMC contraction to the overall mechanical behavior of cerebral arteries is an important consideration, especially considering that over half of the arterial wall is composed of SMCs (Humphrey, 2002). Both active and passive mechanical properties of cerebral arteries have been measured to a limited extent in animals. For example, activation of SMCs in rabbit basilar arteries with the

vasoconstrictor endothelin-1 (ET-1) (Wagner and Humphrey, 2011) during pressure inflation tests at a fixed length shows that the axial force required to maintain a set axial length decreases as SMC tone increases. This study also showed an increase in circumferential stiffness with increased SMC activation. A second study, on rat MCA (Coulson et al., 2004), showed that SMC contraction induced by increased internal pressure also increased circumferential stress at a given level of circumferential stretch. However, when the overall mechanical response is mathematically separated into the individual contributions from passive structures and active SMC contraction, the passive stiffness in both directions seems to decrease with increasing SMC contraction (Baek et al., 2007a).

A large number of strain energy functions have been proposed to describe arterial mechanical behavior (Holzapfel et al., 2000; Humphrey, 1995). Strain energy functions are scalar mathematical relationships that relate the stored strain energy to the deformation gradient. In other words, they relate the energy required to deform a material to the matching level of stretch. Such a function can then be used to predict stress from the applied stretch. The parameters for these functions are derived by iteratively optimizing the function so that the mathematically predicted stresses best match corresponding experimentally measured stress values. One important consideration in this regard is, similar to many biological soft tissues, cerebral arteries exhibit hysteresis or a loss of energy between the loading and unloading of the material. Therefore, current strain energy functions can only be fitted to either the loading or the unloading portions of the data, not both at once. Typically, the loading portion of the data is chosen resulting in the psuedoelasticity assumption (Fung et al., 1979). There are two basic categories of

strain energy functions, phenomenological and microstructurally-based. While microstructurally-based functions have the potential to describe contributions from, and changes in, various components in the arterial wall, they are more computationally demanding and more difficult to validate (Holzapfel et al., 2000). However, while phenomenological models may not be as versatile, they are significantly simpler and can still potentially represent arterial mechanical behavior equally well (Bell and Monson, 2012).

Phenomenological strain energy functions simply utilize an optimized mathematical expression to replicate stress response without regard to the underlying microstructure. Examples of phenomenological functions have been based on exponential (Delfino et al., 1997; Fung et al., 1979; Vaishnav et al., 1973) or logarithmic equations (Takamizawa and Hayashi, 1987). One of the most commonly used phenomenological models is the exponential Fung strain energy function (Bell et al., 2013; Bell and Monson, 2012; Fung et al., 1979; Garcia et al., 2013; Keyes et al., 2013; Monson et al., 2008). The Fung strain energy function as applied to cerebral arteries has only four independent material parameters and is more fully described in Chapter 2 (Bell et al., 2013).

Microstructurally-based strain energy functions divide the overall mechanical behavior into more basic components, such as an isotropic elastic base material and reinforcing collagen fibers (Baek et al., 2007a; Holzapfel et al., 2000; Wicker et al., 2008). Holzapfel et al. (Holzapfel et al., 2000) have also proposed treating the media and adventitia as two connected materials with differing material properties. One previous function, mentioned briefly above, has a third division in the total mechanical behavior to

represent the contribution from contracting SMCs (Eq. 1.1) (Baek et al., 2007a).

$$\boldsymbol{W = W(elastin) + W(collagen) + W(active)} \tag{1.1}$$

This function (Eq. 1.2) accounts for 4 collagen fiber families, each having a unique orientation, stiffness, and degree of nonlinearity, except that material parameters for families 3 and 4 are defined as having equal stiffnesses and nonlinearity. Superscript *k* signifies the fiber family where, in the reference configuration, family 1 is oriented along the axial direction ($\alpha^1 = 0^\circ$), family 2 is oriented circumferentially ($\alpha^2 = 90^\circ$), and families 3 and 4 are oriented helically ($\alpha^3 = \alpha^*$ and $\alpha^4 = -\alpha^*$).

$$\boldsymbol{W = \frac{c_1}{2}(I_1 - 3) + \sum_k \frac{c_2^k}{4c_3^k}\left\{exp\left(c_3^k\left(\left(\lambda^k\right)^2 - 1\right)^2\right) - 1\right\}} \tag{1.2a}$$

$$\boldsymbol{+K_{act}\left\{\lambda_\theta + \frac{1}{3}\frac{(\lambda_M - \lambda_\theta)^2}{(\lambda_M - \lambda_o)^3}\right\}}$$

The stretch of the $k^{\text{th}}$ fiber family is defined as

$$\boldsymbol{\lambda^k = \sqrt{\lambda_z^2 cos^2\alpha^k + \lambda_\theta^2 sin^2\alpha^k}} \tag{1.2b}$$

and $I_1$is the first invariant of the right Cauchy-Green stretch tensor. Parameter $c_1$ is a material parameter for the elastin with units of stress. Parameters $c_2^k$ (stress units) and $c_3^k$ (unitless) are material parameters for the $k^{\text{th}}$ fiber family. Parameter $K_{act}$ is an

experimentally measured parameter related to the level of SMC activation. The various other stretch measurements are current axial stretch ($\lambda_z$), current circumferential stress ($\lambda_\theta$), stretch where SMC contraction is maximum ($\lambda_M$), and stretch where SMC force generation stops ($\lambda_o$). All four of these stretch metrics are experimentally measured. All together, there are eight independent material parameters to optimize. The Baek function has more capability than the Fung phenomenological model, but twice as many material parameters. Therefore, when selecting a strain energy function for investigation of cerebral artery mechanical behavior, one should bear in mind the two factors of what does the function need to do, and the minimization of computational expense should it later be utilized in a computational model of TBI.

There is a limited amount of data for mechanical characterization of human cerebral arteries within the physiological loading range. Circumferential inflation tests on vessels taken from autopsy have revealed that while cerebral vessels get stiffer with age, they are stiffer than peripheral vessels at all ages (Busby and Burton, 1965; Hayashi et al., 1980). Axial stretch tests on unpressurized cerebral vessels from autopsy (Chalupnik, 1971) and live surgical resection (Monson et al., 2003) have shown the mechanical response is not strain rate dependent from quasi-static rates up to 500 $s^{-1}$. However, cerebral vessels from autopsy exhibit a higher stiffness than do fresh vessels from surgical resection (Monson et al., 2005). Additionally, when biaxial loading is utilized, the axial stress at any given level of axial stretch is higher than in previous unpressurized tests (Monson et al., 2008). Unfortunately, limited availability of human tissue is a barrier to additional research.

In order to try to make up for this shortfall in human cerebrovascular tissue,

cerebral artery mechanics under physiological loading levels have been investigated in various animal models. Circumferential active and passive mechanics have been measured in rat MCAs (Coulson et al., 2004; Hogestatt et al., 1983). Certain pathological conditions have been shown to change these mechanical properties. For example, both ischemia (Coulson et al., 2002) and chronic hypertension has been shown to increase the passive circumferential stiffness in large rat cerebral arteries (Hajdu and Baumbach, 1994). While the biaxial active and passive mechanical properties had been measured in rabbit basilar arteries prior to this dissertation (Baek et al., 2007a; Wicker et al., 2008), the rat is a far more common experimental model for TBI (DeWitt and Prough, 2003). Previous measurements of mechanical properties in rodent cerebral vessels have been limited to the circumferential direction (Coulson et al., 2002; Coulson et al., 2004; Hajdu and Baumbach, 1994). Additionally, it has been argued previously that the primary mode of loading experienced by cerebral vessels during TBI is axial stretch (Goldsmith, 2001; Monson et al., 2003). To address this lack of axial rat mechanical data, Chapter 2 of this dissertation (Bell et al., 2013) measured the passive biaxial mechanical properties of rat MCAs.

Since the initial mechanical loading of TBI commonly results in hemorrhage due to vessel rupture, knowing the failure characteristics of cerebral vessels is critical to determining strain injury thresholds. Failure properties of cerebral vessels have been shown to be strain rate independent in humans (Chalupnik, 1971; Lee and Haut, 1989; Monson et al., 2003) and ferrets (Lee and Haut, 1992) for rates ranging from quasi-static up to 500 $s^{-1}$ and 200 $s^{-1}$, respectively. However, near failure stretch levels the incompressibility assumption is potentially no longer valid (Bell et al., 2013) due to the

large strains involved. Unpressurized axial stretch tests to failure on human cerebral vessels from autopsy display a higher failure stress but a lower failure stretch than did fresh cerebral vessels (Monson et al., 2005). With this in mind, it is interesting to note that axial failure stress and stretch from unpressurized human autopsy arteries are 1.06 MPa and 1.34, respectively (Steiger et al., 1989), while these values are 4 MPa and 1.4 for pressurized failure tests on fresh human cerebral arteries (Monson et al., 2008). Considering the higher failure stress in human cerebral arteries from autopsy when unpressurized, the higher failure stress in fresh cerebral vessels when pressurized is all the more pronounced. This emphasizes the need for investigations of injury thresholds to utilize biaxial loading. During the course of the work in this dissertation, axial failure properties under biaxial loading were also defined for rat (Bell et al., 2013) and sheep (Bell et al., 2015) MCAs. Rat MCAs fail at a higher failure stretch but lower failure stress than human cerebral vessels do (Bell et al., 2013). The sheep failure properties were not compared to humans in the study in Chapter 4. However, the sheep MCA failure stress (3.44 MPa) is comparable to humans and the failure stretch (1.7) seems to be higher than for human cerebral arteries.

In addition to injury thresholds that would lead to immediate structural failure, strain thresholds resulting in subfailure cerebrovascular damage are also important to the understanding of TBI. Prior experiments on aorta indicate that the endothelium ruptures under mechanical stretch before other vascular layers (Vaishnav and Vossoughi, 1987). Those authors postulate that this could be due to elevated initial strain in the endothelium due to layer specific residual strains. While it has not yet been extensively studied, preliminary observations in our lab show rupture of endothelium and/or IEL following

subfailure axial overstretch (**Figure 1.3** and **Figure 1.4**). Additionally, other preliminary data show layer-specific alteration and/or damage to the collagen structure within the wall of lamb cerebral arteries following subfailure mechanical overstretch (**Figure 1.5**) (Walther, 2015). Prior to the work of this dissertation, supraphysiological stretch had been shown to reduce the stiffness of peripheral arteries without obvious structural damage in both the circumferential and axial directions, a phenomenon known as strain softening (Alastrue et al., 2008; Holzapfel and Gasser, 2007; Horný et al., 2010; Maher et al., 2012; Peña et al., 2010), but not in cerebral arteries. This reduction in axial stiffness following subfailure mechanical deformation has now been confirmed and characterized in cerebral arteries as well (Bell et al., 2015) (see Chapter 4). Subsequent preliminary data also indicates the presence of circumferential mechanical softening following axial overstretch (Converse and Monson, 2014).

While this subfailure stretch induced strain softening would not necessarily affect the deformation of the brain during the initial traumatic loading, it could play a role in secondary complications. It has been shown that the contractile behavior of vascular SMCs is dependent on the stiffness of the extracellular matrix (Steucke et al., 2015). Furthermore, previous TBI is clinically correlated with an increased risk of stroke up to 5 years later (Burke et al., 2013; Chen et al., 2011; Hills et al., 2012). This may be due to a persistent change in mechanical properties due to overstretch, or possibly be the result of maladaptations to the vasculature due to the reduced axial stress following softening (Humphrey et al., 2009). Finally, as is illustrated in the subfailure rupture of endothelium mentioned above (Vaishnav and Vossoughi, 1987), mechanical overstretch also has the potential to damage other vascular cells inducing autoregulatory dysfunction.

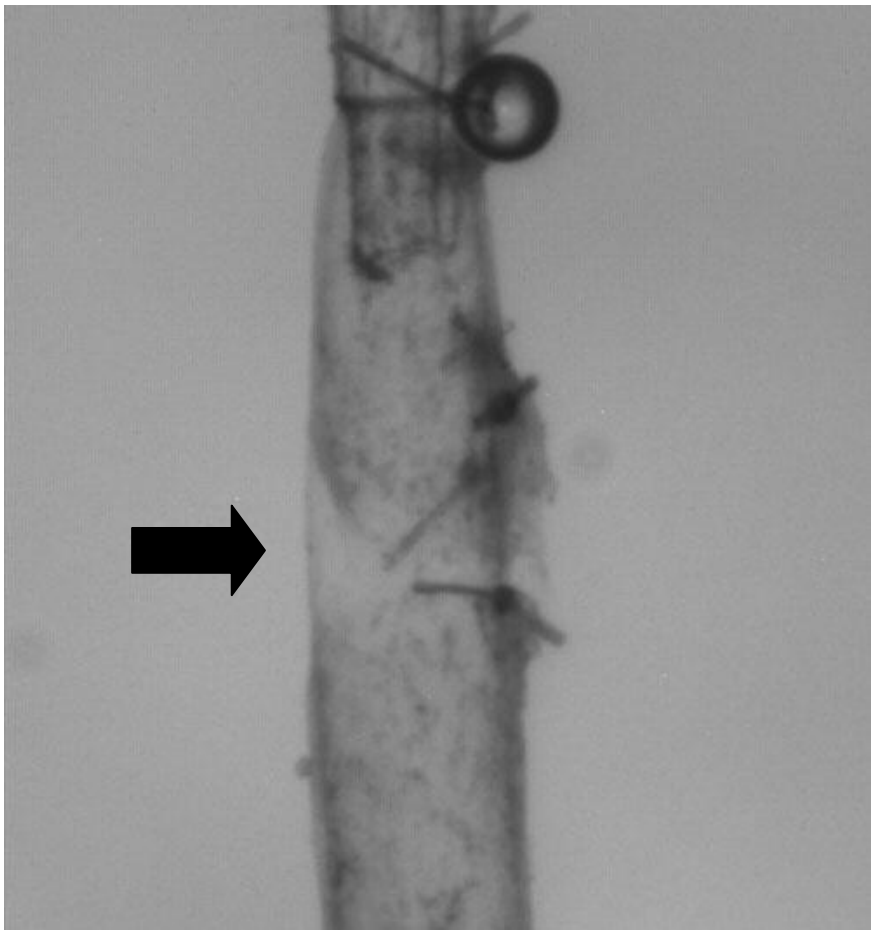

**Figure 1.3: Observed failure of endothelium in rat middle cerebral artery prior to pressure loss or structural failure during pressurized (100 mmHg) axial stretch test to failure.** Intima was stained with nigrosin dye for contrast. It is unknown if IEL was also ruptured in this image.

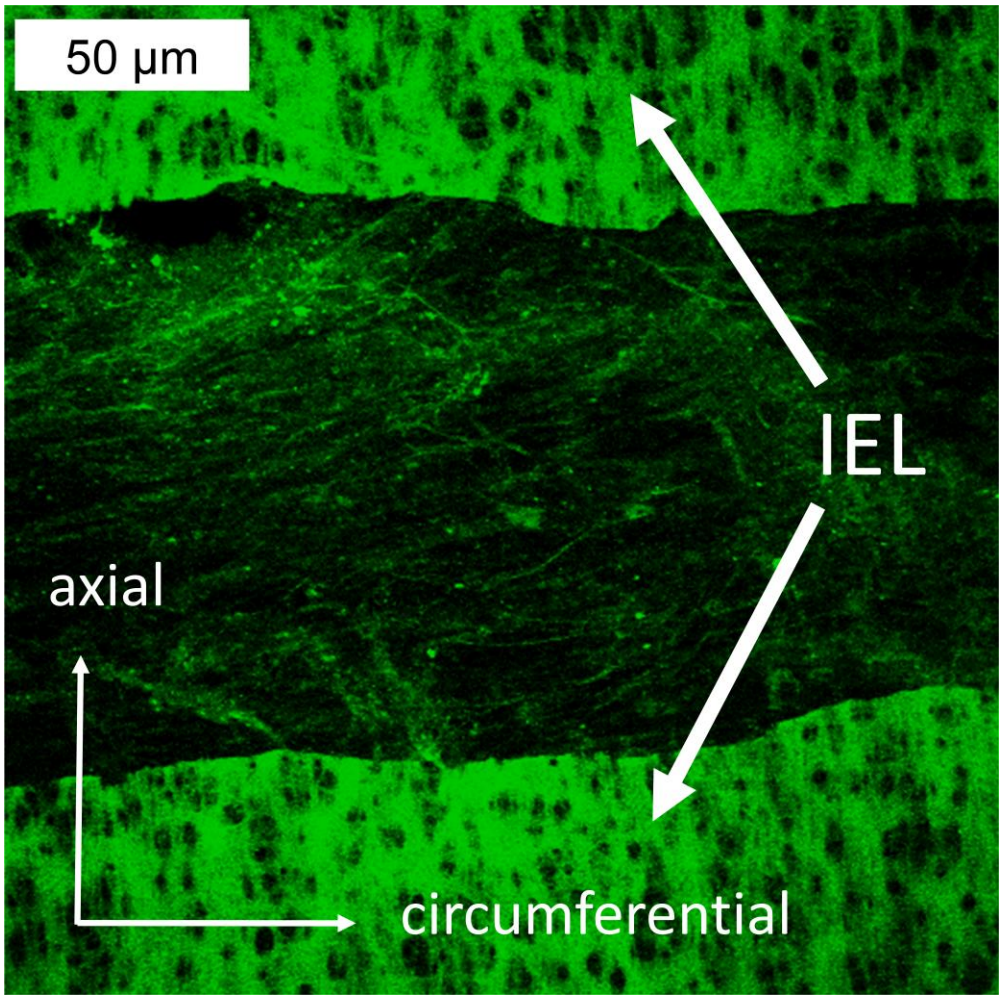


**Figure 1.4: Observed rupture of internal elastic lamina (IEL) following subfailure axial overstretch of lamb middle cerebral artery.** IEL imaged with confocal microscopy. Image from unpublished preliminary data related to (Converse and Monson, 2014).

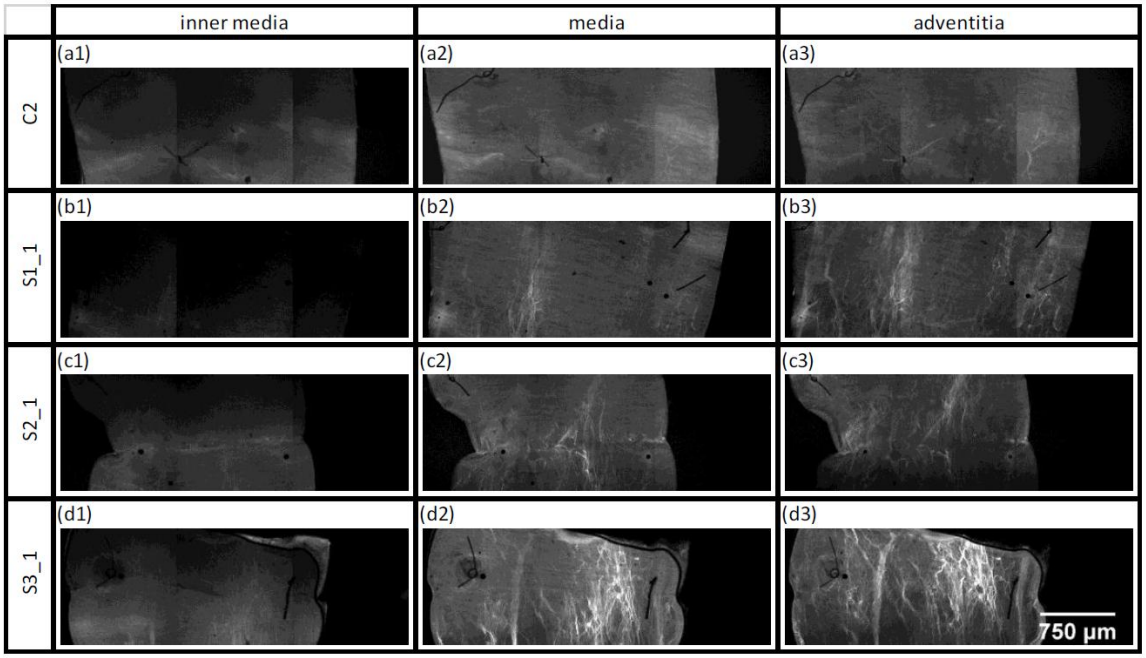


**Figure 1.5: Confocal images of lamb middle cerebral arteries subjected to subfailure axial overstretch. White streaks indicate binding of collagen mimetic peptide to damaged collagen.** Axial direction is vertical and circumferential is horizontal. [C2, control (no overstretch); S1_1 ($\lambda z = 1.3$); S2_1 ($\lambda z = 1.4$); S3_1 ($\lambda z = 1.6$)]. (Walther, 2015) Reproduced with permission.

## 1.4 Cerebrovascular Autoregulation and TBI-Induced Dysfunction

Cerebrovascular autoregulation is the process by which the SMCs in cerebral arteries alter their level of contraction so as to provide the needed level of cerebral blood flow (CBF) in order to maintain homeostasis and match the regional metabolic needs in the brain. In humans, autoregulation of CBF can be sustained within the range of mean arterial blood pressure of approximately 50-150 mmHg (Humphrey, 2002; Phillips and Whisnant, 1992). Above the upper pressure limit, CBF increases with increasing cerebral perfusion pressure (CPP) as SMCs can no longer contract sufficiently to restrict flow (Cipolla and Osol, 1998). Below the lower pressure limit, CBF decreases with decreasing CPP as SMC can no longer dilate sufficiently to allow enough flow, resulting in

hypoperfusion and ischemia (Hossmann, 1994). There are several autoregulatory mechanisms in the cerebrovasculature, many of which are disrupted following TBI. More complete reviews of normal cerebral autoregulation (Brian, 1998; Edvinsson et al., 1993; Faraci and Brian, 1994; Kontos, 1981; Kulik et al., 2008; Meininger and Davis, 1992; Paulson et al., 1990) and TBI-induced autoregulatory dysfunction (DeWitt and Prough, 2003; Golding, 2002; Golding et al., 1999a; Kenney et al., 2016; Kramer et al., 2013; Kreipke et al., 2013; Rangel-Castilla et al., 2008) are available elsewhere.

The scope of this summary of cerebral autoregulation is limited to larger cerebral arteries, such as the pial arteries utilized in this dissertation. These larger cerebral arteries provide as much as 45-50% of the total resistance in the cerebral vasculature in rats (Faraci and Heistad, 1990; Harper et al., 1984). Further, regulation of blood flow for localized needs in the brain requires a vascular response in both the localized vasculature as well as upstream vessels (Faraci and Heistad, 1990), allowing maintenance of local blood flow without drastic alterations in local blood pressure. Therefore, this resistance in the larger cerebral arteries is vital for the protection of the smaller vessels downstream (Faraci and Heistad, 1990). While these larger vessels commonly rupture and bleed during TBI, they can also become dysfunctional, exposing the more distal microvasculature to supraphysiological pressures (Tsubokawa and Katayama, 1998), resulting in diffuse injury such as vasogenic edema and hemorrhage of the microvasculature, both of which are commonly observed post-TBI (Kenney et al., 2016; Tsubokawa and Katayama, 1998). One potential way to clinically evaluate the degree of autoregulatory dysfunction noninvasively post-TBI is the evaluation of blood flow in large cerebral vessels, such as the MCA, using transcranial Doppler ultrasound

(Panerai,1998) or near-infrared spectroscopy (Highton et al., 2015; Panerai, 1998). Additionally, the effects evoked by various signals to the cerebrovasculature change based on where in the vascular tree the signal is applied. For example, norepinephrine causes contraction in pial arteries via interaction with SMC α1-adrenoceptors (Lincoln, 1995; Sandor, 1999), while causing dilation in subcortical arterioles via interaction with β-adrenoceptors which are predominate in these smaller arterioles (Lincoln, 1995; Mayhan, 1994; Rosendorff et al., 1976). Also, the peak myogenic response occurs at decreasing pressure levels as the diameter of the artery decreases (Golding et al., 1998b). Therefore, a better understanding of mechanically-induced autoregulatory dysfunction of larger cortical vessels, like the MCA, may contribute to the planning of treatments based on noninvasive clinical measurements of blood flow within these vessels.

Cerebrovascular autoregulation takes place via the complex interplay of several mechanisms which are here divide into four basic categories for discussion: neurogenic, metabolic, endothelial, and myogenic.

### *1.4.1 Neurogenic autoregulation*

Pial arteries receive nervous signals from nerves originating in the peripheral nervous system (Hamel, 2006). These nerves are located in the adventitia, their density begins to decrease as arteries enter the cortex, and they are not present in subcortical arterioles (Handa et al., 1990). The role and importance of these pial artery perivascular nerves is not well understood and is still an open debate (Sandor, 1999; Strandgaard and Sigurdsson, 2008; van Lieshout and Secher, 2008). Additionally, while it has been shown that these perivascular nerves do not have a significant effect on cerebral blood flow

under physiological conditions, contraction of pial arteries due to sympathetic nerve signals during hypertension do significantly reduce cerebral blood flow, protecting downstream portions of the vasculature from damage (Tuor, 1992; Wahl, 1985).

These perivascular nerves are capable of releasing neurotransmitters that can potentially alter the level of SMC contraction. Norepinephrine (NE) interacts with α1-adrenoceptors in SMCs, and serotonin (5-HT) interacts with 5-HT1B receptors, both leading to contraction of pial arteries (Hogestatt and Andersson, 1984b; Lincoln, 1995; Sandor, 1999). Further, while interaction of acetylcholine (ACh) with muscarinic receptors in SMCs can potentially lead to weak contraction, ACh evokes a much more pronounced dilation in cerebral arteries by triggering the release of nitric oxide (NO) from endothelial cells as explained in the endothelial autoregulation section below in greater detail (Lee, 2002). The density and functionality of these perivascular nerves varies by location within the brain, which may serve to accommodate the varied metabolic needs in differing regions of the brain (Bleys et al., 1996; Handa et al., 1990; Hogestatt and Andersson, 1984b). For example, perivascular nerve density is lower in human anterior cerebral arteries than in posterior cerebral arteries (Bleys et al., 1996), while reactivity to NE is higher in feline anterior cerebral arteries than in posterior cerebral arteries (Hamel et al., 1988).

TBI leads to damage of this system in addition to altered response to signaling. Perivascular nerves in the basilar and internal carotid arteries have been shown to be physically damaged following impact TBI in rats (Ueda et al., 2006). Also, following fluid percussion injury, 5-HT induced vasoconstriction is eliminated or even changed to mild dilation (Kontos and Wei, 1992).

*1.4.2 Metabolic autoregulation*

Metabolic autoregulation refers to alteration in SMC tone in response to the chemical signals associated with metabolic needs. While metabolic signals exert some influence on cerebrovascular tone regardless of pressure level, they are likely the primary means of autoregulation at pressures below the autoregulatory pressure range (Kontos et al., 1978). This section will briefly discuss the regulatory mechanisms associated with maintenance of physiological levels of carbon dioxide ($CO_2$) and oxygen ($O_2$).

Either hypocapnia or hypercapnia in the brain result in compensatory responses from cerebrovascular SMCs. The physiological partial pressure of $CO_2$ ($PCO_2$) in CSF is approximately 55 mmHg (Andrews et al., 1994). When $PCO_2$ is elevated, SMC vasodilation results in order to clear the excess $CO_2$. The primary mechanism for this is the SMC response to the associated change in the surrounding pH. Excess $CO_2$ reacts with extracellular $H_2O$ to form carbonic acid ($CO_2 + H_2O \leftrightarrow H_2CO_3 \leftrightarrow H^+ + HCO_3^-$). This increases the concentration of extracellular $H^+$ which then interact with SMCs and cause dilation (Kontos et al., 1977). The concept that this is the primary mechanism for hypercapnic vasodilation is further supported by the finding that changes in $PCO_2$ or bicarbonate concentrations alone do not affect vascular tone (Kontos et al., 1977). Hypocapnia results in vasoconstriction due to the same relationship between the concentration of extracellular $H^+$ and the level of SMC contraction.

Levels of $O_2$ in the brain produce vasoactive responses independent of the level of $CO_2$. While the partial pressure of $O_2$ ($PO_2$) varies dramatically from one region of the brain to another (Masamoto and Tanishita, 2009), hypoxia-induced vasodilation typically begins when mean arterial blood pressure (MAP) falls below 50 mmHg (Humphrey,

2002; Masamoto and Tanishita, 2009). There are several factors which are released from nonvascular brain tissues in response to hypoxia that can induce vasodilation and increase blood flow (Pearce, 1995). While it is still a matter of debate which is the primary mechanism for hypoxia mediated vasodilation (Masamoto and Tanishita, 2009; Pearce, 1995), a few of them are presented here. Neural cells release potassium ions ($K^+$) under hypoxic conditions. Small increases of extracellular $K^+$ lead to dilation of SMCs through the action of inward rectifying potassium channels ($K_{ir}$) (Golding et al., 2000; Johnson et al., 1998). Hypoxic neurons also release $H^+$, the effect of which was discussed above. Adenosine is normally released by and then acts on endothelial cells to produce vasodilation (Coney and Marshall, 1998). However, under hypoxic conditions, nonvascular brain tissue also release adenosine which then interacts directly with SMCs causing dilation. There is also a direct effect of hypoxia on SMCs. Reduced adenosine triphosphate (ATP) levels in SMCs open ATP sensitive $K^+$ channels which result in hyperpolarization and vasodilation (Taguchi et al., 1994). Under hyperoxic conditions, the elevated levels of $PO_2$ have been shown to increase concentrations of ET-1, a potent vasoconstrictor (Armstead, 1999). Also it is theorized that free floating NO, basally acting as a vasodilator, is inactivated by superoxide anions that form during hyperoxia resulting in decreased dilation (Zhilyaev et al., 2003).

TBI leads to impairment of metabolically-based autoregulatory mechanisms. It is important to note here that the metabolic demand in the brain decreases post-TBI. However, the decrease in CBF due to autoregulatory dysfunction is greater than would be justified by this reduced metabolic demand (DeWitt and Prough, 2003). Decreased vascular reactivity to elevated $CO_2$ in the brain following TBI has been observed

experimentally (Golding et al., 1999b). Additionally, ATP sensitive $K^+$ channels in SMCs, involved in the dilation associated with hypoxia, have been shown to be impaired following fluid percussion injury (Armstead, 1997a).

*1.4.3 Endothelial autoregulation*

Vascular endothelial cells play a vital role in the regulation of CBF through the action of both chemical and mechanical signals. Endothelial cells also provide a wide variety of other essential functions such as acting as a selective barrier between blood and brain, providing a nonthrombogenic surface, and facilitating blood clotting, inflammation, and angiogenesis (Kropinski et al., 2013). Some examples of the vasoactive substances produced by endothelial cells are NO, endothelial-derived hyperpolarizing factor (EDHF), and endothelin.

Nitric oxide is a potent vasodilator and is consistently produced at a basal level by endothelial cells. Production of NO is dependent on endothelial cytosolic calcium levels (Szabo, 1996). Some examples of the stronger methods to increase cytosolic calcium are shear stress applied by flowing blood (Mashour and Boock, 1999), interaction of NO synthase (NOS) with the endothelial cell membrane, and binding of ACh to the cell membrane (Szabo, 1996). The three sources of NOS are the endothelial cells themselves (eNOS), neurons (nNOS), and inducible NOS (iNOS) which is not normally present in the healthy brain (Szabo, 1996) but can be expressed following TBI (Szabo, 1996; Villalba et al., 2014).

Endothelial derived hyperpolarizing factor is the residual dilational effect endothelial cells can exhibit on SMCs in the absence of chemical dilators like NO,

prostaglandin, or cyclooxygenase. No specific chemical has been associated with this effect to date. It is thought that when endothelial cytosolic calcium increases due to various agonists, this opens calcium-mediated $K^+$ channels, hyperpolarizing the endothelial cell membrane. This process then results in relaxation in adjacent SMCs (Busse et al., 2002). This phenomenon is not fully understood, but some possible explanations include direct transfer of membrane potential between endothelial and SMCs via gap junctions (Busse et al., 2002; Griffith, 2004), and expulsion of $K^+$ from the endothelium into the extracellular space inducing hyperpolarization of SMC via $K^+$ channels or $Na^+$- $K^+$ ATPase (Busse et al., 2002).

While endothelin peptides are produced by endothelial cells, there are also significant amounts produced by astrocytes, and neurons under normal physiological conditions (Petrov et al., 2002). The primary endothelin peptides produced in the brain are ET-1 and ET-3, but ET-1 is thought to be the predominantly vasoactive of the two (Kuwaki et al., 1997; MacCumber et al., 1990), and concentrations of ET-1 are typically much higher in CSF than in plasma (Kuwaki et al., 1997). ET-1 has a complicated effect on the vasculature causing dilation at low concentrations, and contraction at higher concentrations (Armstead et al., 1989). Vasoconstriction induced by ET-1 is the result of its interaction with ETA receptors on SMCs which activate of the G-protein cascade. This results in the formation of inositol triphosphate which then binds to SMC calcium channels to increase influx of calcium, leading to contraction (Hirata et al., 1988). The contractile effects of ET-1 are long lasting, persisting for several hours after ET-1 is no longer associated with the receptor (Clarke et al., 1989). The binding of ET-1 with ETB receptors on endothelial cells evokes vasodilation by triggering eNOS and NO

production. ETB receptors also activate cell survival pathways and providing clearance of ET-1 (Kropinski et al., 2013; Touzani et al., 1997).

There is a number of studies showing endothelial autoregulatory pathways are disrupted following TBI. NO-mediated dilation is impaired following subarachnoid hemorrhage (SAH) as hemoglobin is a potent NO scavenger leading to vasoconstriction (Szabo, 1996). Fluid percussion injury eliminates ACh-mediated dilation and even results in mild vasoconstriction due to ACh interaction with muscarinic receptors on SMCs (Ellison et al., 1989; Kontos and Wei, 1992). Toklu et al. (Toklu et al., 2015) have shown that exposure to blast overpressure results in both a decrease to ACh mediated dilation, as well as an increase in ET-1 induced contraction. Increased levels of ET-1 in plasma and CSF following experimental (Foley et al., 1994; Petrov, 2009; Petrov et al., 2002) and human (Beuth et al., 2001; Salonia et al., 2010) TBI have been linked to hypoperfusion and ischemic brain damage. It should be noted that the increase in production of ET-1 following TBI is much more pronounced in macrophages, astrocytes, and neurons then in endothelial cells (Petrov et al., 2002). Since experimental application of ET-1 to the adventitia has a significantly stronger response than luminal application (Salom et al., 1995), it is possible that elevated production of ET-1 by nonvascular cells post-TBI plays a larger role in the post-TBI vasospasm than alterations to endothelial ET-1 production do. However, the specific role of ET-1 in TBI-induced vasospasm is still not well defined (Kropinski et al., 2013).

*1.4.4 Myogenic autoregulation*

The myogenic response, also known as the Bayliss effect, involves alteration of SMC contraction caused by changes in luminal pressure. It was first observed by Sir William Bayliss over 100 years ago in dogs.

> When the pressure was raised inside the artery it was seen at first to swell, but immediately, and while the mercury was still kept at its height, a powerful contraction took place, in which the artery appeared to writhe like a worm. If pressure was suddenly lowered again the artery did not return merely to the state corresponding to the lesser pressure, but underwent a considerable relaxation... (Bayliss, 1902) (page 229; used with permission)

There are two main divisions to this effect, generation of basal tone (myogenic tone) and regulation of tone thereafter (myogenic reactivity) (Osol et al., 2002). Both have been shown to be affected by TBI (Armstead, 1997b; Mathew et al., 1999; Villalba et al., 2014).

The development of myogenic tone takes place within the pressure range of 40-60 mmHg in rats (Osol et al., 2002). Luminal pressure stretches SMC membranes resulting in depolarization caused in part by opening of stretch activated cation channels, such as transient receptor potential channels (Welsh et al., 2002). SMC membrane depolarization causes the opening of voltage sensitive calcium channels which facilitate influx of extracellular calcium (Knot and Nelson, 1998; McCarron et al., 1997). Elevated intracellular calcium increases myosin light-chain phosphorylation, resulting in SMC contraction, and a decrease in vessel diameter (Somlyo et al., 1999). Additionally, activation of calcium sensitive $K^+$ channels by increased intracellular calcium results in membrane hyperpolarization, thus providing negative feedback to control the level of stretch induced myogenic contraction (Jaggar et al., 2000).

The mechanisms of myogenic reactivity differ from those of myogenic tone

development. The pressure range in which myogenic reactivity is dominant is 60-140 mmHg in rats (Osol et al., 2002) and 60-160 mmHg in humans (Phillips and Whisnant, 1992). It has been shown experimentally in rats that increases in luminal pressure within this range produce increased wall tension, but the diameter is kept relatively constant (Osol et al., 2002). Increased myosin light-chain phosphorylation in this case is due to heightened sensitivity to calcium in SMCs, while the intracellular calcium levels do not significantly increase (Lagaud et al., 2002; Somlyo et al., 1999). This increase in calcium sensitivity is achieved by activation of Rho kinase and protein kinase C (Lagaud et al., 2002; Osol et al., 1991; Schubert et al., 2002). The reverse of both these processes takes place in response to decreased luminal pressure, resulting in decreased wall tension and eventually, vasodilation (Bayliss, 1902; Osol et al., 2002).

Both myogenic tone and reactivity are affected by TBI. Specifically, controlled cortical impact TBI in rats impairs both mechanisms (Golding et al., 1998a). Also, myogenic tone development to increasing luminal pressure is impaired after fluid percussion injury, which the authors attributed to expression of iNOS and elevated levels of NO preventing contraction (Villalba et al., 2014). Additionally, calcium sensitive $K^+$ channels, involved in the reduction of myogenic tone to decreased luminal pressure, have been shown to be impaired following fluid percussion injury (Armstead, 1997b; Mathew et al., 1999), possibly caused by inactivation by elevated oxygen free radicals (DeWitt et al., 2001).

*1.4.5 Mechanisms of autoregulatory dysfunction (physical vs. chemical interplay)*

Cerebrovascular autoregulatory dysfunction following TBI is a combination of the repercussions from the initial injury and the subsequently altered chemical environment in the injured brain. Good reviews on the combined initial mechanical and secondary injury caused by TBI are available (Davis, 2000; Kreipke et al., 2013; Ommaya, 1995). The importance of the interaction between these two comorbid factors and the need to identify the specific role cerebrovasculature injury plays is well stated by DeWitt.

> It is somewhat artificial to separate traumatic injury to the brain from traumatic injury to the vasculature since injury to the brain likely contributes to cerebral vascular injury and vice versa. However, it may prove important to separate the mechanisms of vascular and brain injury because different types of damage may require different preventative or treatment strategies. (DeWitt and Prough, 2003) (page 802; used with permission)

While the need for properly functioning cerebrovascular autoregulation is vital, aside from altered chemical signaling, autoregulatory dysfunction could just as well be influenced by subfailure mechanical damage to cerebral vessels. The need to better understand the subsequent mechanically related pathology, and the potential of such knowledge, was voiced by a foundational researcher of TBI, Ayub Ommaya.

> If knowledge of the specific biomechanics of any head injury were available and the clinical and physiopathologic boundary conditions in the earliest period were also known and subsequently could be adequately controlled, then it would be possible to predict the outcome of that head injury at a very early stage. (Ommaya, 1995) (page 534; used with permission)

As a result, it is necessary to examine the effects to cerebral autoregulation resulting from both the initial mechanical injury, as well as subsequent chemical insults, to the cerebrovasculature associated with TBI.

The scope of this section is to focus specifically on a few examples of how

mechanical and chemical insults may separately affect the functionality of cerebrovascular autoregulation following TBI. There are other serious secondary complications that follow TBI that are not necessarily directly related to vascular injury, and are subsequently outside the scope of this dissertation, such as inflammation (Ziebell and Morganti-Kossmann, 2010) and cytotoxic edema (Marmarou, 2007; Unterberg et al., 2004). However, these conditions do play a part in the altered chemical milieu in the brain post-TBI. Another such condition is the elevation of intracranial pressure (ICP) frequently observed after TBI (Tang et al., 2015; Tasker, 2014). Given a constant MAP, increased ICP leads to a drop in the CPP (CPP = MAP - ICP). This has been referred to as false autoregulatory dysfunction as otherwise unimpeded CBF is restored when elevated ICP is relieved (Enevoldsen and Jensen, 1977).

Several autoregulatory mechanisms are strongly related to the arterial mechanical environment. Myogenic autoregulation is entirely driven by applied luminal pressure (Bayliss, 1902). Shear forces caused by blood flow stimulate endothelial production of NO (Mashour and Boock, 1999). It has also been shown that the behavior of vascular SMCs are altered following mechanical stretch (Alford et al., 2011; Arutiunov et al., 1974; Boock, 1991). Specifically, short-term cerebral vasospasm lasting less than 20 minutes has been produced experimentally by mechanically stretching connective tissue attached to cerebral arteries, but not when stretch was applied to the vessel itself (Arutiunov et al., 1974). Further, mechanical stretch applied directly to isolated femoral arteries has led to vasospasm, but this was even shorter in duration, lasting 2 minutes or less (Boock, 1991). Long-term increase in SMC contractility, lasting at least 24 hours, has been observed following rapid stretch of cultured SMCs (Alford et al., 2011). In

contrast however, the application of rapid in vitro axial overstretch to rat MCAs in Chapter 3 led to a decrease in SMC contraction.

The intrinsic mechanical properties of cerebral arteries can also be effected by TBI. As mentioned in the previous section, contractile behavior of SMCs is dependent on the stiffness of the extracellular matrix (Steucke et al., 2015). Supraphysiological deformation of arteries produces strain softening (Alastrue et al., 2008; Bell et al., 2015; Holzapfel and Gasser, 2007; Horný et al., 2010; Maher et al., 2012; Peña et al., 2010), potentially due to changes in the stiffness of the ECM. Further, decreased wall tension in cerebral vessels correlates clinically with impaired autoregulation (Varsos et al., 2014). So even in the absence of chemically induced changes, cerebral autoregulation can be negatively affected by the initial mechanical insult associated with TBI.

There are several aspects of the altered chemical environment post-TBI which could play a role in autoregulatory dysfunction. Specifically, vasospasm leads to hypoperfusion and subsequent ischemia (Kramer et al., 2013). Independent of any mechanically-induced increase in contraction, several chemical changes take place following TBI which can induce vasospasm. Following TBI, there is frequently an increase in extracellular $K^+$ concentrations released from neurons (Golding et al., 2000; Katayama et al., 1990; Nilsson et al., 1993; Takahashi et al., 1981), potentially returning to normal within an hour (Nilsson et al., 1993). Under physiological conditions, where extracellular $K^+$ concentrations are approximately 4 mM, slight increases in extracellular $K^+$ result in vasodilation (Golding et al., 2000; Johnson et al., 1998). However, the increased concentration of extracellular $K^+$ post-TBI can reach 50-60 mM (Nilsson et al., 1993; Takahashi et al., 1981) which evokes strong vasocontraction via direct

depolarization of SMCs (Golding et al., 2000; Hogestatt and Andersson, 1984a).

Another change in the post-TBI chemical environment linked to vasospasm is the clinically observed increase of ET-1 concentrations in CSF following SAH (Mascia et al., 2001; Volker Seifert et al., 1995). Similar ET-1 increases are observed following experimental weight drop TBI (Petrov, 2009). In humans, elevated ET-1 post-TBI has been associated with unfavorable clinical outcomes (Salonia et al., 2010). Unfortunately, while endothelin antagonists have been shown to reduce cerebral vasospasm after brain injury (Armstead, 2004; Roux et al., 1999; Schubert et al., 2011), clinical outcomes and mortality rates are not similarly improved (Kramer and Fletcher, 2009)

Concentrations of 5-HT are also increased in CSF following SAH (Cambj-Sapunar et al., 2003). As discussed above, 5-HT normally leads to vasoconstriction by interaction with SMCs, but following fluid percussion injury, 5-HT-induced vasoconstriction has been shown to be eliminated, or even changed to mild dilation (Kontos and Wei, 1992). This is interesting considering others have noted increased sensitivity to both ET-1 and 5-HT after SAH (Edvinsson and Povlsen, 2011).

Chemical signals normally associated with vasodilation are also altered following TBI. Concentrations of ACh in the brain following TBI are increased (Hayes et al., 1991; Lyeth and Hayes, 1992). Following fluid percussion injury, Ach-mediated dilation is eliminated and application of ACh produces mild contraction via interaction with muscarinic receptors on SMCs (Kontos and Wei, 1992). In the case of hemorrhage, hemoglobin that has breached the blood brain barrier scavenges free NO leading to vasoconstriction (Szabo, 1996), as mentioned earlier. Oxygen free radicals, such as superoxide, are dramatically increased in the brain following experimental TBI (Fabian et

al., 1995; Kontos and Wei, 1986). It has been suggested that these free radicals could inactivate NO leading to vasoconstriction (Szabo, 1996). However, experimentally observed decreases in myogenic contraction following TBI have been attributed to increased NO levels (also an oxygen radical) resulting from iNOS expression. It should be noted that this latter conclusion was not confirmed with measured NO levels. This increase in oxygen free radicals post-TBI can also lead to production of $ONOO^-$ which inhibit $K^+$ channels necessary for hyperpolarization of SMCs, thus increasing vascular tone and reducing myogenic reactivity to decreasing pressure (DeWitt et al., 2001).

## 1.5 Summary of Chapters

This dissertation examined the biaxial mechanical and functional properties of cerebral arteries, and how these properties are changed following determined thresholds of axial stretch. The current research is presented in the following chapters as two previously published and one in progress manuscript.

Chapter 2 presents a published study (Bell et al., 2013) which measured the biaxial and failure properties of rat MCAs and then compared these properties to previously collected data from human pial arteries (Monson et al., 2008). The dual purpose of this study was to both better define the passive mechanical behavior of rat cerebral arteries and to provide translatability between the measured cerebrovascular mechanics of rat and human cerebral vessels. It was determined that the passive mechanical behavior of rat and human cerebral arteries is qualitatively similar. Specifically, they are both anisotropic with the axial direction being stiffer than the circumferential. Also, the ratio between the stiffness in the axial vs. circumferential

directions was statistically similar between the two species. This defined relationship between the passive mechanics of rat and human arteries allows more accurate application of the results from other rat studies to humans. Further, the failure stretch levels measured in the study were also used to inform the target stretch levels in a subsequent subfailure injury threshold study (Chapter 3).

The study in Chapter 3 (manuscript for publication in progress) investigates the thresholds of axial stretch, as well as strain rate, that result in alterations to the SMC function of rat cerebral arteries. Since proper functioning of the SMC in cerebral arteries is vital for the regulation of CBF, this study focuses specifically on how the contractile ability of these SMCs are affected by axial overstretch. This contractile behavior was measured by observing the dose response relationship of extracellular $K^+$-induced contraction. While the applied overstretches in the study did not alter the baseline or maximally induced levels of contraction in samples, the level of contraction for sub-maximal doses of extracellular $K^+$ was reduced following axial overstretch. This was reflected in an increase in the $K^+$ concentration required to evoke half the maximum contraction. This change in contraction was dependent on both the magnitude and strain rate of the applied overstretch. These mechanically-induced changes to SMC contraction could contribute to second impact syndrome (Cantu and Gean, 2010; Laskowski et al., 2015) as well as highlight a potentially treatable mechanism of autoregulatory dysfunction.

In Chapter 4 (Bell et al., 2015), the level of axial stretch which led to alterations in the axial passive mechanical behavior of cerebral arteries was investigated. Unfortunately, due to the small absolute value of forces associated with axial stretch of

rat cerebral arteries, this study had to be conducted in MCAs taken from sheep, which are much larger in size. It was shown that there is a threshold of axial overstretch below which passive mechanical properties in cerebral arteries do not change. However, above this threshold, the stiffness decreases as applied overstretch increases until a second stretch threshold is reached. Beyond this second upper threshold, the change in stiffness does not continue to decrease until a failure inducing axial stretch is reached. Interestingly, neither the failure stress or stretch levels were significantly affected by overstretch. These results demonstrate that subfailure levels of axial stretch can lead to alterations in the passive mechanics of cerebral arteries, possibly due to alterations in the underlying microstructure. These alterations to the cerebrovascular microstructure could be a driving factor in the subsequent increased risk for stroke up to 5 years after a TBI event (Burke et al., 2013; Chen et al., 2011; Hills et al., 2012). As a result, these results could be used to inform treatments aimed to reduce these complications post-TBI as they provide a greater understanding of the status of cerebral arteries at the initiation of the biochemical cascades following TBI.

A discussion of the combined results and conclusions from all three studies is contained in Chapter 5. The applicability of these results, along with limitations of the work, are discussed. Additional unanswered questions related to these studies, and related to the cerebrovasculature during TBI in general, are also discussed. Potential goals and experimental methods for future studies are also presented.

## 1.6 References

Adelson, P.D., Clyde, B., Kochanek, P.M., Wisniewski, S.R., Marion, D.W., Yonas, H., 1997. Cerebrovascular response in infants and young children following severe traumatic brain injury: a preliminary report. Pediatric Neurosurgery 26, 200-207.

Akima, M., Nonaka, H., Kagesawa, M., Tanaka, K., 1986. A study on the microvasculature of the cerebral cortex. Fundamental architecture and its senile change in the frontal cortex. Laboratory Investigation; A Journal of Technical Methods and Pathology 55, 482-489.

Alastrue, V., Pena, E., Martinez, M.A., Doblare, M., 2008. Experimental study and constitutive modelling of the passive mechanical properties of the ovine infrarenal vena cava tissue. Journal of Biomechanics 41, 3038-3045.

Alcolado, R., Weller, R.O., Parrish, E.P., Garrod, D., 1988. The cranial arachnoid and pia mater in man: anatomical and ultrastructural observations. Neuropathology and Applied Neurobiolgy 14, 1-17.

Alem, N.M., Stalnaker, R.L., Melvin, J.W., 1997. Measurement of head impact response. In International IRCOBI: Conference on the Biomechanics of Impact. Berlin, Germany.

Alford, P.W., Dabiri, B.E., Goss, J.A., Hemphill, M.A., Brigham, M.D., Parker, K.K., 2011. Blast-induced phenotypic switching in cerebral vasospasm. Proceedings of the National Academy of Sciences of the United States of America 108, 12705-12710.

Andrews, B.T., Dujovny, M., Mirchandani, H.G., Ausman, J.I., 1989. Microsurgical anatomy of the venous drainage into the superior sagittal sinus. Neurosurgery 24, 514-520.

Andrews, R.J., Bringas, J.R., Alonzo, G., 1994. Cerebrospinal fluid pH and $PCO_2$ rapidly follow arterial blood pH and $PCO_2$ with changes in ventilation. Neurosurgery 34, 466-470; discussion 470.

Armstead, W.M., 1997a. Brain injury impairs ATP-sensitive $K^+$ channel function in piglet cerebral arteries. Stroke 28, 2273-2280.

Armstead, W.M., 1997b. Role of impaired cAMP and calcium-sensitive $K^+$ channel function in altered cerebral hemodynamics following brain injury. Brain Research 768, 177-184.

Armstead, W.M., 1999. Endothelin-1 contributes to normocapnic hyperoxic pial artery vasoconstriction. Brain Research 842, 252-255.

Armstead, W.M., 2004. Endothelins and the role of endothelin antagonists in the management of posttraumatic vasospasm. Current Pharmaceutical Design 10, 2185-2192.

Armstead, W.M., Mirro, R., Leffler, C.W., Busija, D.W., 1989. Influence of endothelin on piglet cerebral microcirculation. American Journal of Physiology 257, H707-710.

Arutiunov, A.I., Baron, M.A., Majorova, N.A., 1974. The role of mechanical factors in the pathogenesis of short-term and prolonged spasm of the cerebral arteries. Journal of Neurosurgery 40, 459-472.

Asgharpour, Z., Baumgartner, D., Willinger, R., Graw, M., Peldschus, S., 2014. The validation and application of a finite element human head model for frontal skull fracture analysis. Journal of the Mechanical Behavior of Biomedical Materials 33, 16-23.

Baek, S., Gleason, R.L., Rajagopal, K.R., Humphrey, J.D., 2007a. Theory of small on large: potential utility in computations of fluid-solid interactions in arteries. Computer Methods in Applied Mechanics and Engineering 196, 3070-3078.

Baek, S., Valentin, A., Humphrey, J.D., 2007b. Biochemomechanics of cerebral vasospasm and its resolution: II. constitutive relations and model simulations. Annals of Biomedical Engineering 35, 1498-1509.

Ballabh, P., Braun, A., Nedergaard, M., 2004. The blood-brain barrier: an overview: structure, regulation, and clinical implications. Neurobiology of Disease 16, 1-13.

Bassan, H., Limperopoulos, C., Visconti, K., Mayer, D.L., Feldman, H.A., Avery, L., Benson, C.B., Stewart, J., Ringer, S.A., Soul, J.S., Volpe, J.J., du Plessis, A.J., 2007. Neurodevelopmental outcome in survivors of periventricular hemorrhagic infarction. Pediatrics 120, 785-792.

Bayliss, W.M., 1902. On the local reactions of the arterial wall to changes of internal pressure. Journal of Physiology 28, 220-231.

Bell, E.D., Kunjir, R.S., Monson, K.L., 2013. Biaxial and failure properties of passive rat middle cerebral arteries. Journal of Biomechanics 46, 91-96.

Bell, E.D., Monson, K.L., 2012. The fung strain energy function captures passive middle cerebral artery response, Biomedical Engineering Society 2012 Annual Meeting, Atlanta, GA.

Bell, E.D., Sullivan, J.W., Monson, K.L., 2015. Subfailure overstretch induces persistent changes in the passive mechanical response of cerebral arteries. Frontiers in Bioengineering and Biotechnology 3.

Bell, J.D., Thomas, T.C., Lass, E., Ai, J., Wan, H., Lifshitz, J., Baker, A.J., Macdonald, R.L., 2014. Platelet-mediated changes to neuronal glutamate receptor expression at sites of microthrombosis following experimental subarachnoid hemorrhage. Journal of Neurosurgery 121, 1424-1431.

Bendjellal, F., Tarriere, C., Gillet, D., Mack, P., Guillon, F., 1987. Head and neck responses under high G-level lateral deceleration. SAE Technical Paper 872196.

Bergel, D.H., 1961. The static elastic properties of the arterial wall. Journal of Physiology 156, 445-457.

Beuth, W., Kasprzak, H., Kotschy, M., Wozniak, B., Kulwas, A., Sniegocki, M., 2001. Endothelin in the plasma and cerebrospinal fluid of patients after head injury. Neurologia i Neurochirurgia Polska 35 Suppl 5, 125-129.

Black, P.M., 1986. Hydrocephalus and vasospasm after subarachnoid hemorrhage from ruptured intracranial aneurysms. Neurosurgery 18, 12-16.

Bleys, R.L., Cowen, T., Groen, G.J., Hillen, B., Ibrahim, N.B., 1996. Perivascular nerves of the human basal cerebral arteries: I. topographical distribution. Journal of Cerebral Blood Flow and Metabolism 16, 1034-1047.

Boock, R.J., 1991. Vascular Response to Mechanical Deformations. University of Pennsylvania, Philadelphia.

Bramlett, H.M., Dietrich, W.D., Green, E.J., 1999. Secondary hypoxia following moderate fluid percussion brain injury in rats exacerbates sensorimotor and cognitive deficits. Journal of Neurotrauma 16, 1035-1047.

Brian, J.E., Jr., 1998. Carbon dioxide and the cerebral circulation. Anesthesiology 88, 1365-1386.

Brossollet, L.J., Vito, R.P., 1995. An alternate formulation of blood vessel mechanics and the meaning of the in vivo property. Journal of Biomechanics 28, 679-687.

Brozici, M., van der Zwan, A., Hillen, B., 2003. Anatomy and functionality of leptomeningeal anastomoses: a review. Stroke 34, 2750-2762.

Burke, J.F., Stulc, J.L., Skolarus, L.E., Sears, E.D., Zahuranec, D.B., Morgenstern, L.B., 2013. Traumatic brain injury may be an independent risk factor for stroke. Neurology 81, 33-39.

Busby, D.E., Burton, A.C., 1965. The effect of age on the elasticity of the major brain arteries. Canadian Journal of Physiology and Pharmacology 43, 185-202.

Busse, R., Edwards, G., Feletou, M., Fleming, I., Vanhoutte, P.M., Weston, A.H., 2002. EDHF: bringing the concepts together. Trends in Pharmacological Sciences 23, 374-380.

Cambj-Sapunar, L., Yu, M., Harder, D.R., Roman, R.J., 2003. Contribution of 5-hydroxytryptamine1β receptors and 20-hydroxyeiscosatetraenoic acid to fall in cerebral blood flow after subarachnoid hemorrhage. Stroke 34, 1269-1275.

Cantu, R.C., Gean, A.D., 2010. Second-impact syndrome and a small subdural hematoma: an uncommon catastrophic result of repetitive head injury with a characteristic imaging appearance. Journal of Neurotrauma 27, 1557-1564.

Carew, T.E., Vaishnav, R.N., Patel, D.J., 1968. Compressibility of the arterial wall. Circulation Research 23, 61-68.

Cassot, F., Lauwers, F., Fouard, C., Prohaska, S., Lauwers-Cances, V., 2006. A novel three-dimensional computer-assisted method for a quantitative study of microvascular networks of the human cerebral cortex. Microcirculation 13, 1-18.

Cassot, F., Lauwers, F., Lorthois, S., Puwanarajah, P., Cances-Lauwers, V., Duvernoy, H., 2010. Branching patterns for arterioles and venules of the human cerebral cortex. Brain Research 1313, 62-78.

CDC, 2013. CDC grand rounds: reducing severe traumatic brain injury in the United States. MMWR: Morbidity and Mortality Weekly Report 62, 549-552.

Chalupnik, J.D., Daly, C.H., Merchant, H.C., 1971. Material Properties of Cerebral Blood Vessels. Deptartment of Mechanical Engineering, University of Washington, Seattle, WA.

Chen, Y.H., Kang, J.H., Lin, H.C., 2011. Patients with traumatic brain injury: population-based study suggests increased risk of stroke. Stroke 42, 2733-2739.

Cherian, L., Robertson, C.S., Goodman, J.C., 1996. Secondary insults increase injury after controlled cortical impact in rats. Journal of Neurotrauma 13, 371-383.

Chesnut, R.M., Marshall, S.B., Piek, J., Blunt, B.A., Klauber, M.R., Marshall, L.F., 1993. Early and late systemic hypotension as a frequent and fundamental source of cerebral ischemia following severe brain injury in the Traumatic Coma Data Bank. Acta Neurochirurgica Supplementum 59, 121-125.

Chow, M.J., Turcotte, R., Lin, C.P., Zhang, Y., 2014. Arterial extracellular matrix: a mechanobiological study of the contributions and interactions of elastin and collagen. Biophysical Journal 106, 2684-2692.

Christ, A.F., Franze, K., Gautier, H., Moshayedi, P., Fawcett, J., Franklin, R.J., Karadottir, R.T., Guck, J., 2010. Mechanical difference between white and gray matter in the rat cerebellum measured by scanning force microscopy. Journal of Biomechanics 43, 2986-2992.

Chuong, C.J., Fung, Y.C., 1986. On residual stresses in arteries. Journal of Biomechanical Engineering 108, 189-192.

Cipolla, M.J., Osol, G., 1998. Vascular smooth muscle actin cytoskeleton in cerebral artery forced dilatation. Stroke 29, 1223-1228.

Clarke, J.G., Benjamin, N., Larkin, S.W., Webb, D.J., Davies, G.J., Maseri, A., 1989. Endothelin is a potent long-lasting vasoconstrictor in men. American Journal of Physiology 257, H2033-2035.

Compton, J.S., Teddy, P.J., 1987. Cerebral arterial vasospasm following severe head injury: a transcranial doppler study. British Journal of Neurosurgery 1, 435-439.

Coney, A.M., Marshall, J.M., 1998. Role of adenosine and its receptors in the vasodilatation induced in the cerebral cortex of the rat by systemic hypoxia. The Journal of Physiology 509, 507-518.

Converse, M., Monson, K.L., 2014. Alteration and failure of cerebral artery internal elastic lamina following mechanical insult, 7th World Congress of Biomechanics, Boston, MA.

Coronado, V.G., Xu, L., Basavaraju, S.V., McGuire, L.C., Wald, M.M., Faul, M.D., Guzman, B.R., Hemphill, J.D., 2011. Surveillance for traumatic brain injury-related deaths--United States, 1997-2007. MMWR: Morbidity and Mortality Weekly Report Surveillance Summaries 60, 1-32.

Coulson, R.J., Chesler, N.C., Vitullo, L., Cipolla, M.J., 2002. Effects of ischemia and myogenic activity on active and passive mechanical properties of rat cerebral arteries. American Journal of Physiology: Heart and Circulation Physiology 283, H2268-2275.

Coulson, R.J., Cipolla, M.J., Vitullo, L., Chesler, N.C., 2004. Mechanical properties of rat middle cerebral arteries with and without myogenic tone. Journal of Biomechanical Engineering 126, 76-81.

Crooks, D.A., 1991. Pathogenesis and biomechanics of traumatic intracranial haemorrhages. Virchows Archiv A, Pathological Anatomy and Histopathology 418, 479-483.

Czosnyka, M., Smielewski, P., Kirkpatrick, P., Menon, D.K., Pickard, J.D., 1996. Monitoring of cerebral autoregulation in head-injured patients. Stroke 27, 1829-1834.

Davis, A.E., 2000. Mechanisms of traumatic brain injury: biomechanical, structural and cellular considerations. Critical Care Nursing Quarterly 23, 1-13.

Delfino, A., Stergiopulos, N., Moore, J.E., Jr., Meister, J.J., 1997. Residual strain effects on the stress field in a thick wall finite element model of the human carotid bifurcation. Journal of Biomechanics 30, 777-786.

DeWitt, D.S., Mathew, B.P., Chaisson, J.M., Prough, D.S., 2001. Peroxynitrite reduces vasodilatory responses to reduced intravascular pressure, calcitonin gene-related peptide, and cromakalim in isolated middle cerebral arteries. Journal of Cerebral Blood Flow and Metabolism 21, 253-261.

DeWitt, D.S., Prough, D.S., 2003. Traumatic cerebral vascular injury: the effects of concussive brain injury on the cerebral vasculature. Journal of Neurotrauma 20, 795-825.

Duvernoy, H.M., Delon, S., Vannson, J.L., 1981. Cortical blood vessels of the human brain. Brain Research Bulletin 7, 519-579.

Edvinsson, L., MacKenzie, E.T., McCulloch, J., 1993. Cerebral Blood Flow and Metabolism. Raven Press, New York.

Edvinsson, L., Povlsen, G.K., 2011. Late cerebral ischaemia after subarachnoid haemorrhage: is cerebrovascular receptor upregulation the mechanism behind? Acta Physiologica (Oxford, England) 203, 209-224.

Ellison, M.D., Erb, D.E., Kontos, H.A., Povlishock, J.T., 1989. Recovery of impaired endothelium-dependent relaxation after fluid-percussion brain injury in cats. Stroke 20, 911-917.

Enevoldsen, E.M., Jensen, F.T., 1977. "False" autoregulation of cerebral blood flow in patients with acute severe head injury. Acta Neurologica Scandinavica. Supplementum 64, 514-515.

Fabian, R.H., DeWitt, D.S., Kent, T.A., 1995. In vivo detection of superoxide anion production by the brain using a cytochrome c electrode. Journal of Cerebral Blood Flow and Metabolism 15, 242-247.

Fahlstedt, M., Depreitere, B., Halldin, P., Vander Sloten, J., Kleiven, S., 2015. Correlation between injury pattern and finite element analysis in biomechanical reconstructions of traumatic brain injuries. Journal of Biomechanics 48, 1331-1335.

Faraci, F.M., Brian, J.E., Jr., 1994. Nitric oxide and the cerebral circulation. Stroke 25, 692-703.

Faraci, F.M., Heistad, D.D., 1990. Regulation of large cerebral arteries and cerebral microvascular pressure. Circulation Research 66, 8-17.

Finkelstein, E.A., Corso, P.S., Miller, T.R., 2006. The Incidence and Economic Burden of Injuries in the United States. Oxford University Press, New York.

Foley, P.L., Caner, H.H., Kassell, N.F., Lee, K.S., 1994. Reversal of subarachnoid hemorrhage-induced vasoconstriction with an endothelin receptor antagonist. Neurosurgery 34, 108-112; discussion 112-103.

Fuchs, R.F., 1900. Zur physiologie und wachstumsmechanik des blutgefass-systems. Archiv für Anatomie Physiologie, 102-154.

Fung, Y.C., 1993. Biomechanics: Mechanical Properties of Living Tissues, 2nd ed. Springer-Verlag, New York.

Fung, Y.C., Fronek, K., Patitucci, P., 1979. Pseudoelasticity of arteries and the choice of its mathematical expression. American Journal of Physiology 237, H620-631.

Garcia, J.R., Lamm, S.D., Han, H.C., 2013. Twist buckling behavior of arteries. Biomechanics and Modeling in Mechanobiology 12, 915-927.

Gennarelli, T., Thibault, L.E., Tomei, G., Wiser, R., Graham, D., Adams, J., 1987. Directional dependence of axonal brain injury due to centroidal and non-centroidal acceleration. SAE Technical Paper 872197.

Golding, E.M., 2002. Sequelae following traumatic brain injury. The cerebrovascular perspective. Brain Research Review 38, 377-388.

Golding, E.M., Contant, C.F., Jr., Robertson, C.S., Bryan, R.M., Jr., 1998a. Temporal effect of severe controlled cortical impact injury in the rat on the myogenic response of the middle cerebral artery. Journal of Neurotrauma 15, 973-984.

Golding, E.M., Robertson, C.S., Bryan, R.M., Jr., 1998b. Comparison of the myogenic response in rat cerebral arteries of different calibers. Brain Research 785, 293-298.

Golding, E.M., Robertson, C.S., Bryan, R.M., Jr., 1999a. The consequences of traumatic brain injury on cerebral blood flow and autoregulation: a review. Clinical and Experimental Hypertension 21, 299-332.

Golding, E.M., Steenberg, M.L., Contant, C.F., Jr., Krishnappa, I., Robertson, C.S., Bryan, R.M., Jr., 1999b. Cerebrovascular reactivity to $CO_2$ and hypotension after mild cortical impact injury. American Journal of Physiology 277, H1457-1466.

Golding, E.M., Steenberg, M.L., Johnson, T.D., Bryan, R.M., Jr., 2000. The effects of potassium on the rat middle cerebral artery. Brain Research 880, 159-166.

Goldsmith, W., 2001. The state of head injury biomechanics: past, present, and future: part 1. Critical Reviews in Biomedical Engingeering 29, 441-600.

Goldsmith, W., Monson, K.L., 2005. The state of head injury biomechanics: past, present, and future part 2: physical experimentation. Critical Reviews in Biomedical Engingeering 33, 105-207.

Griffith, T.M., 2004. Endothelium-dependent smooth muscle hyperpolarization: do gap junctions provide a unifying hypothesis? British Journal of Pharmacology 141, 881-903.

Hajdu, M.A., Baumbach, G.L., 1994. Mechanics of large and small cerebral arteries in chronic hypertension. American Journal of Physiology 266, H1027-1033.

Hamel, E., 2006. Perivascular nerves and the regulation of cerebrovascular tone. Journal of Applied Physiology 100, 1059-1064.

Hamel, E., Edvinsson, L., MacKenzie, E.T., 1988. Heterogeneous vasomotor responses of anatomically distinct feline cerebral arteries. British Journal of Pharmacology 94, 423-436.

Han, H., Tao, W., Zhang, M., 2007. The dural entrance of cerebral bridging veins into the superior sagittal sinus: an anatomical comparison between cadavers and digital subtraction angiography. Neuroradiology 49, 169-175.

Handa, Y., Caner, H., Hayashi, M., Tamamaki, N., Nojyo, Y., 1990. The distribution pattern of the sympathetic nerve fibers to the cerebral arterial system in rat as revealed by anterograde labeling with WGA-HRP. Experimental Brain Research 82, 493-498.

Harper, S.L., Bohlen, H.G., Rubin, M.J., 1984. Arterial and microvascular contributions to cerebral cortical autoregulation in rats. American Journal of Physiology 246, H17-24.

Hassler, O., Larsson, S.E., 1962. The external elastic layer of the cerebral arteries in different age-groups. Acta Anatomica 48, 1-6.

Hayashi, K., Nagasawa, S., Naruo, Y., Okumura, A., Moritake, K., Handa, H., 1980. Mechanical properties of human cerebral arteries. Biorheology 17, 211-218.

Hayes, R.L., Jenkings, L.W., Lyeth, B.G., 1991. Neuropharmacological mechanisms of traumatic brain injury: acetylcholine and excitatory amino acids. Journal of Neurotrauma 8, S173-S187.

Highton, D., Ghosh, A., Tachtsidis, I., Panovska-Griffiths, J., Elwell, C.E., Smith, M., 2015. Monitoring cerebral autoregulation after brain injury: multimodal assessment of cerebral slow-wave oscillations using near-infrared spectroscopy. Anesthesia and Analgesia 121, 198-205.

Hills, N.K., Johnston, S.C., Sidney, S., Zielinski, B.A., Fullerton, H.J., 2012. Recent trauma and acute infection as risk factors for childhood arterial ischemic stroke. Annals of Neurology 72, 850-858.

Hirata, Y., Yoshimi, H., Takata, S., Watanabe, T.X., Kumagai, S., Nakajima, K., Sakakibara, S., 1988. Cellular mechanism of action by a novel vasoconstrictor endothelin in cultured rat vascular smooth muscle cells. Biochemical and Biophysical Research Communications 154, 868-875.

Ho, J., Kleiven, S., 2007. Dynamic response of the brain with vasculature: a three-dimensional computational study. Journal of Biomechanics 40, 3006-3012.

Hogestatt, E.D., Andersson, K.E., 1984a. Mechanisms behind the biphasic contractile response to potassium depolarization in isolated rat cerebral arteries. Journal of Pharmacology and Experimental Therapeutics 228, 187-195.

Hogestatt, E.D., Andersson, K.E., 1984b. On the postjunctional alpha-adrenoreceptors in rat cerebral and mesenteric arteries. Journal of Autonomic Pharmacology 4, 161-173.

Hogestatt, E.D., Andersson, K.E., Edvinsson, L., 1983. Mechanical properties of rat cerebral arteries as studied by a sensitive device for recording of mechanical activity in isolated small blood vessels. Acta Physiologica Scandinavica 117, 49-61.

Holzapfel, G., Gasser, T., Ogden, R., 2000. A new constitutive framework for arterial wall mechanics and a comparative study of material models. Journal of Elasticity 61, 1-48.

Holzapfel, G.A., Gasser, T.C., 2007. Computational stress-deformation analysis of arterial walls including high-pressure response. International Journal of Cardiology 116, 78-85.

Holzapfel, G.A., Sommer, G., Auer, M., Regitnig, P., Ogden, R.W., 2007. Layer-specific 3D residual deformations of human aortas with non-atherosclerotic intimal thickening. Annals of Biomedical Engineering 35, 530-545.

Horný, L., Gultova, E., Chlup, H., Sedláček, R., Kronek, J., Veselý, J., Žitný, R., 2010. Mullins effect in an aorta and limiting extensibility evolution. Czech Technical University in Prague, Prague.

Hossmann, K.A., 1994. Viability thresholds and the penumbra of focal ischemia. Annals of Neurology 36, 557-565.

Humphrey, J.D., 1995. Mechanics of the arterial wall: review and directions. Critical Reviews in Biomedical Engineering 23, 1-162.

Humphrey, J.D., 2002. Cardiovascular Solid Mechanics : Cells, Tissues, and Organs. Springer, New York.

Humphrey, J.D., Eberth, J.F., Dye, W.W., Gleason, R.L., 2009. Fundamental role of axial stress in compensatory adaptations by arteries. Journal of Biomechanics 42, 1-8.

Jaggar, J.H., Porter, V.A., Lederer, W.J., Nelson, M.T., 2000. Calcium sparks in smooth muscle. American Journal of Physiology, Cell Physiology 278, C235-256.

Ji, S., Ghadyani, H., Bolander, R.P., Beckwith, J.G., Ford, J.C., McAllister, T.W., Flashman, L.A., Paulsen, K.D., Ernstrom, K., Jain, S., Raman, R., Zhang, L., Greenwald, R.M., 2014. Parametric comparisons of intracranial mechanical responses from three validated finite element models of the human head. Annals of Biomedical Engineering 42, 11-24.

Johnson, T.D., Marrelli, S.P., Steenberg, M.L., Childres, W.F., Bryan, R.M., Jr., 1998. Inward rectifier potassium channels in the rat middle cerebral artery. American Journal of Physiology 274, R541-547.

Katayama, Y., Becker, D.P., Tamura, T., Hovda, D.A., 1990. Massive increases in extracellular potassium and the indiscriminate release of glutamate following concussive brain injury. Journal of Neurosurgery 73, 889-900.

Kenney, K., Amyot, F., Haber, M., Pronger, A., Bogoslovsky, T., Moore, C., Diaz-Arrastia, R., 2016. Cerebral vascular injury in traumatic brain injury. Experimental Neurology 275 Pt 3, 353-366.

Keyes, J.T., Lockwood, D.R., Utzinger, U., Montilla, L.G., Witte, R.S., Vande Geest, J.P., 2013. Comparisons of planar and tubular biaxial tensile testing protocols of the same porcine coronary arteries. Annals of Biomedical Engineering 41, 1579-1591.

King, A.I., Yang, K.H., L., Z., Hardy, W., Viano, D.C., 2003 Is head injury caused by linear or angular acceleration? In 2003 International Conference on the Biomechanics of Impacts. Lisbon, Portugal.

Kleiven, S., 2007. Predictors for traumatic brain injuries evaluated through accident reconstructions. Stapp Car Crash Journal 51, 81-114.

Knot, H.J., Nelson, M.T., 1998. Regulation of arterial diameter and wall [Ca2+] in cerebral arteries of rat by membrane potential and intravascular pressure. The Journal of Physiology 508 ( Pt 1), 199-209.

Kontos, H.A., 1981. Regulation of the cerebral circulation. Annual Review of Physiology 43, 397-407.

Kontos, H.A., Raper, A.J., Patterson, J.L., 1977. Analysis of vasoactivity of local pH, $PCO_2$ and bicarbonate on pial vessels. Stroke 8, 358-360.

Kontos, H.A., Wei, E.P., 1986. Superoxide production in experimental brain injury. Journal of Neurosurgery 64, 803-807.

Kontos, H.A., Wei, E.P., 1992. Endothelium-dependent responses after experimental brain injury. Journal of Neurotrauma 9, 349-354.

Kontos, H.A., Wei, E.P., Raper, A.J., Rosenblum, W.I., Navari, R.M., Patterson, J.L., Jr., 1978. Role of tissue hypoxia in local regulation of cerebral microcirculation. American Journal of Physiology 234, H582-591.

Kramer, A., Fletcher, J., 2009. Do endothelin-receptor antagonists prevent delayed neurological deficits and poor outcomes after aneurysmal subarachnoid hemorrhage?: a meta-analysis. Stroke 40, 3403-3406.

Kramer, D.R., Winer, J.L., Pease, B.A., Amar, A.P., Mack, W.J., 2013. Cerebral vasospasm in traumatic brain injury. Neurology Research International 2013, 415813.

Kreipke, C.W., Rafols, J.A., Betrus, C., Graves, J., Kane, M.J., Perez, M.A., Briggs, D.I., Viano, D.C., Kuhn, D.M., Haacke, E.M., Raza, W., Wu, B., Kou, Z., Kropinski, A., Dore-Duffy, P., Armstead, W.M., Vavilala, M.S., Tiesma, D., Kaufman, M., Schafer, S., Kuhn, D.M., 2013. Cerebral Blood Flow, Metabolism, and Head Trauma: The Pathotrajectory of Traumatic Brain Injury. Springer, New York.

Kropinski, A., Dore-Duffy, P., Kreipke, C.W., 2013. Situating the Endothelin System in the Pathotrajectory of TBI-Induced Changes in Hemodynamics, in: Kreipke, C.W., Rafols, J.A. (Eds.), Cerebral Blood Flow, Metabolism, and Head Trauma: The Pathotrajectory of Traumatic Brain Injury. Springer, New York, pp. 95-133.

Kulik, T., Kusano, Y., Aronhime, S., Sandler, A.L., Winn, H.R., 2008. Regulation of cerebral vasculature in normal and ischemic brain. Neuropharmacology 55, 281-288.

Kuwaki, T., Kurihara, H., Cao, W.H., Kurihara, Y., Unekawa, M., Yazaki, Y., Kumada, M., 1997. Physiological role of brain endothelin in the central autonomic control: from neuron to knockout mouse. Progress in Neurobiology 51, 545-579.

Lagaud, G., Gaudreault, N., Moore, E.D., Van Breemen, C., Laher, I., 2002. Pressure-dependent myogenic constriction of cerebral arteries occurs independently of voltage-dependent activation. American Journal of Physiology: Heart and Circulatory Physiology 283, H2187-2195.

Laskowski, R.A., Creed, J.A., Raghupathi, R., 2015. Pathophysiology of Mild TBI: Implications for Altered Signaling Pathways, in: Kobeissy, F.H.P. (Ed.), Brain Neurotrauma: Molecular, Neuropsychological, and Rehabilitation Aspects, Boca Raton (FL).

Lassen, N.A., 1974. Control of cerebral circulation in health and disease. Circulation Research 34, 749-760.

Lee, M.C., Haut, R.C., 1989. Insensitivity of tensile failure properties of human bridging veins to strain rate: implications in biomechanics of subdural hematoma. Journal of Biomechanics 22, 537-542.

Lee, M.C., Haut, R.C., 1992. Strain rate effects on tensile failure properties of the common carotid artery and jugular veins of ferrets. Journal of Biomechanics 25, 925-927.

Lee, R.M., 1995. Morphology of cerebral arteries. Pharmacology and Therapeutics 66, 149-173.

Lee, T.J.F., 2002. Adrenergic and cholinergic modulation of cerebrovascular nitrergic vasodilation. International Congress Series 1235, 337-345.

Lincoln, J., 1995. Innervation of cerebral arteries by nerves containing 5-hydroxytryptamine and noradrenaline. Pharmacology and Therapeutics 68, 473-501.

Liu, S.Q., Fung, Y.C., 1988. Zero-stress states of arteries. Journal of Biomechanical Engineering 110, 82-84.

Lyeth, B.G., Hayes, R.L., 1992. Cholinergic and opioid mediation of traumatic brain injury. Journal of Neurotrauma 9 (Supplement 2), S463-474.

Maas, A.I., Stocchetti, N., Bullock, R., 2008. Moderate and severe traumatic brain injury in adults. Lancet Neurology 7, 728-741.

MacCumber, M.W., Ross, C.A., Snyder, S.H., 1990. Endothelin in brain: receptors, mitogenesis, and biosynthesis in glial cells. Proceedings of the National Academy of Science of the United States of America 87, 2359-2363.

Maher, E., Creane, A., Lally, C., Kelly, D.J., 2012. An anisotropic inelastic constitutive model to describe stress softening and permanent deformation in arterial tissue. Journal of the Mechanical Behavior of Biomedical Materials 12, 9-19.

Marmarou, A., 2007. A review of progress in understanding the pathophysiology and treatment of brain edema. Neurosurgical Focus 22, E1.

Martin, N.A., Doberstein, C., Zane, C., Caron, M.J., Thomas, K., Becker, D.P., 1992. Posttraumatic cerebral arterial spasm: transcranial Doppler ultrasound, cerebral blood flow, and angiographic findings. Journal of Neurosurgery 77, 575-583.

Martin, N.A., Patwardhan, R.V., Alexander, M.J., Africk, C.Z., Lee, J.H., Shalmon, E., Hovda, D.A., Becker, D.P., 1997. Characterization of cerebral hemodynamic phases following severe head trauma: hypoperfusion, hyperemia, and vasospasm. Journal of Neurosurgery 87, 9-19.

Masamoto, K., Tanishita, K., 2009. Oxygen transport in brain tissue. Journal of Biomechanical Engineering 131, 074002.

Mascia, L., Fedorko, L., Stewart, D.J., Mohamed, F., terBrugge, K., Ranieri, V.M., Wallace, M.C., 2001. Temporal relationship between endothelin-1 concentrations and cerebral vasospasm in patients with aneurysmal subarachnoid hemorrhage. Stroke 32, 1185-1190.

Mashour, G.A., Boock, R.J., 1999. Effects of shear stress on nitric oxide levels of human cerebral endothelial cells cultured in an artificial capillary system. Brain Research 842, 233-238.

Mathew, B.P., DeWitt, D.S., Bryan, R.M., Jr., Bukoski, R.D., Prough, D.S., 1999. Traumatic brain injury reduces myogenic responses in pressurized rodent middle cerebral arteries. Journal of Neurotrauma 16, 1177-1186.

Mayhan, W.G., 1994. Responses of cerebral arterioles to activation of beta-adrenergic receptors during diabetes mellitus. Stroke 25, 141-146.

McAllister, T.W., Ford, J.C., Ji, S., Beckwith, J.G., Flashman, L.A., Paulsen, K., Greenwald, R.M., 2012. Maximum principal strain and strain rate associated with concussion diagnosis correlates with changes in corpus callosum white matter indices. Annals of Biomedical Engineering 40, 127-140.

McCarron, J.G., Crichton, C.A., Langton, P.D., MacKenzie, A., Smith, G.L., 1997. Myogenic contraction by modulation of voltage-dependent calcium currents in isolated rat cerebral arteries. Journal of Physiology 498 ( Pt 2), 371-379.

Meaney, D.F., Morrison, B., Dale Bass, C., 2014. The mechanics of traumatic brain injury: a review of what we know and what we need to know for reducing its societal burden. Journal of Biomechanical Engineering 136, 021008.

Meder, J.F., Chiras, J., Roland, J., Guinet, P., Bracard, S., Bargy, F., 1994. Venous territories of the brain. Journal of Neuroradiology 21, 118-133.

Meininger, G.A., Davis, M.J., 1992. Cellular mechanisms involved in the vascular myogenic response. American Journal of Physiology 263, H647-659.

Melvin, J.W., Fuller, P.M., Daniel, R.P., Pavliscak, G.M., 1969. Human head and knee tolerance to localized impacts. SAE Technical Paper 690477.

Melvin, J.W., Lighthall, J.W., Ueno, H., 1993. Brian Injury Biomechanics, in: Nahum, A.M., Melvin, J.W. (Eds.), Accidental Injury: Biomechanics and Prevention. Springer-Verlag, New York, pp. 268-291.

Monson, K.L., Barbaro, N.M., Manley, G.T., 2008. Biaxial response of passive human cerebral arteries. Annals of Biomedical Engineering 36, 2028-2041.

Monson, K.L., Goldsmith, W., Barbaro, N.M., Manley, G.T., 2003. Axial mechanical properties of fresh human cerebral blood vessels. Journal of Biomechanical Engineering 125, 288-294.

Monson, K.L., Goldsmith, W., Barbaro, N.M., Manley, G.T., 2005. Significance of source and size in the mechanical response of human cerebral blood vessels. Journal of Biomechanics 38, 737-744.

Nahum, A.M., Smith, R.W., 1976. An experimental model for closed head impact injury. SAE Technical Paper 760825.

Nilsson, P., Hillered, L., Olsson, Y., Sheardown, M.J., Hansen, A.J., 1993. Regional changes in interstitial K+ and Ca2+ levels following cortical compression contusion trauma in rats. Journal of Cerebral Blood Flow and Metabolism 13, 183-192.

Nusholtz, G.S., Kaiker, P.S., Lehman, R.J., 1986. Critical limitations on significant factors in head injury research. SAE Technical Paper 861890.

Oka, K., Rhoton, A.L., Jr., Barry, M., Rodriguez, R., 1985. Microsurgical anatomy of the superficial veins of the cerebrum. Neurosurgery 17, 711-748.

Ommaya, A.K., 1995. Head injury mechanisms and the concept of preventive management: a review and critical synthesis. Journal of Neurotrauma 12, 527-546.

Omori, K., Zhang, L., Yang, K.H., King, A.I., 2000. Effect of cerebral vasculatures on the mechanical response of brain tissue: a preliminary study, in: Mahmood, H.F., Barbat, S.D., Baccouche, M.R. (Eds.), Crashworthiness, Occupant Protection, and Biomechanics in Transportation Systems, ASME Mechanical Engineering Congress and Exposition. ASME, Orlando, FL, pp. 167-174.

Osol, G., Brekke, J.F., McElroy-Yaggy, K., Gokina, N.I., 2002. Myogenic tone, reactivity, and forced dilatation: a three-phase model of in vitro arterial myogenic behavior. American Journal of Physiology: Heart and Circulatory Physiology 283, H2260-2267.

Osol, G., Laher, I., Cipolla, M., 1991. Protein kinase C modulates basal myogenic tone in resistance arteries from the cerebral circulation. Circulation Research 68, 359-367.

Panerai, R.B., 1998. Assessment of cerebral pressure autoregulation in humans--a review of measurement methods. Physiological Measurement 19, 305-338.

Parnaik, Y., Beillas, P., Demetropoulos, C.K., Hardy, W.N., Yang, K.H., King, A.I., 2004. The influence of surrogate blood vessels on the impact response of a physical model of the brain. Stapp Car Crash Journal 48, 259-277.

Paulson, O.B., Strandgaard, S., Edvinsson, L., 1990. Cerebral autoregulation. Cerebrovascular and Brain Metabolism Reviews 2, 161-192.

Pearce, W.J., 1995. Mechanisms of hypoxic cerebral vasodilatation. Pharmacology and Therapeutics 65, 75-91.

Peña, E., Alastrue, V., Laborda, A., Martinez, M.A., Doblare, M., 2010. A constitutive formulation of vascular tissue mechanics including viscoelasticity and softening behaviour. Journal of Biomechanics 43, 984-989.

Petrov, T., 2009. Amelioration of hypoperfusion after traumatic brain injury by in vivo endothelin-1 knockout. Canadian Journal of Physiology and Pharmacology 87, 379-386.

Petrov, T., Steiner, J., Braun, B., Rafols, J.A., 2002. Sources of endothelin-1 in hippocampus and cortex following traumatic brain injury. Neuroscience 115, 275-283.

Phillips, S.J., Whisnant, J.P., 1992. Hypertension and the brain. The National High Blood Pressure Education Program. Archives of Internal Medicine 152, 938-945.

Post, A., Hoshizaki, T.B., Gilchrist, M.D., Brien, S., Cusimano, M., Marshall, S., 2015. Traumatic brain injuries: the influence of the direction of impact. Neurosurgery 76, 81-91.

Rangel-Castilla, L., Gasco, J., Nauta, H.J., Okonkwo, D.O., Robertson, C.S., 2008. Cerebral pressure autoregulation in traumatic brain injury. Neurosurgery Focus 25, E7.

Reina-De La Torre, F., Rodriguez-Baeza, A., Sahuquillo-Barris, J., 1998. Morphological characteristics and distribution pattern of the arterial vessels in human cerebral cortex: a scanning electron microscope study. Anatomical Record 251, 87-96.

Robertson, C.S., Contant, C.F., Gokaslan, Z.L., Narayan, R.K., Grossman, R.G., 1992. Cerebral blood flow, arteriovenous oxygen difference, and outcome in head injured patients. Journal of Neurology, Neurosurgery, and Psychiatry 55, 594-603.

Rosendorff, C., Mitchell, G., Scriven, D.R., Shapiro, C., 1976. Evidence for a dual innervation affecting local blood flow in the hypothalamus of the conscious rabbit. Circulation Research 38, 140-145.

Roux, S., Breu, V., Ertel, S.I., Clozel, M., 1999. Endothelin antagonism with bosentan: a review of potential applications. Journal of Molecular Medicine (Berlin) 77, 364-376.

Salom, J.B., Torregrosa, G., Alborch, E., 1995. Endothelins and the cerebral circulation. Cerebrovascular and Brain Metabolism Reviews 7, 131-152.

Salonia, R., Empey, P.E., Poloyac, S.M., Wisniewski, S.R., Klamerus, M., Ozawa, H., Wagner, A.K., Ruppel, R., Bell, M.J., Feldman, K., Adelson, P.D., Clark, R.S., Kochanek, P.M., 2010. Endothelin-1 is increased in cerebrospinal fluid and

associated with unfavorable outcomes in children after severe traumatic brain injury. Journal of Neurotrauma 27, 1819-1825.

Sandor, P., 1999. Nervous control of the cerebrovascular system: doubts and facts. Neurochemistry International 35, 237-259.

Saunders, M.L., Miller, J.D., Stablein, D., Allen, G., 1979. The effects of graded experimental trauma on cerebral blood flow and responsiveness to $CO_2$. Journal of Neurosurgery 51, 18-26.

Schrauwen, J.T., Vilanova, A., Rezakhaniha, R., Stergiopulos, N., van de Vosse, F.N., Bovendeerd, P.H., 2012. A method for the quantification of the pressure dependent 3D collagen configuration in the arterial adventitia. Journal of Structural Biololgy 180, 335-342.

Schubert, G.A., Seiz, M., Hegewald, A.A., Manville, J., Thome, C., 2011. Hypoperfusion in the acute phase of subarachnoid hemorrhage. Acta Neurochirurgica Supplement 110, 35-38.

Schubert, R., Kalentchuk, V.U., Krien, U., 2002. Rho kinase inhibition partly weakens myogenic reactivity in rat small arteries by changing calcium sensitivity. American Journal of Physiology: Heart and Circulatory Physiology 283, H2288-2295.

Siedler, D.G., Chuah, M.I., Kirkcaldie, M.T., Vickers, J.C., King, A.E., 2014. Diffuse axonal injury in brain trauma: insights from alterations in neurofilaments. Frontiers in cellular neuroscience 8, 429.

Somlyo, A.P., Wu, X., Walker, L.A., Somlyo, A.V., 1999. Pharmacomechanical coupling: the role of calcium, G-proteins, kinases and phosphatases. Reviews of physiology, biochemistry and pharmacology 134, 201-234.

Stalnaker, R.L., Melvin, J.W., Nusholtz, G.S., Alem, N.M., Benson, J.B., 1977. Head impact response. SAE Technical Paper 770921.

Stalnaker, R.L., Roberts, V.L., McElhaney, J.H., 1973. Side impact tolerance to blunt trauma. SAE Technical Paper 730979.

Stehbens, W.E., 1972. Pathology of the Cerebral Blood Vessels. C. V. Mosby.

Steiger, H.J., Aaslid, R., Keller, S., Reulen, H.J., 1989. Strength, elasticity and viscoelastic properties of cerebral aneurysms. Heart and Vessels 5, 41-46.

Stephens, R.B., Stilwell, D.L., 1969. Arteries and Veins of the Human Brain. Thomas, Springfield, Ill.

Steucke, K.E., Tracy, P.V., Hald, E.S., Hall, J.L., Alford, P.W., 2015. Vascular smooth muscle cell functional contractility depends on extracellular mechanical properties. Journal of Biomechanics 48, 3044-3051.

Strandgaard, S., Sigurdsson, S.T., 2008. Point:Counterpoint: Sympathetic activity does/does not influence cerebral blood flow. Counterpoint: Sympathetic nerve activity does not influence cerebral blood flow. Journal of Applied Physiology 105, 1366-1367; discussion 1367-1368.

Szabo, C., 1996. Physiological and pathophysiological roles of nitric oxide in the central nervous system. Brain Research Bulletin 41, 131-141.

Taguchi, H., Heistad, D.D., Kitazono, T., Faraci, F.M., 1994. ATP-sensitive K+ channels mediate dilatation of cerebral arterioles during hypoxia. Circulation Research 74, 1005-1008.

Takahashi, A., Ushiki, T., Abe, K., Houkin, K., Abe, H., 1994. Scanning electron microscopic studies of the medial smooth muscles in human major intracranial arteries. Archives of Histology and Cytology 57, 341-350.

Takahashi, H., Manaka, S., Sano, K., 1981. Changes in extracellular potassium concentration in cortex and brain stem during the acute phase of experimental closed head injury. Journal of Neurosurgery 55, 708-717.

Takamizawa, K., Hayashi, K., 1987. Strain energy density function and uniform strain hypothesis for arterial mechanics. Journal of Biomechanics 20, 7-17.

Tang, A., Pandit, V., Fennell, V., Jones, T., Joseph, B., O'Keeffe, T., Friese, R.S., Rhee, P., 2015. Intracranial pressure monitor in patients with traumatic brain injury. Journal of Surgical Research 194, 565-570.

Tasker, R.C., 2014. Intracranial pressure and cerebrovascular autoregulation in pediatric critical illness. Seminars in Pediatric Neurology 21, 255-262.

Thibault, L.E., Margulies, S.S., Gennarelli, T.A., 1987. The temporal and spacial deformation response of a brain model in inertial loading. SAE Technical Paper 872200.

Toklu, H.Z., Muller-Delp, J., Yang, Z., Oktay, S., Sakarya, Y., Strang, K., Ghosh, P., Delp, M.D., Scarpace, P.J., Wang, K.K., Tumer, N., 2015. The functional and structural changes in the basilar artery due to overpressure blast injury. Journal of Cerebral Blood Flow and Metabolism 35, 1950-6.

Touzani, O., Galbraith, S., Siegl, P., McCulloch, J., 1997. Endothelin-B receptors in cerebral resistance arterioles and their functional significance after focal cerebral ischemia in cats. Journal of Cerebral Blood Flow and Metabolism 17, 1157-1165.

Tse, K.M., Tan, L.B., Lee, S.J., Lim, S.P., Lee, H.P., 2015. Investigation of the relationship between facial injuries and traumatic brain injuries using a realistic subject-specific finite element head model. Accident; Analysis and Prevention 79, 13-32.

Tsubokawa, T., Katayama, Y., 1998. Cerebral vasomotor reactivity in head-injured patients. Critical Reviews in Neurosurgery 8, 112-121.

Tuor, U.I., 1992. Acute hypertension and sympathetic stimulation: local heterogeneous changes in cerebral blood flow. American Journal of Physiology 263, H511-518.

Ueda, Y., Walker, S.A., Povlishock, J.T., 2006. Perivascular nerve damage in the cerebral circulation following traumatic brain injury. Acta Neuropathologica 112, 85-94.

Unterberg, A.W., Stover, J., Kress, B., Kiening, K.L., 2004. Edema and brain trauma. Neuroscience 129, 1021-1029.

Ursino, M., 1994. Regulation of the circulation of the brain, in: Bevan, R.D., Bevan, J.A. (Eds.), The Human Brain Circulation: Functional Changes in Disease. Humana Press, Totowa, NJ, pp. 291-318.

Vaishnav, R.N., Vossoughi, J., 1987. Residual stress and strain in aortic segments. Journal of Biomechanics 20, 235-239.

Vaishnav, R.N., Young, J.T., Patel, D.J., 1973. Distribution of stresses and of strain-energy density through the wall thickness in a canine aortic segment. Circulation Research 32, 577-583.

van Lieshout, J.J., Secher, N.H., 2008. Point:Counterpoint: Sympathetic activity does/does not influence cerebral blood flow. Point: Sympathetic activity does influence cerebral blood flow. Journal of Applied Physiology (1985) 105, 1364-1366.

Van Loon, P., 1977. Length-force and volume-pressure relationships of arteries. Biorheology 14, 181-201.

Varsos, G.V., Budohoski, K.P., Kolias, A.G., Liu, X., Smielewski, P., Varsos, V.G., Hutchinson, P.J., Pickard, J.D., Czosnyka, M., 2014. Relationship of vascular wall tension and autoregulation following traumatic brain injury. Neurocritical Care 21, 266-274.

Villalba, N., Sonkusare, S.K., Longden, T.A., Tran, T.L., Sackheim, A.M., Nelson, M.T., Wellman, G.C., Freeman, K., 2014. Traumatic brain injury disrupts cerebrovascular tone through endothelial inducible nitric oxide synthase expression and nitric oxide gain of function. Journal of the American Heart Association 3, e001474.

Volker Seifert, Bernd-Michael Löffler, Michael Zimmermann, Sébastiên Roux, Dietmar Stolke, 1995. Endothelin concentrations in patients with aneurysmal subarachnoid hemorrhage. Journal of Neurosurgery 82, 55-62.

Vossoughi, J., Bandak, F.A., 1995. Mechanical characteristics of vascular tissue and their role in brain injury modeling: a review. J Neurotrauma 12, 755-763.

Wagner, H.P., Humphrey, J.D., 2011. Differential passive and active biaxial mechanical behaviors of muscular and elastic arteries: basilar versus common carotid. Journal of Biomechanical Engineering 133, 051009.

Wahl, M., 1985. Local chemical, neural, and humoral regulation of cerebrovascular resistance vessels. Journal of Cardiovascular Pharmacology 7 Suppl 3, S36-46.

Walther, R.G., 2015. Collagen Mimetic Peptide as a Marker of Mechanical Damage in Cerebral Arteries. University of Utah.

Wang, R., Gleason, R.L., Jr., 2010. A mechanical analysis of conduit arteries accounting for longitudinal residual strains. Annals of Biomedical Engineering 38, 1377-1387.

Wang, R., Gleason, R.L., Jr., 2014. Residual shear deformations in the coronary artery. Journal of Biomechanical Engineering 136, 061004.

Weisbecker, H., Viertler, C., Pierce, D.M., Holzapfel, G.A., 2013. The role of elastin and collagen in the softening behavior of the human thoracic aortic media. Journal of Biomechanics 46, 1859-1865.

Weizsacker, H.W., Lambert, H., Pascale, K., 1983. Analysis of the passive mechanical properties of rat carotid arteries. Journal of Biomechanics 16, 703-715.

Welsh, D.G., Morielli, A.D., Nelson, M.T., Brayden, J.E., 2002. Transient receptor potential channels regulate myogenic tone of resistance arteries. Circulation Research 90, 248-250.

Wicker, B.K., Hutchens, H.P., Wu, Q., Yeh, A.T., Humphrey, J.D., 2008. Normal basilar artery structure and biaxial mechanical behaviour. Computer Methods in Biomechanics and Biomedical Engineering 11, 539-551.

Wolff, H.G., 1936. The cerebral circulation. Physiological Reviews 16, 545-596.

Yamashima, T., Friede, R.L., 1984. Why do bridging veins rupture into the virtual subdural space? Journal of Neurology, Neurosurgery and Psychiatry 47, 121-127.

Yang, B., Tse, K.M., Chen, N., Tan, L.B., Zheng, Q.Q., Yang, H.M., Hu, M., Pan, G., Lee, H.P., 2014. Development of a finite element head model for the study of impact head injury. BioMed Research International 2014, 408278.

Zeinali-Davarani, S., Wang, Y., Chow, M.J., Turcotte, R., Zhang, Y., 2015. Contribution of collagen fiber undulation to regional biomechanical properties along porcine thoracic aorta. Journal of Biomechanical Engineering 137, 051001.

Zhang, L., Bae, J., Hardy, W.N., Monson, K.L., Manley, G.T., Goldsmith, W., Yang, K.H., King, A.I., 2002. Computational study of the contribution of the vasculature on the dynamic response of the brain. Stapp Car Crash Journal 46, 145-164.

Zhang, R., Behbehani, K., Levine, B.D., 2009. Dynamic pressure-flow relationship of the cerebral circulation during acute increase in arterial pressure. Journal of Physiology 587, 2567-2577.

Zhilyaev, S.Y., Moskvin, A.N., Platonova, T.F., Gutsaeva, D.R., Churilina, I.V., Demchenko, I.T., 2003. Hyperoxic vasoconstriction in the brain is mediated by inactivation of nitric oxide by superoxide anions. Neuroscience and Behavioral Physiology 33, 783-787.

Ziebell, J.M., Morganti-Kossmann, M.C., 2010. Involvement of pro- and anti-inflammatory cytokines and chemokines in the pathophysiology of traumatic brain injury. Neurotherapeutics : The Journal of the American Society for Experimental NeuroTherapeutics 7, 22-30.

# CHAPTER 2

# BIAXIAL AND FAILURE PROPERTIES OF PASSIVE RAT MIDDLE CEREBRAL ARTERIES

Reprinted from Journal of Biomechanics, 46, Bell, E. D., Kunjir, R. S., Monson, K. L., Biaxial and failure properties of passive rat middle cerebral arteries. Pages 91-96, © (2013), with permission from Elsevier.

Journal of Biomechanics 46 (2013) 91–96

Contents lists available at SciVerse ScienceDirect

Journal of Biomechanics

journal homepage: www.elsevier.com/locate/jbiomech
www.JBiomech.com

# Biaxial and failure properties of passive rat middle cerebral arteries

E. David Bell [a], Rahul S. Kunjir [b], Kenneth L. Monson [a,b,*]

[a] Department of Bioengineering, University of Utah, Salt Lake City, UT 84112, USA
[b] Department of Mechanical Engineering, University of Utah, 50 S. Central Campus Drive, MEB 2132, Salt Lake City, UT 84112, USA

ARTICLE INFO

*Article history:*
Accepted 10 October 2012

*Keywords:*
Traumatic brain injury
Rat cerebral arteries
Passive biaxial mechanical properties

ABSTRACT

Rodents are commonly used as test subjects in research on traumatic brain injury and stroke. However, study of rat cerebral vessel properties has largely been limited to pressure–diameter response within the physiological loading range. A more complete, multiaxial description is needed to guide experiments on rats and rat vessels and to appropriately translate findings to humans. Accordingly, we dissected twelve rat middle cerebral arteries (MCAs) and subjected them to combined inflation and axial stretch tests around physiological loading conditions while in a passive state. The MCAs were finally stretched axially to failure. Results showed that MCAs under physiological conditions were stiffer in the axial than circumferential direction by a mean ($\pm$standard deviation) factor of 1.72 ($\pm$0.73), similar to previously reported behavior of human cerebral arteries. However, the stiffness for both directions was lower in rat MCA than in human cerebral arteries ($p < 0.01$). Failure stretch values were higher in rat MCA (1.35 $\pm$ 0.08) than in human vessels (1.24 $\pm$ 0.09) ($p$=0.003), but corresponding 1st Piola Kirchhoff stress values for rats (0.42 $\pm$ 0.09 MPa) were considerably lower than those for humans (3.29 $\pm$ 0.64 MPa) ($p < 0.001$). These differences between human and rat vessel properties should be considered in rat models of human cerebrovascular injury and disease.



## 1. Introduction

Disruption of cerebral blood vessel function leads to stroke and is a common outcome of traumatic brain injury (TBI). In the United States, 52,000 deaths result from over 1.7 million cases of TBI annually (Faul et al., 2010); the number of deaths is over 140,000 per year for stroke (Lloyd-Jones et al., 2010). Total annual costs associated with TBI and stroke have been estimated at 60 (Faul et al., 2010) and 65.5 (Rosamond et al., 2008) billion dollars, respectively.

Efforts to better prevent and treat cerebrovascular injury and disease are, in part, dependent upon a more complete understanding of vessel mechanics. This includes definition of blood vessel injury thresholds as well as characterization of relationships between applied forces and vessel function. Experiments on human cerebral vessels have revealed some characteristics of these tissues (Busby and Burton, 1965; Hayashi et al., 1980; Monson et al., 2008; Scott et al., 1972), but the limited availability of human specimens is a barrier to additional research.

Rodents are commonly used as models for both TBI and stroke (Coulson et al., 2002, 2004; Gonzalez et al., 2005; Hajdu and Baumbach, 1994; Hogestatt et al., 1983). Rodent cerebral vessels have also been studied in isolation, but the mechanical properties of these vessels have not been fully characterized. Emphasis has mainly been on circumferential behavior within the physiological loading range (Coulson et al., 2002, 2004; Hajdu and Baumbach, 1994). A more complete definition of these properties is an important step toward addressing questions more specific to cerebral vessel injury and disease. Accordingly, the aim of this research was to define the biaxial and failure properties of passive rat middle cerebral arteries (MCAs) and to compare these characteristics to those of previously studied human cerebral vessels.

## 2. Methods

### 2.1. Vessel dissection and cannulation

The MCA was dissected from 12 male Sprague Dawley rats (389 $\pm$ 41 g). All procedures met requirements established by the Institutional Animal Use and Care Committee at the University of Utah. Rats were anesthetized with isoflurane and exsanguinated via cardiac perfusion using Hank's Buffered Saline Solution (HBSS; KCl 5.37, $KH_2PO_4$ 0.44, NaCl 136.9, $Na_2HPO_4$ 0.34, D-Glucose 5.55, $NaHCO_3$ 4.17; concentrations in mM), followed by a 1% nigrosin dye (Sigma-Aldrich, St. Louis, MO) HBSS solution. The dye enhanced visibility of the artery and its branches during dissection. MCA side branches were ligated with individual fibrils from unwound 6-0 silk suture, and the vessel was cannulated with glass tip needles and secured with 6-0 silk suture and cyanoacrylate glue. Lack of calcium in the HBSS ensured a passive response.

* Corresponding author at: University of Utah, Mechanical Engineering, 50 S. Central Campus Drive, MEB 2132, Salt Lake City, UT 84112, United States. Tel.: +1 801 585 5191; fax: +1 801 585 9826.
*E-mail address:* ken.monson@mech.utah.edu (K.L. Monson).

0021-9290/$ - see front matter © 2012 Elsevier Ltd. All rights reserved.
http://dx.doi.org/10.1016/j.jbiomech.2012.10.015

### 2.2. Experimental apparatus and methodology

Mechanical testing methodology was similar to that described previously (Monson et al., 2008). Briefly, the needles on which the MCA were mounted, and the associated fixtures, were attached to a custom vertical linear stage (Parker Automation, Cleveland, OH). The upper fixture was suspended from a 250 g capacity load cell (Model 31 Low, Honeywell, Golden Valley, MN) through an X–Y stage (MS-125-XY, Newport, Irvine, CA) that allowed for correction of any needle misalignment. The lower fixture was mounted to the stage via a vertical, low friction sled supported by a voice coil actuator (MGV52-25-1.0, Akribis, Singapore). Displacement of this actuator moved the lower fixture vertically along the sled track, axially stretching the MCA. A narrow, glass water bath, filled with HBSS and surrounding the MCA and needles, was attached to the lower fixture. Specimens were viewed via a digital video camera (PL-A641, Pixelink, Ottawa, Canada) equipped with a zoom lens (VZM 450i, Edmund Optics, Barrington, NJ). Vessels were perfused with HBSS originating from a syringe attached to a computer-controlled linear actuator (D-A0.25-AB-HT17075-4-P, Ultra Motion, Cutchogue, NY) and passing through the lower fixture, the mounted MCA, and the upper fixture. Pressure was determined by averaging the signals of pressure transducers (26PCDFM6G, Honeywell, Golden Valley, MN) located at each end of the vessel. Test control, as well as data and video acquisition, were accomplished using a custom LabVIEW program (National Instruments, Austin, TX). Actuator positions were given by digital encoders (resolution 1.0 μm).

Following mounting of the MCA, it was preconditioned by oscillating the luminal pressure (6.7–20 kPa; 50–150 mmHg) for five cycles while length was held constant at various sub-failure axial stretch values up to $\lambda_z \approx 1.2$. The zero-load length (corresponding with $\lambda_z = 1.0$) of each MCA was then estimated as that length where the measured axial load began to increase during an unpressurized (0.25 kPa to maintain an open lumen) axial stretch test. This was followed by a series of six sub-failure, quasi-static, biaxial sequences, consisting of three inflation tests at constant axial stretch ($\lambda_z \approx 1.1$, 1.15, 1.2) and three axial stretch tests at constant luminal pressure (20, 13.3, and 6.7 kPa). Finally, the vessel was stretched axially to failure, at a pressure of 13.3 kPa, to study deformations relevant to TBI.

### 2.3. Data analysis

Data from the encoders, load cell, and pressure transducers were recorded at 100 Hz. Noise observed in the load cell readings was smoothed using the SAE J211 filter (SAE, 1995). Images were acquired at 3 Hz, and current outer diameter ($d_e$) was measured via image analysis software (Vision Assistant; National Instruments, Austin, TX). Similarly, the reference diameter ($D_e$) was measured from an image taken from the zero load length test at $\lambda_z = 1.0$. Since images were obtained at a lower rate than the other signals, additional diameter data were defined using interpolation to allow one-to-one correspondence. Following the method defined by Wicker et al. (2008), wall volume was determined at six different configurations (each combination of $\lambda_z \approx 1.1$, 1.15, 1.2 and pressure $p_i = 0.25$,10.6 kPa) by measuring inner diameter ($d_i$), $d_e$, and vessel length ($l$) in the images and calculating the associated wall volume of a tube. The average wall volume ($V$), along with the incompressibility assumption, was used to calculate $d_i$ from the measured $d_e$ in subsequent analysis, including the reference inner diameter ($D_i$) from $D_e$ (Eq. (1)).

$$d_i = \sqrt{d_e^2 - 4V/(\pi l)} \tag{1}$$

Vessels were assumed to be homogeneous circular cylinders, with mid-wall stretch defined by Eqs. (2)

$$\lambda_\theta = \left(\frac{d_i + d_e}{D_i + D_e}\right) \tag{2a}$$

$$\lambda_z = \left(\frac{l}{L}\right) \tag{2b}$$

where the subscripts $\theta$ and $z$ refer to the local cylindrical coordinates in the circumferential and axial directions, respectively. Enforcing equilibrium in the two directions results in the mean Cauchy stresses defined in Eqs. (3)

$$T_\theta = p_i \left(\frac{d_i}{d_e - d_i}\right) \tag{3a}$$

$$T_z = \frac{\lambda_z}{A}\left(F_z + \frac{\pi}{4} p_i d_i^2\right) \tag{3b}$$

where $F_z$ represents the experimental axial force. Residual stresses were not considered due to large variations in measured opening angle.

As a first step in characterizing response in the axial and circumferential directions, stress–stretch data around approximate in vivo conditions were examined. Axial in vivo length was determined for each sample by observing the pressure-axial force response during preconditioning tests (Van Loon, 1977). Circumferential in vivo stiffness was defined as the slope of the stress–stretch curve in the inflation test with an axial stretch value closest to the axial in vivo stretch. An exponential function was fit through the data around the point corresponding to a pressure of 13.3 kPa (100 mmHg), and the value of the function's derivative at 13 kPa was taken as circumferential stiffness. Axial in vivo stiffness was defined in a similar manner from the axial stretch test conducted at a luminal pressure of 13.3 kPa, with the location where stiffness was calculated corresponding to the in vivo length. Note that stiffness is used here as a measure of the resistance of the vessel structure to deformation, rather than as an intrinsic tissue property.

A hyperelastic constitutive model, based on a phenomenological approach, was additionally applied to parameterize the biaxial response of the vessels based on the data from inflation tests. Data from axial stretch tests were not included since they resulted in slight unloading in the circumferential direction during axial stretch, inconsistent with requirements of pseudoelasticity (Humphrey et al., 1990). We applied the Fung-type strain energy function with the zero-load state as the reference configuration shown in Eq. (4) (Fung, 1993)

$$W = \frac{1}{2} c(e^Q - 1) \tag{4}$$

where $Q = c_1 E_{\theta\theta}^2 + c_2 E_{zz}^2 + 2c_3 E_{\theta\theta} E_{zz}$, $W$ represents the strain energy per unit mass of the material, $E_{\theta\theta}$ and $E_{zz}$ refer to the Green strains in the circumferential and axial directions, and $c$ (units kPa), $c_1$, $c_2$ and $c_3$ are material parameters. Shear strains were ignored owing to the axisymmetric loading conditions and observed response. Incompressibility was enforced directly (Humphrey, 2002). The associated mean Cauchy stress values are shown in Eq. (5)

$$t_{\theta\theta} = \lambda_\theta^2 \frac{\partial W}{\partial E_{\theta\theta}} = \lambda_\theta^2 c(c_1 E_{\theta\theta} + c_3 E_{zz}) e^Q \tag{5a}$$

$$t_{zz} = \lambda_z^2 \frac{\partial W}{\partial E_{zz}} = \lambda_z^2 c(c_2 E_{zz} + c_3 E_{\theta\theta}) e^Q \tag{5b}$$

where $t_{\theta\theta}$ and $t_{zz}$ correspond to the theoretical Cauchy stress values in the circumferential and axial directions, respectively. Radial stresses were assumed to be small based on findings from our previous work on human arteries (Monson et al., 2008). Mean values of $t_{\theta\theta}$ and $t_{zz}$ were calculated for comparison to experimentally derived stresses (Eqs. (3)). Material parameters $c$, $c_1$, $c_2$ and $c_3$ that best fit the experimental data were computed by employing a nonlinear regression routine (fminsearch) in MATLAB (Mathworks, Natick, MA) to minimize the objective function $f$ (Eq. (6))

$$f = \sum_{i=1}^{N} \left[ \left(\frac{t_{\theta\theta} - T_\theta}{T_\theta}\right)_i^2 + \left(\frac{t_{zz} - T_z}{T_z}\right)_i^2 \right] \tag{6}$$

where $N$ represents the total number of data points, and the stresses are defined in Eqs. (3) and (5). Previously collected data from human cerebral arteries were similarly fit for comparison.

Two-tailed, unpaired $t$-tests were used to determine the significance of any differences between determined values, with $p < 0.01$ indicating statistical significance.

## 3. Results

Twelve arteries were successfully tested. Mean (±standard deviation) unloaded outer diameter and length of these specimens were 0.25 (±0.02) and 2.11 (±0.51) mm, respectively. Typical response is shown in Figs. 1 and 2 and is qualitatively similar to what we have previously reported for biaxial behavior of human cerebral arteries.

Rat MCA in vivo stretch was 1.10 (±0.03) and 1.27 (±0.11) for the axial and circumferential directions, respectively. At these stretch levels, axial stiffness was 1.14 (±0.37) MPa and circumferential stiffness was 0.73 (±0.29) MPa ($p = 0.006$), resulting in a ratio of 1.72 (±0.73) between the two directions; the ratio ranged from 1.05 (M5, Fig. 4) to 3.30 (M6, Fig. 4). For clarity, the rat data used to determine the axial and circumferential in vivo stiffnesses are identified as $S_{13}$ and the inflation test having the lowest value of axial stretch, respectively, in Figs. 3 and 4. The inflation test having the lowest value of axial stretch was selected as it was consistently closest to the in vivo stretch. However, in most cases it was not exactly at the in vivo axial stretch since this value could only be precisely determined during post-processing.

The Fung-type constitutive model fit the rat MCA data well, as shown for a representative data set in Fig. 5. Further, best-fit material parameters showed that $c_2$ was consistently larger than $c_1$ ($p < 0.001$) (Table 1). These best fit parameters, along with the

in vivo stiffness measurements, indicate that the mechanical behavior in the axial direction was consistently stiffer than in the circumferential direction in the rat MCA. Requirements imposed by energy conservation for orthotropic symmetry ($c_1$, $c_2$, $c_3 > 0$ and $\sqrt{c_1 * c_2} > c_3$) were met by the determined material parameters (excepting M2 and M4) (Holzapfel et al., 2000); it is unclear why $c_3$was negative for M2 and M4.

The responses of rat MCA and human cerebral arteries were qualitatively similar. The ratio of in vivo stiffness values, with means ($\pm$ standard deviation) 1.72 ($\pm$0.73) for rat MCA and 1.87 ($\pm$0.84) from human pial arteries (Monson et al., 2008), were not statistically different ($p$=0.67), indicating that the difference between the stiffness in the axial and circumferential directions in the rat MCA (Fig. 3) is proportional to the difference in human pial arteries. However, the magnitude of the in vivo stiffness was lower for both directions in rat MCAs compared to human cerebral arteries, with axial stiffnesses of 1.1 ($\pm$0.4) and 2.9 ($\pm$1.4) MPa for rat and human arteries, respectively ($p$=0.005), and circumferential stiffnesses of 0.7 ($\pm$0.3) and 1.6 ($\pm$0.5) MPa for the two tissues ($p < 0.001$) (Fig. 3). This trend is also supported by best fit values for $c_1$ and $c_2$ reported in Table 1, but since the fit of the Fung-type model was poor for the human cerebral arteries, a statistical comparison of these fitted parameters between the vessel types was not considered to be meaningful. Additionally, the mean axial in vivo stretch for the rat MCAs, 1.10 ($\pm$0.03), was larger than that for human arteries, 1.07 ($\pm$0.04). This difference approached statistical significance ($p$=0.04) but was above our threshold of $p < 0.01$. The circumferential in vivo stretch was not statistically different between rat MCAs, 1.27 ($\pm$0.11), and human arteries, 1.33 ($\pm$0.17) ($p$=0.37).

Failure values for the twelve tested MCA samples, along with those from human cerebral arteries tested in our laboratory, are plotted in Fig. 6. For rat MCAs, the mean axial stretch at failure was 1.35 ($\pm$0.08) and the corresponding axial 1st Piola–Kirchhoff stress ($F_z/A$) was 0.42 ($\pm$0.09) MPa. These two values for human vessels were 1.24 ($\pm$0.09) and 3.29 ($\pm$0.64) MPa, respectively, indicating that the rat MCAs had a lower failure stress ($p < 0.001$) but a higher failure stretch ($p$=0.003) as compared to human cerebral arteries. Five rat vessels failed near a suture tie-off, while seven failed in mid-section. Failure values were not a function of failure location ($p > 0.50$) (Fig. 6). Stress values are reported in 1st Piola–Kirchhoff form because the incompressibility assumption commonly yielded a complex number for inner diameter in the current configuration, suggesting that large vessel deformations are not isochoric.

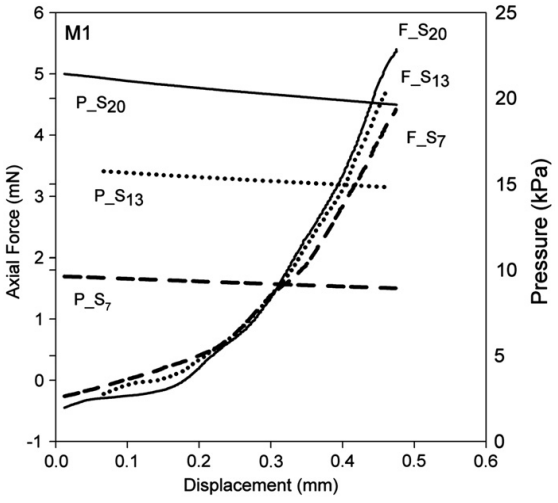


**Fig. 1.** Axial force ($F\_S_m$) and luminal pressure ($P\_S_m$) for a representative MCA sample (M1) during axial stretch tests. Label subscript $m$ indicates the approximate luminal pressure for these axial stretch tests.

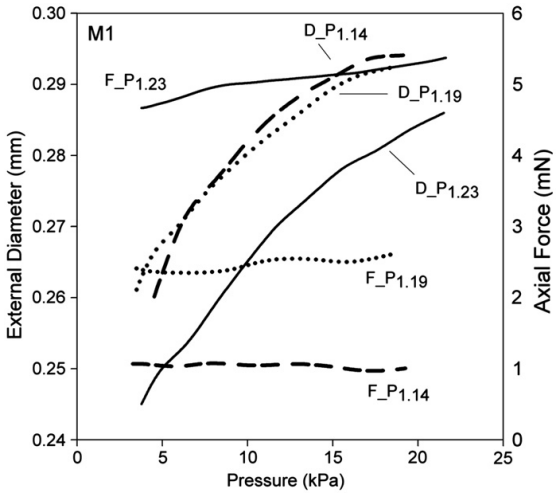


**Fig. 2.** Outer diameter ($D\_P_n$) and axial force ($F\_P_n$) responses for a representative MCA sample (M1) during inflation tests. Label subscript $n$ indicates the axial stretch for these inflation tests.

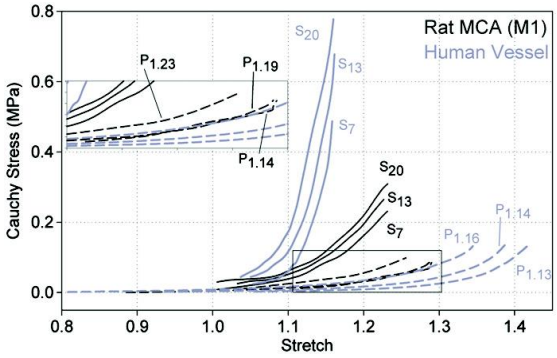


**Fig. 3.** Cauchy stress–stretch response curves for representative rat MCA (M1) and human cerebral artery (Monson et al., 2008) samples in the axial ($S_m$) and circumferential ($P_n$) directions. Label subscript $m$ indicates the luminal pressure during axial stretch tests while subscript $n$ indicates the axial stretch during inflation tests.

## 4. Discussion

The present study aimed to characterize the biaxial mechanical properties of passive rat MCAs and to compare them to those of human cerebral arteries. Qualitatively, rat MCA response was similar to that of the human vessels. Stiffness around the in vivo configuration was also found to be higher axially than circumferentially, as in human arteries, but the human vessels were stiffer in both directions compared to rat arteries. Additionally, failure stretch values were slightly higher and failure stresses were considerably lower for rat arteries. These similarities and differences should be considered in the translation of knowledge gained from rat models of TBI and stroke to the human system.

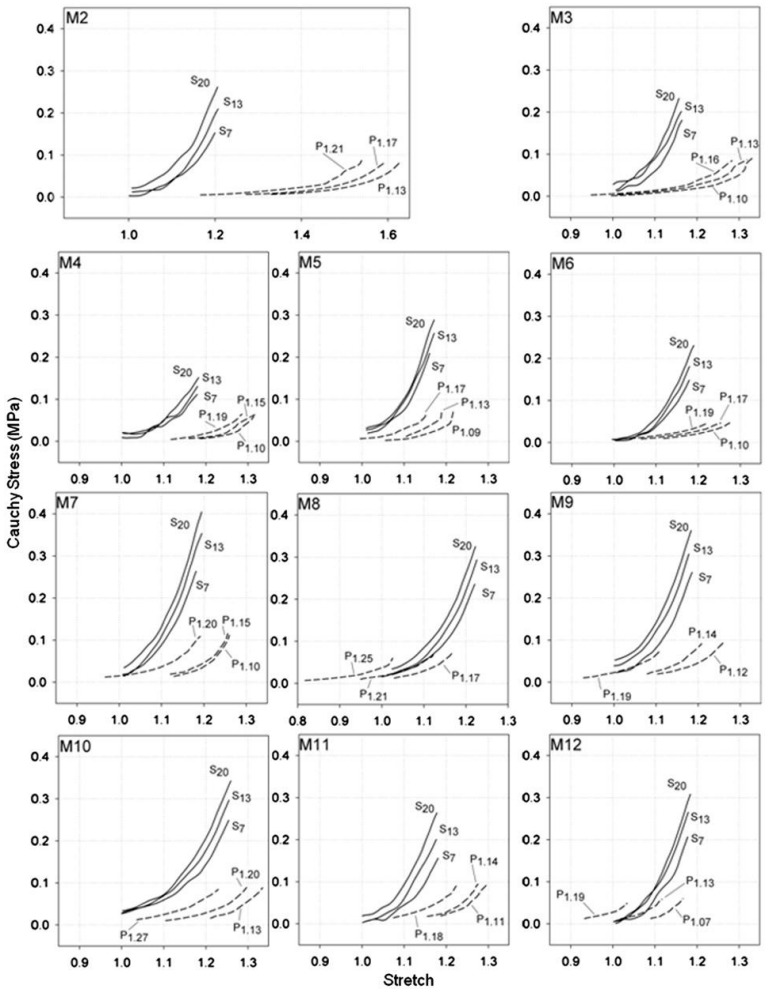


**Fig. 4.** Cauchy stress–stretch response curves for remaining rat MCAs in the axial ($S_m$) and circumferential ($P_n$) directions. Label subscript $m$ indicates the luminal pressure during axial stretch tests while subscript $n$ indicates the axial stretch during inflation tests.

Based on the observed rat MCA stress–stretch response and the corresponding material parameter values, it is clear that axial and circumferential responses are statistically different. This agrees with our previous work showing that behavior is considerably stiffer axially than circumferentially in human cerebral arteries (Monson et al., 2008). Reasons for the observed differences between rat and human arteries are unknown, but it is important to note that rat data were obtained from MCAs while human data were collected from pial arteries on the surface of the temporal lobe, two different locations in the cerebral circulation. Our previous work comparing these two sites in humans (Monson et al., 2005) indicated that differences between them were not significant, but any similarity between rat MCA and pial artery is currently undefined. Dissimilarities in the general structure of rat and human cerebral arteries may also contribute to the observed differences (Lee, 1995) and should be further investigated through histological studies.

It is interesting to note the good quality of fit obtained here for the rat MCAs using the Fung-type strain energy function, in contrast to our previous efforts to fit this function to human data (Monson et al., 2008). It should be emphasized that the function was here fitted to data from inflation tests only, whereas the previous effort also included data from axial stretch tests. Initial efforts to fit Eq. (4) to the rat MCA data included results from both types of test, and the quality of that combined fit was also poor, consistent with our previous experience. This was also the case for a more complex, microstructure-based strain energy function (Baek et al., 2007; Wagner and Humphrey, 2011; Wicker et al., 2008) that we initially fitted to both the human and rat MCA data. This more complex model did not provide a substantial increase in the quality of fit to either data set so its performance is not reported here. The decision to limit the data used for fitting was based on the recognition that the circumferential direction unloads slightly during axial stretch tests, inconsistent with requirements of pseudoelasticity (Humphrey et al., 1990). Despite the use of this limited data set, it is interesting that the resulting fit of the human data was still poor.

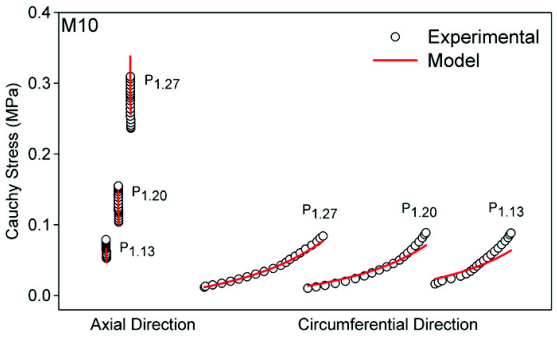


**Fig. 5.** Experimental and predicted axial and circumferential stress values from inflation tests only ($P_n$) for a representative rat MCA (M10). M10 was selected here since it has a fit parameter closest to that of the mean fit for all the samples, without violating the pseudoelasticity assumption. Predicted values are derived from best-fit parameters from the Fung-type constitutive model. Label subscript $n$ indicates the axial stretch during inflation tests. Datasets having the same label are from the same test.

**Table 1**
Rat MCA best-fit material parameters computed for inflation tests (Eq. (4)), with mean and standard deviation shown for each. Corresponding summary of human cerebral artery inflation tests also shown (Monson et al., 2008).

| Sample No. | Fung-type material parameters | | | | |
|---|---|---|---|---|---|
| | $c$ (kPa) | $c_1$ | $c_2$ | $c_3$ | $f$ |
| | | **Rat MCAs** | | | |
| **M1** | 14.98 | 1.87 | 12.60 | 1.56 | 5.74 |
| **M2** | 5.95 | 1.34 | 25.33 | −0.55 | 3.00 |
| **M3** | 8.79 | 3.46 | 27.47 | 1.44 | 1.62 |
| **M4** | 6.58 | 4.37 | 25.29 | −1.65 | 5.67 |
| **M5** | 4.94 | 8.71 | 40.78 | 0.85 | 5.75 |
| **M6** | 12.71 | 3.06 | 18.08 | 0.75 | 1.34 |
| **M7** | 21.13 | 3.02 | 19.30 | 1.22 | 4.21 |
| **M8** | 13.32 | 3.93 | 16.93 | 2.86 | 1.43 |
| **M9** | 6.26 | 5.85 | 33.95 | 4.23 | 1.28 |
| **M10** | 13.19 | 3.12 | 12.47 | 0.48 | 2.14 |
| **M11** | 3.59 | 8.58 | 37.39 | 0.14 | 0.63 |
| **M12** | 5.59 | 12.25 | 37.03 | 6.16 | 1.97 |
| | | **Summary** | | | |
| **Mean** | 9.75 | 4.96 | 25.55 | 1.46 | 2.90 |
| **Std. Dev.** | 5.28 | 3.28 | 9.94 | 2.11 | 1.93 |
| | | **Human cerebral arteries Summary** | | | |
| **Mean** | 2.88 | 5.14 | 179.29 | 2.66 | 19.17 |
| **Std. Dev.** | 2.63 | 3.35 | 199.63 | 14.59 | 18.20 |

The primary challenge with conducting the current experiments, relative to previous work on human vessels, was the small size of the specimens, and errors related to size could lead to some of the differences observed here. Forces measured were not far above the specified error of the load cell in some tests, but results for axial stretch tests at different pressures were discernible from one another and were consistent with the multi-axial behavior observed in other vessels. Also, filtered force traces were always compared to raw data to ensure fidelity.

Despite the significance of the stress–strain relationship in cerebrovascular mechanics, previous studies on rat cerebral vessels have mostly focused on analyzing the pressure–diameter response for different purposes (Coulson et al., 2002, 2004; Hajdu and Baumbach, 1994). Coulson et al. (2004) have examined the rat MCA mechanical behavior in both a myogenically active state and a drug-induced passive state, but they limited their study to uniaxial circumferential testing only. Our circumferential

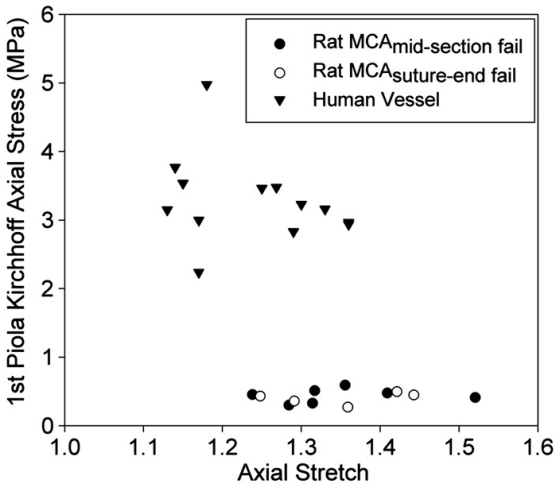


**Fig. 6.** 1st Piola–Kirchhoff ultimate failure stress–stretch values for rat MCAs and human cerebral vessels.

findings compare well with theirs, i.e. the pressure–diameter relationship is non-linear and lies within a similar range. Apart from that, other related studies have either examined rat cerebral arteries in a different state or have focused on a different aspect. As far as we know, no researchers have conducted multiaxial testing and analysis of rat middle cerebral arteries.

While our findings shed light on the mechanical behavior of rat cerebral arteries and their relationship to those of human cerebral arteries, further work is needed to more completely define both types of vessels. In particular, the use of the zero-load state as the reference configuration ignores contributions from residual stresses (Chuong and Fung, 1986). Further investigation including through-wall stress distribution is needed to better identify conditions associated with disease development and injury, and should utilize the zero-stress state as reference. Future work should also address the multiple layers present in any vessel and how specific components of these layers are loaded, especially during injury. Based on preliminary fits of the current data to more advanced models that incorporate arterial microstructure (Baek et al., 2007; Holzapfel et al., 2000; Wagner and Humphrey, 2011; Wicker et al., 2008), the more complex functions do not currently provide substantial fitting advantages over the simpler Fung-type model, but functions that accurately simulate microstructure have intrinsically greater potential to capture the complex behavior of these tissues and should continue to be developed. Additionally, cerebral artery response varies with smooth muscle tone (Coulson et al., 2004; Wagner and Humphrey, 2011), and our study focused only on passive properties. The nature of this contribution needs further attention, as do other questions related to tethering (Steelman et al., 2010) and the influence of fluid flow, in order to more completely define cerebrovasculature function in health and disease.

## Conflict of interest statement

The authors have no conflict of interest.

## Acknowledgments

This work was supported by grants from the National Institutes of Health (5K25HD048643) and the Department of Defense (W81XWH-08-1-0295).

## References

Baek, S., Gleason, R.L., Rajagopal, K.R., Humphrey, J.D., 2007. Theory of small on large: potential utility in computations of fluid–solid interactions in arteries. Computer Methods in Applied Mechanics and Engineering 196, 3070–3078.

Busby, D.E., Burton, A.C., 1965. The effect of age on the elasticity of the major brain arteries. Canadian Journal of Physiology and Pharmacology 43, 185–202.

Chuong, C.J., Fung, Y.C., 1986. On residual stresses in arteries. Journal of Biomechanical Engineering 108, 189–192.

Coulson, R.J., Chesler, N.C., Vitullo, L., Cipolla, M.J., 2002. Effects of ischemia and myogenic activity on active and passive mechanical properties of rat cerebral arteries. American Journal of Physiology - Heart and Circulatory Physiology 283, H2268–2275.

Coulson, R.J., Cipolla, M.J., Vitullo, L., Chesler, N.C., 2004. Mechanical properties of rat middle cerebral arteries with and without myogenic tone. Journal of Biomechanical Engineering 126, 76–81.

Faul, M., Xu, L., Wald, M.M., Coronado, V.G., 2010. Traumatic Brain Injury in the United States: Emergency Department Visits, Hospitalizations and Deaths 2002–2006. Centers for Disease Control and Prevention, National Center for Injury Prevention and Control, Atlanta, GA.

Fung, Y.C., 1993. Biomechanics: Mechanical Properties of Living Tissues, second ed. Springer, New York.

Gonzalez, J.M., Briones, A.M., Starcher, B., Conde, M.V., Somoza, B., Daly, C., Vila, E., McGrath, I., Gonzalez, M.C., Arribas, S.M., 2005. Influence of elastin on rat small artery mechanical properties. Experimental Physiology 90, 463–468.

Hajdu, M.A., Baumbach, G.L., 1994. Mechanics of large and small cerebral arteries in chronic hypertension. American Journal of Physiology 266, H1027–1033.

Hayashi, K., Nagasawa, S., Naruo, Y., Okumura, A., Moritake, K., Handa, H., 1980. Mechanical properties of human cerebral arteries. Biorheology 17, 211–218.

Hogestatt, E.D., Andersson, K.E., Edvinsson, L., 1983. Mechanical properties of rat cerebral arteries as studied by a sensitive device for recording of mechanical activity in isolated small blood vessels. Acta Physiologica Scandinavica 117, 49–61.

Holzapfel, G., Gasser, T., Ogden, R., 2000. A new constitutive framework for arterial wall mechanics and a comparative study of material models. Journal of Elasticity 61, 1–48.

Humphrey, J.D., 2002. Cardiovascular Solid Mechanics: Cells, Tissues, and Organs. Springer, New York.

Humphrey, J.D., Strumpf, R.K., Yin, F.C., 1990. Determination of a constitutive relation for passive myocardium: II. Parameter estimation. The Journal of Biomechanical Engineering 112, 340–346.

Lee, R.M., 1995. Morphology of cerebral arteries. Pharmacology and Therapeutics 66, 149–173.

Lloyd-Jones, D., Adams, R.J., Brown, T.M., Carnethon, M., Dai, S., De Simone, G., Ferguson, T.B., Ford, E., Furie, K., Gillespie, C., Go, A., Greenlund, K., Haase, N., Hailpern, S., Ho, P.M., Howard, V., Kissela, B., Kittner, S., Lackland, D., Lisabeth, L., Marelli, A., McDermott, M.M., Meigs, J., Mozaffarian, D., Mussolino, M., Nichol, G., Roger, V.L., Rosamond, W., Sacco, R., Sorlie, P., Roger, V.L., Thom, T., Wasserthiel-Smoller, S., Wong, N.D., Wylie-Rosett, J., 2010. Heart disease and stroke statistics—2010 update: a report from the American Heart Association. Circulation 121, e46–e215.

Monson, K.L., Barbaro, N.M., Manley, G.T., 2008. Biaxial response of passive human cerebral arteries. Annals of Biomedical Engineering 36, 2028–2041.

Monson, K.L., Goldsmith, W., Barbaro, N.M., Manley, G.T., 2005. Significance of source and size in the mechanical response of human cerebral blood vessels. Journal of Biomechanics 38, 737–744.

Rosamond, W., Flegal, K., Furie, K., Go, A., Greenlund, K., Haase, N., Hailpern, S.M., Ho, M., Howard, V., Kissela, B., Kittner, S., Lloyd-Jones, D., McDermott, M., Meigs, J., Moy, C., Nichol, G., O'Donnell, C., Roger, V., Sorlie, P., Steinberger, J., Thom, T., Wilson, M., Hong,, Y., 2008. Heart disease and stroke statistics—2008 update: a report from the American Heart Association Statistics Committee and Stroke Statistics Subcommittee. Circulation, e25–146.

SAE, 1995. S.A.E. Instrumentation for Impact Test. Part 1: Electronic Instrumentation, SAE J211-1. Society of Automotive Engineers, Warrendale, PA.

Scott, S., Ferguson, G.G., Roach, M.R., 1972. Comparison of the elastic properties of human intracranial arteries and aneurysms. Canadian Journal of Physiology and Pharmacology 50, 328–332.

Steelman, S.M., Wu, Q., Wagner, H.P., Yeh, A.T., Humphrey, J.D., 2010. Perivascular tethering modulates the geometry and biomechanics of cerebral arterioles. Journal of Biomechanics 43, 2717–2721.

Van Loon, P., 1977. Length-force and volume-pressure relationships of arteries. Biorheology 14, 181–201.

Wagner, H.P., Humphrey, J.D., 2011. Differential passive and active biaxial mechanical behaviors of muscular and elastic arteries: basilar versus common carotid. The Journal of Biomechanical Engineering 133, 051009.

Wicker, B.K., Hutchens, H.P., Wu, Q., Yeh, A.T., Humphrey, J.D., 2008. Normal basilar artery structure and biaxial mechanical behaviour. Computer Methods in Biomechanics and Biomedical Engineering 11, 539–551.

# CHAPTER 3

# CEREBROVASCULAR DYSFUNCTION FOLLOWING SUBFAILURE AXIAL STRETCH

## 3.1 Abstract

Cerebral vessels are vital to maintaining health in the brain. Failure of cerebral vessels to maintain homeostasis in the brain, or autoregulatory dysfunction, can occur following traumatic brain injury (TBI), but mechanisms are not understood. Even in cases without cerebral hemorrhage, vessels are deformed with the surrounding brain tissue. This subfailure deformation could affect the contractile behavior of smooth muscle cells (SMCs). Further, the level of autoregulatory dysfunction has been shown to be dependent on the rate of loading in closed head impacts. This study investigates the effect of overstretch on the contractile behavior of SMCs in middle cerebral arteries, with the hypothesis that this contractile behavior will be altered above a threshold of stretch and strain rate.

Twenty-four MCAs from Sprague Dawley rats were tested. Following development of basal SMC tone, vessels were subjected to increasing levels of isosmotic extracellular potassium ($K^+$) to characterize the SMC contractile response. Samples were then subjected to a target levels of axial overstretch of either $1.2*\lambda_{IV}$ or $1.3*\lambda_{IV}$, at target strain rates of 0.2 $s^{-1}$ or 20 $s^{-1}$. After overstretch, SMC contractile behavior was again

characterized, via repeated $K^+$ dose response tests, both immediately and 60 minutes after overstretch. Control vessels were subjected to the same protocol except no overstretch was imposed between the first two characterization tests. SMC contractile behavior was defined via both percent contraction (%C) relative to the fully dilated inner diameter and the $K^+$ dose required to evoke the half maximal contractile response (EC50). Control vessels exhibited increased sensitivity to $K^+$ in successive characterization tests so all effects were quantified relative to the time-matched control response.

Samples exhibited the typical biphasic response to extracellular $K^+$, dilating to small $K^+$ increases and contracting to larger $K^+$ increases. As hypothesized, axial overstretched altered SMC contractile behavior, as seen in a decrease in %C for sub-maximal contractile $K^+$ doses ($p<0.05$) and an increase in EC50 ($p<0.01$), but only for the test group stretched rapidly to $1.3*\lambda_{IV}$. While the change in %C was only significantly different immediately after overstretch, the change to EC50 persisted for 60 minutes. These results indicate that mechanical injury can alter SMC contractile behavior and thus play a role in cerebrovascular autoregulatory dysfunction independent of the pathological chemical environment in the brain post-TBI.

## 3.2 Introduction

Traumatic brain injury (TBI) is a devastating cause of disability, leading to an estimated 53,000 deaths annually in the United States alone (Coronado et al., 2011), with the incidence of TBI increasing significantly across the globe (Maas et al., 2008). While this death toll is staggering, the majority of the estimated 2.4 million annual cases in the United States (CDC, 2013) result in survival, highlighting the importance of clinical

methods to reduce the risk of secondary complications.

The cerebrovasculature plays a critical role in the maintenance of the healthy brain. Specifically, the ability of the cerebral vessels to generate intrinsic tone in the smooth muscle cells (SMCs) (Ursino, 1994), and then alter that level of tone to maintain appropriate cerebral blood flow (CBF), is vital to the maintenance of homeostasis in the brain (Lassen, 1974; Ursino, 1994). This process, known as autoregulation, has been shown to be disrupted following TBI (Golding, 2002; Golding et al., 1999a; Martin et al., 1992; Zubkov et al., 2000), resulting in unfavorable clinical outcomes (Czosnyka et al., 1996; Robertson et al., 1992). A few examples of disrupted autoregulation following TBI include vasospasm (Compton and Teddy, 1987; Kramer et al., 2013; Martin et al., 1992; Martin et al., 1997), secondary hypoxia or hypoperfusion (Bramlett et al., 1999; Cherian et al., 1996; Chesnut et al., 1993), and decreased vascular reactivity to hypercapnia in the surrounding brain tissue (Saunders et al., 1979).

There are a number of autoregulatory mechanisms in healthy cerebrovasculature (Johnson, 1986; Udomphorn et al., 2008). Endothelial cells can produce both vasodilation and vasoconstriction. For example, endothelial cells can release nitric oxide (a potent SMC dilator) in response to mechanical signals, such as shear from luminal flow (Seals et al., 2011), and certain chemical signals like acetylcholine (Hamel, 2006). Endothelin-1, a potent vasoconstrictor, is also produced by endothelial cells (Armstead, 1999). Smooth muscle cells can also be directly affected by mechanical and nonendothelial chemical signals. As luminal pressure changes within the autoregulatory range, the SMCs contract in response to increased pressure and dilate with decreased pressure (Bayliss, 1902; Davis, 1993; Osol et al., 2002), a process known as myogenic contraction. Further, SMCs

dilate in direct response to increased extracellular $H^+$, associated with hypoxia (Kontos et al., 1977), and with exposure to nitric oxide released from neurons (Talman and Nitschke Dragon, 2007). Finally, potassium ($K^+$) in surrounding tissue interacts directly with SMCs to produce either dilation or contraction. Mild increases in $K^+$ result in SMC dilation in MCAs via the action of inward rectifying potassium channels ($K_{ir}$) (Golding et al., 2000; Johnson et al., 1998), while larger increases in $K^+$ result in a strong contraction via direct depolarization of the SMCs (Golding et al., 2000; Hogestatt and Andersson, 1984).

A number of previous studies have carefully investigated vascular dysfunction following TBI. Investigations performed in vivo have shown that both endothelial cell-mediated dilation (Ellison et al., 1989; Kontos and Wei, 1992; Toklu et al., 2015) and myogenic pressure response (Golding et al., 1998a; Mathew et al., 1999) are impaired following TBI. However, other studies testing cerebral vessel function in vitro have shown no change in some autoregulatory mechanisms when the vessel was removed quickly from the brain post-TBI. Bukoski et al. (Bukoski et al., 1997) showed lack of deficits in both endothelial cell-mediated dilation and $K^+$-induced force generation in rat posterior and middle cerebral arteries isolated 30 minutes after midline fluid percussion. One hour after controlled cortical impact, Golding et al. (Golding et al., 1999b) showed altered reactivity to $CO_2$ in rat vessels originating at the impact site when tested in vivo, but not when tested in vitro. This has led some to conclude that dysfunction following TBI is not due to mechanical damage to the vessels, but is instead associated with the milieu of the injured brain following TBI. However, it should be noted that the vessels tested in vitro which did not show dysfunction were taken from a portion of the brain

either far removed from the site of injury (Bukoski et al., 1997) or where the mechanical deformation experienced by the tested samples was not well understood (Golding et al., 1999b). Therefore, these studies do not directly address mechanical damage as a potential contributor to autoregulatory dysfunction.

Mechanical injury of the cerebrovasculature might be expected to both alter passive mechanical properties and cause cellular dysfunction, through damage to the extracellular matrix and cells, respectively. We have previously shown that the passive mechanical properties of cerebral vessels are altered following in vitro axial stretch above a threshold beyond the in vivo length (Bell et al., 2015). Additionally, the degree of TBI-induced autoregulatory dysfunction in rats, along with the time frame for the onset of that dysfunction, has been shown to be dependent on impact velocity in closed head injury (Prat et al., 1997). This further suggests a role for mechanics in cellular dysfunction but may also simply indicate that more dysfunction results from a more severe injury.

In order to better define the role of mechanics in cerebrovascular dysfunction, the objective of the current study was to evaluate the contractile behavior of isolated rat middle cerebral arteries (MCAs) before and after axial overstretch. We hypothesized that subfailure mechanical deformation would induce a change in the contractile behavior of rat MCAs that would be dependent upon both the level and rate of applied overstretch. This study focused on the response of SMCs to increasing levels of isotonic extracellular potassium ($K^+$), a pathway independent of the endothelium (Golding et al., 2000).

## 3.3 Methods

### *3.3.1 Sample acquisition and preparation*

The right MCA was dissected from 24 male Sprague Dawley rats (371 ± 24 grams). All procedures met the requirements established by the Institutional Animal Use and Care Committee at the University of Utah. Rats were euthanized via isoflurane overdose and decapitation. The brain was immediately removed and placed in a 5° C physiological saline solution (PSS; NaCl 144.9; KCl 4.7; $CaCl_2$ 2; $MgSO_4$ 1.2; $NaH_2PO_4$ 1.2; D-Glucose 5; Pyruvic Acid 2.5; MOPS 3.3; EDTA 2.2; BSA 0.15; concentrations in mM; pH 7.4) (Donato et al., 2007) for dissection of the MCA. MCA side branches were ligated with individual fibrils from unwound 6-0 silk suture. The MCA was then cannulated with glass needles approximately 200 μm in diameter and secured with 11-0 monofilament nylon suture. Ceramic coated forceps (Roboz Surgical Instruments, Gaithersburg, MD) were utilized for dissection and mounting in order to prevent any depolarization of SMCs via environmental static electricity.

### *3.3.2 Test apparatus*

The needles on which the MCA sample was mounted were oriented horizontally in a temperature controlled bath, filled with PSS, and maintained at 37° C. This bath had a glass window in the bottom for light and a submersible glass viewing window above the MCA. One needle was stationary and mounted to an X-Y stage (MS-125-XY, Newport, Irvine, CA) that allowed for correction of any needle misalignment. The other needle was mounted to the tester via a horizontal, low friction sled which was connected to a voice coil actuator (MGV52-25-1.0, Akribis, Singapore). Movement of the actuator moved the

proximal needle horizontally along the sled track, axially stretching the MCA. Actuator position was given by a digital encoder (resolution 1.0 μm). The MCA was viewed via a digital video camera (PL-A641, Pixelink, Ottawa, Canada) mounted to a light microscope (Ziess 2000C, Carl Zeiss Microscopy, Thornwood, NY) in order to record vessel dimensions during testing. The MCA was perfused with warm PSS originating from an open syringe hanging at the appropriate height to provide static fluid pressure. The fluid path passed through the proximal needle, mounted MCA, and the distal needle. Inline pressure transducers (26PCDFM6G, Honeywell, Golden Valley, MN) were located both proximal and distal to the mounted MCA, equidistant from the vessel. The average between these two transducers was taken to be the pressure inside the MCA, or the luminal pressure. Data and video acquisition, as well as control of the test set-up, were accomplished by a custom LabVIEW program (National Instruments, Austin, TX).

*3.3.3 Test procedure*

Four test groups (n=4 or 5 each), and one time-matched control group (n=5), were included in the study, as detailed below. Briefly, samples were subjected to $K^+$ dose response tests to characterize the sample specific baseline response. Following this initial characterization test, an axial stretch beyond the in vivo length was applied using group specific stretch levels and strain rates. The $K^+$ characterization test was then repeated both immediately and 60 minutes following overstretch. Time-matched control samples were subjected to the same schedule of $K^+$ characterization tests without any applied overstretch.

After mounting the MCA, the luminal pressure was slowly raised from 2 kPa to

the testing pressure of 6.65 kPa (50 mmHg) in approximately 0.5 kPa increments every 5 minutes. During this period, the length of the vessel was also gradually increased to approximately in vivo length ($\lambda_{IV}$), corresponding to an axial stretch of $\lambda_z = 1.1$ (Bell et al., 2013). Once the MCA was up to pressure, it was allowed to equilibrate for 40 minutes in order to develop basal smooth muscle tone. Vessels which failed to develop basal tone or that leaked were discarded. Throughout the entire duration of MCA testing, the PSS in the bath was changed at least every 20 minutes.

In order to determine the baseline level of contractile functionality of the SMCs, MCAs were subjected to $K^+$ dose response tests. Serially increasing doses of $K^+$ were applied externally by changing the PSS in the bath for PSS with altered $K^+$ concentrations but equivalent osmolarity. After 5 minutes of exposure to each $K^+$ concentration (10, 30, 40, 60, and 100 mM), the inner diameter was measured from images. Following a complete $K^+$ dose response test, the bath was rinsed and the MCA allowed to equilibrate for 30 minutes to allow the basal tone to redevelop.

Following the baseline characterization via $K^+$ dose response tests and subsequent re-equilibration period, MCAs were stretch beyond the in vivo length to one of two target peak stretch levels ($\lambda_z = 1.2*\lambda_{IV}$ or $1.3*\lambda_{IV}$) at one of two target strain rates (0.2 or 20 $s^{-1}$), giving 4 overstretched sample groups. The $K^+$ dose response test was then repeated twice more with a 30 minute equilibration period between them, providing a characterization of SMC contractility initiated both immediately as well as 60 minutes after overstretch. After the final dose response test, the bath PSS was switched for an isosmotic calcium free PSS (NaCl 146.9; KCl 4.7; $MgSO_4$ 1.2; $NaH_2PO_4$ 1.2; D-Glucose 5; Pyruvic Acid 2.5; MOPS 3.3; EDTA 2.2; BSA 0.15; concentrations in mM; pH 7.4) (Donato et al.,

2007), and the MCA was allowed to dilate for 30 minutes to obtain a maximum diameter measurement. Finally, to ensure complete dilation, sodium nitroprusside (SNP: $10^{-4}$ mM) was added to the bath. The fully dilated inner diameter was measured from images once the diameter was stable, approximately 3 minutes after SNP exposure. To ensure that any changes following overstretch were not simply due to degradation of the MCA in the test system, time-matched control tests were performed without overstretch.

*3.3.4 Data analysis*

The results of $K^+$ dose response tests were quantified using percent contraction (%C), calculated as (Eq. 3.1):

$$\%\boldsymbol{C} = \frac{(\boldsymbol{D_M} - \boldsymbol{D_C})}{\boldsymbol{D_M}} * \mathbf{100} \tag{3.1}$$

where $D_M$ is the maximum dilated inner diameter, and $D_C$ is the current measured inner diameter. Percent contraction, %C, would register as 100% for a closed lumen and 0% for a fully dilated lumen. The baseline levels of contraction observed varied dramatically from sample to sample. Accordingly, the change in the %C (Δ%C) observed relative to the sample specific pre-overstretch response at that $K^+$ dosage was also calculated (Eq. 3.2) to assist in comparing how overstretch affected contraction across multiple samples.

$$\boldsymbol{\Delta}\%\boldsymbol{C} = (\boldsymbol{Post\text{-}overstretch}\ \%\boldsymbol{C}) - (\boldsymbol{Pre\text{-}overstretch}\ \%\boldsymbol{C}) \tag{3.2}$$

Additionally, the $K^+$ dosage resulting in the half maximum contraction (EC50) was also calculated by fitting the normalized dose response data (excluding baseline

values) to a four-parameter logistic function (Eq. 3.3) (Finney, 1976; Jiang and Kopp-Schneider, 2014).

$$\boldsymbol{y = min + \frac{(max - min)}{\left(1 + abs\left(\frac{x}{log_{10}(EC50)}\right)^{Hillslope}\right)}} \tag{3.3}$$

The parameters *min* and *max* correspond to the minimum and maximum level of contraction, while *x* and *y* represent the $\log_{10}$ applied $K^+$ concentration and resulting normalized %C, respectively. *Hillslope* is the slope of the central portion of the curve. Units for EC50 are in mM. To normalize between groups (Control group, $1.2*\lambda_{IV}$ rapid overstretch group, etc.), all %C data gathered were adjusted such that 0% still corresponded to the fully dilated diameter and 100% corresponded to the median maximally observed contraction over all tests performed in that group (pre- or post-overstretch). Further, for fitting of dose response data to Eq. 3.3, the parameters *min*, *max*, and *Hillslope* were enforced to be constant over all three dose response tests performed on that test group. The appropriateness of this constraint on the fitting parameters was confirmed with an F-test for parallelism between curves, as recommended by SigmaPlot (San Jose, CA), which showed the reduction did not statistically affect the resulting EC50 values. Finally, the percent change of EC50 (%ΔEC50) for post-overstretch dose response tests was calculated relative to the vessel specific pre-overstretch EC50 value (Eq. 3.4), where $EC50_{Pre}$ and $EC50_{Post}$ are the EC50 values for the sample specific pre-overstretch and post-overstretch tests, respectively.

$$\%\boldsymbol{\Delta EC50} = \mathbf{100} * \left(\frac{\boldsymbol{EC50_{Post}} - \boldsymbol{EC50_{Pre}}}{\boldsymbol{EC50_{Pre}}}\right) \quad (3.4)$$

For statistical comparison of Δ%C, a Levene test was first used to determine if the variances of interest were statistically different. When variances were not different, a one way ANOVA, followed by a Tukey-Kramer post-hoc test, was performed. For comparisons with statistically different variances, Welsh's ANOVA followed by Games-Howell post-hoc tests were performed to determine significance. The significance threshold used for the Levene tests, as well as the various ANOVAs and post-hoc tests, was $p<0.05$. Both the EC50 values within a test group over time, as well as the %ΔEC50 between groups, were compared using one way ANOVA tests followed by post-hoc two way t-tests utilizing a Bonforroni correction factor, with $p<0.05$ indicating significance. The EC50 and %ΔEC50 post-hoc tests required a resulting corrected p-value below 0.01 for significance.

## 3.4 Results

Twenty-four arteries were successfully tested. Mean (± standard deviation) in vivo length and fully dilated inner diameter of these specimens were 0.61 (± 0.13) and 0.25 (± 0.02) mm, respectively. The overstretch parameters and number of samples for each of the test groups are detailed in **Table 3.1**.

As the increasing doses of $K^+$ were applied to the mounted samples in each dose response test, the level of observed contraction followed the previously observed biphasic

**Table 3.1**

**Summary of overstretch parameters (mean ± standard deviation) and group sizes for each test group.**

| Test Groups | N | Overstretch Level ($X*\lambda_{IV}$) | Strain Rate ($s^{-1}$) |
|---|---|---|---|
| Control | 5 | N/A | N/A |
| $1.2*\lambda_{IV}$ Slow | 4 | 1.18 ± 0.02 | 0.28 ± 0.02 |
| $1.2*\lambda_{IV}$ Fast | 5 | 1.20 ± 0.02 | 20.63 ± 0.59 |
| $1.3*\lambda_{IV}$ Slow | 5 | 1.32 ± 0.02 | 0.33 ± 0.09 |
| $1.3*\lambda_{IV}$ Fast | 5 | 1.31 ± 0.02 | 24.49 ± 1.90 |

potassium response for rat cerebral vessels (**Figure 3.1**) (Golding et al., 2000; Johnson et al., 1998), dilating to the lower concentration (10 mM KCl) and exhibiting increasing levels of contraction to the higher doses (30 - 100 mM KCl). In the control group, the observed levels of %C at a given $K^+$ dosage increased with successive dose response tests for all but the dilatory dose (10 mM) and the maximal dose (100 mM) (**Figure 3.2(A)**). This change in sub-maximal %C for subsequent $K^+$ tests was attributed to sensitization of the SMCs to potassium evoked contraction.

Following overstretch, the $K^+$ dose response tests typically showed a change from group specific pre-overstretch values, as shown by the non-zero values in **Figure 3.2 (B) - (E)**. However, neither of the test groups pulled to $1.2*\lambda_{IV}$ , or the slowly stretched $1.3*\lambda_{IV}$ group, showed a statistically different response from the time-matched control measurement as quantified by Δ%C (**Figure 3.2 (B) - (D)**). The response of the rapidly stretched $1.3*\lambda_{IV}$ group (**Figure 3.2 (E)**) was statistically different for all of the sub-maximal contractile doses (30 - 60 mM KCl) immediately following overstretch.

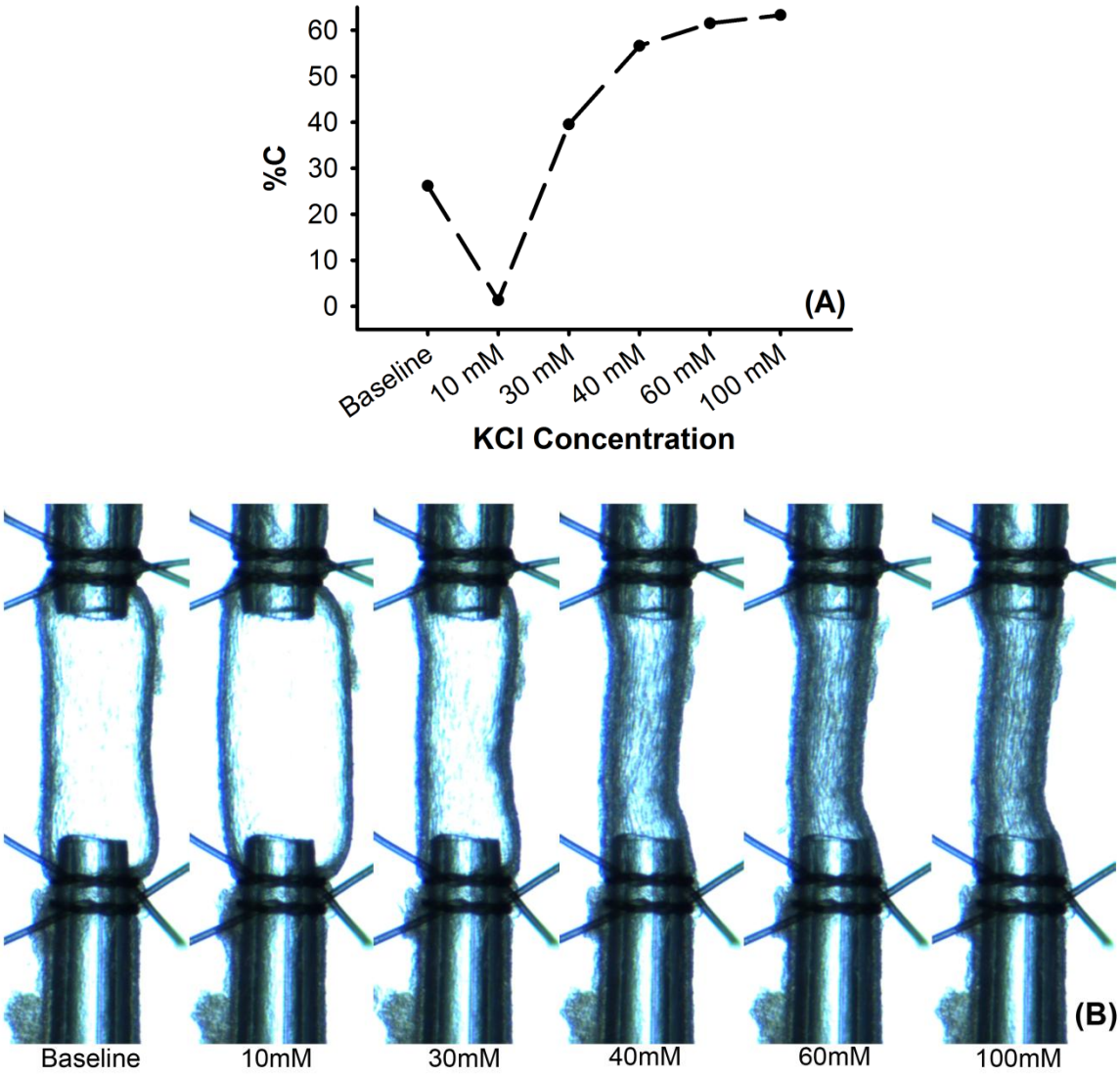


**Figure 3.1: Representative $K^+$ dose response for mounted rat MCA sample (A) as represented by percent contraction (%C), and (B) as viewed by the camera.** Characteristic biphasic response exhibits dilation to small increases of $K^+$ and contraction to high $K^+$ concentrations. Note: Baseline KCl concentration is 4.7 mM.

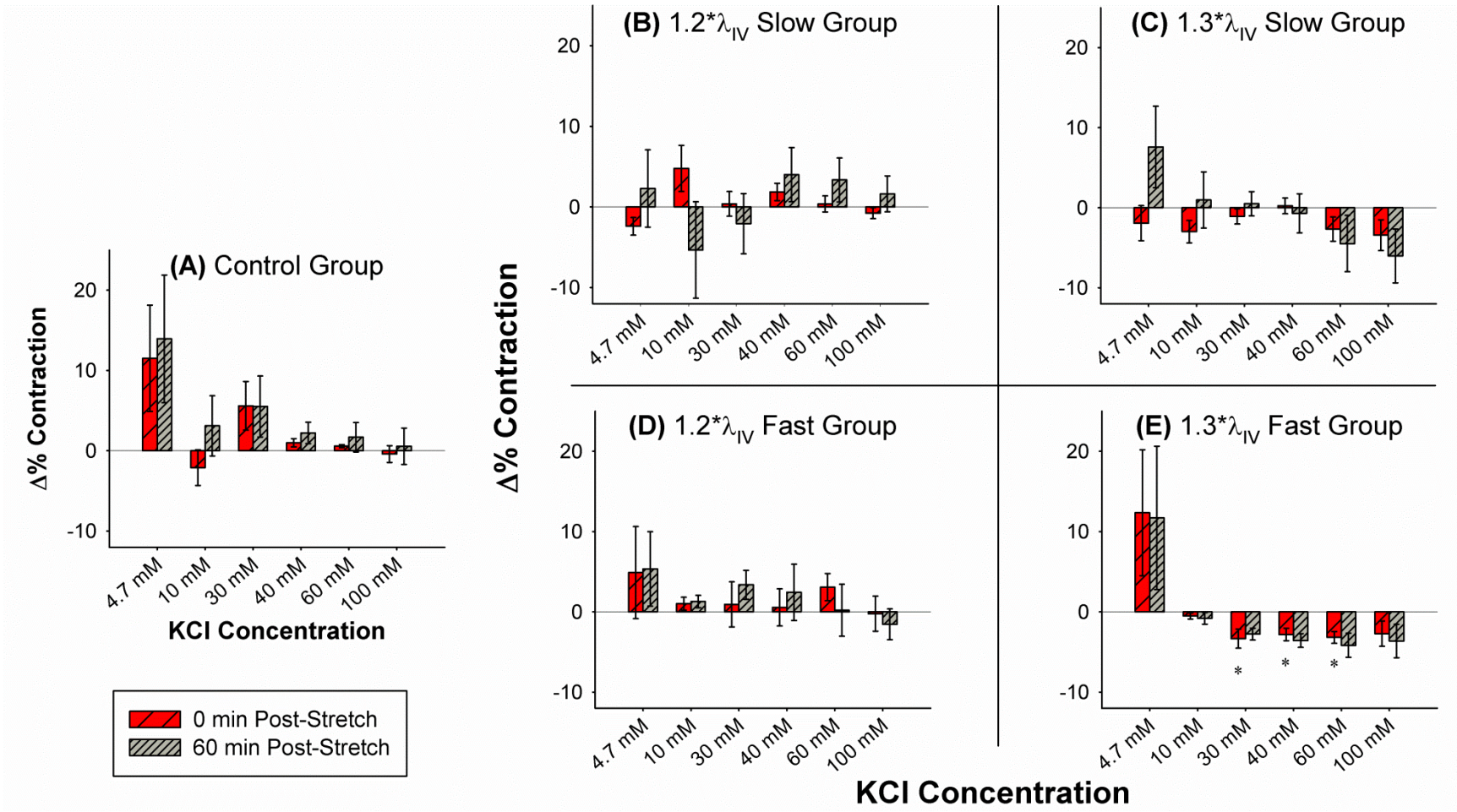


**Figure 3.2: Data for Δ%C from each test group displayed as mean ± standard error.** (*) indicates statistical difference from the time-matched control group measurement.

However, while the Δ%C remained rather consistent between the two post-overstretch dose response tests, the values 60 minutes post-overstretch were no longer considered statistically different from the time-matched control response.

The four-parameter logistic function (Eq. 3.3) was successful at calculating EC50 for the various test groups, but the deviations within the groups were large (**Table 3.2**). Similar to the effect observed over time in the Δ%C results, the EC50 values for the sequentially applied dose response tests in the control group resulted in progressively lower values for EC50. However, these differences in EC50 between subsequent control tests were not statistically significant ($p=0.67$). Further, the direct comparison of the EC50 mean values for all test groups relative to the group-specific pre-overstretch values also did not show statistical differences post-overstretch, which may be due to large deviations in EC50 between samples within a group.

In order to overcome these sample specific variations, %ΔEC50 values were calculated. The only overstretch group that showed a statistical difference relative to the time-matched control %ΔEC50 values was the $1.3*\lambda_{IV}$ fast group ($p<0.01$) (**Figure 3.3**), which agrees well with the observed levels of Δ%C immediately post-overstretch. However, in contrast to the Δ%C statistical analysis, the %ΔEC50 values were considered statistically different both immediately ($p=0.0046$) and 60 minutes ($p=0.0072$) post-overstretch. Considering the consistency of Δ%C between the two post-overstretch response tests, and that the %ΔEC50 remained significantly different over the 60 minute time period for the $1.3*\lambda_{IV}$ fast group, it is possible that the lack of statistical significance in Δ%C 60 minutes post-overstretch could simply be due to the larger deviation present in the time-matched control Δ%C data.

**Table 3.2**

**Best fit parameters for the four parameter logistic function used to calculate EC50 values.**

| | Best Fit Parameters | | | | | | |
|---|---|---|---|---|---|---|---|
| | Shared Parameters | | | | EC50 (mM) | | |
| Test Groups | Min | Max | Hillslope | | Pre-OS | 0 min Post-OS | 60 min Post-OS |
| Control | 8.44 | 99.97 | 3.22 | Mean | 27.57 | 25.25 | 23.90 |
| | | | | St. Dev. | 7.48 | 6.74 | 5.28 |
| 1.2*$\lambda_{IV}$ Slow | 0.16 | 100.59 | 4.48 | Mean | 27.29 | 26.60 | 25.05 |
| | | | | St. Dev. | 7.27 | 7.23 | 5.76 |
| 1.2*$\lambda_{IV}$ Fast | -0.27 | 101.32 | 2.82 | Mean | 30.69 | 28.38 | 28.16 |
| | | | | St. Dev. | 9.65 | 6.45 | 5.61 |
| 1.3*$\lambda_{IV}$ Slow | 4.53 | 104.47 | 2.85 | Mean | 33.23 | 35.09 | 36.57 |
| | | | | St. Dev. | 8.41 | 9.88 | 12.80 |
| 1.3*λIV Fast | -5.10 | 107.09 | 2.24 | Mean | 27.26 | 31.54 | 33.01 |
| | | | | St. Dev. | 13.07 | 14.97 | 17.35 |

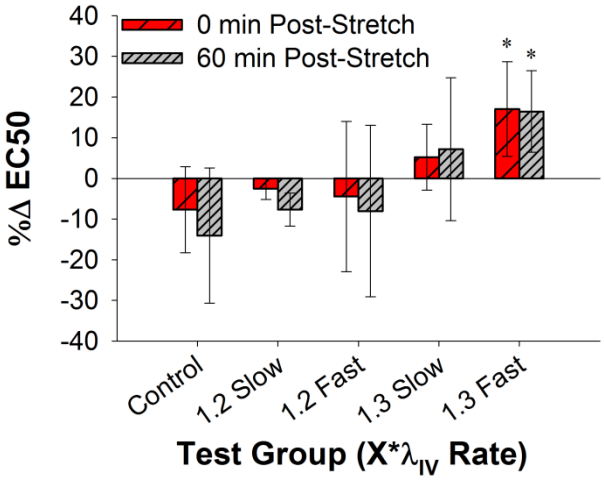


**Figure 3.3: Percent change in EC50 for all five test groups, displayed as mean ± standard deviation.** (*) indicates statistical difference from the time-matched control group measurement.

## 3.5 Discussion

The goal of the present study was to determine if the contractile behavior of cerebral SMCs is altered following axial mechanical stretch. The results show that axial overstretch did not affect the baseline or maximum contraction levels. However, there was a decrease in %C in the sub-maximal contraction levels, shown by a decrease in Δ%C and mirrored by an increase in EC50 for $K^+$-induced contraction. These changes were only significant above thresholds of both axial stretch and strain rate. Over the 60-minute time period of testing, there was no recovery for the EC50 values following overstretch. This observed decrease in SMC sub-maximal contractile response due to a purely mechanical insult is counter to the typically observed vasospasm post-TBI (Compton and Teddy, 1987; Kramer et al., 2013; Martin et al., 1992; Martin et al., 1997). However, coupled with the increase in the corresponding $K^+$ EC50 values, these results indicate that axial mechanical stretch does alter the cerebral SMC function. Therefore, this study lends support to the concept that clinically observed autoregulatory dysfunction

post-TBI may be influenced by mechanical insult to the cerebrovasculature in addition to the altered chemical milieu in the brain associated with TBI (DeWitt and Prough, 2003).

The observed decrease in Δ%C following overstretch was only significantly different from time-matched control values immediately after an overstretch to the $1.3*\lambda_{IV}$ stretch level at the rapid strain rate. Correspondingly, the EC50 value was significantly increased relative to time-matched controls for this test group only. However, this increase in EC50 remained significantly different for the 60 minutes post-overstretch test as well. The fact that the change in the EC50 values for the tests 60 minutes post-overstretch remained statistically different than pre-overstretch baseline values suggests that the lack of significance in the Δ%C changes 60 minutes post-overstretch may be due to the large deviation in the associated Δ%C time-matched control data (**Figure 3.2A**).

Results also indicate a dependence on loading rate for the observed changes in both Δ%C and EC50. These parameters were significantly different than time-matched controls for the test group stretched to $1.3*\lambda_{IV}$ rapidly ($\approx 20\ s^{-1}$) but not in the group overstretched to the same level at a much slower rate ($\approx 0.2\ s^{-1}$); while there does appear to be a similar trend in the low rate data, it was not statistically significant. It thus appears that the vasculature is more sensitive to higher loading rates, such as those associated with a closed head impact. However, in a previous study (Toklu et al., 2015), where the $K^+$ dose response of a rat basilar artery was examined following overpressure-induced TBI, no significant difference was detected in %C or EC50 values compared to control vessels. There are a number of possible reasons for the discrepancy between those results and the current study. In the current investigation, %C was calculated based on the

maximum dilated diameter, while Toklu et al. used the baseline partially contracted diameter. Further, the previous study used three dose levels of KCl for their dose response curve, with a 2-minute equilibration time between application of a dose and measurement of diameter; the current study used 5 doses for the dose response curve (including the 10mM dilatory dose), with a 5-minute equilibration time between application and diameter measurement. It has been stated previously (Hogestatt and Andersson, 1984), and was observed in this study, that contraction in rat cerebral arteries following KCl application requires just under 5 minutes to reach a stable diameter. It is also possible that the larger number of measurement points in the dose response curve, as well as a longer equilibration time between dose application and diameter measurement, are responsible for the observed differences in %C and EC50 following overstretch. Additionally, in the previous study (Toklu et al., 2015), the response of injured vessels was compared to the behavior of control arteries from different animals rather than using a time-matched control test on the same vessel. Finally, the mode, magnitude, and rate of loading in the described overpressure exposure was almost certainly different from the controlled axial overstretch in the current study.

Following overstretch, all test groups had unchanged levels of Δ%C for the baseline as well as the 10 mM $K^+$ dilational response. At lower concentrations of $K^+$, it has been shown that the $K_{ir}$ channels (responsible for dilation) dominate the SMC response (Golding et al., 2000; Johnson et al., 1998). While $K_{ir}$ channel impairment has been observed following ischemia reperfusion injury (Bastide et al., 1999; Marrelli et al., 1998), it has been suggested that this observed impairment may be due to lower density of these channels rather than reduced channel function (Bastide et al., 1999). Further,

there are no studies to-date linking $K_{ir}$ channel dysfunction with the mechanical insult associated with TBI. The current study lends more solid evidence for the lack of a connection between $K_{ir}$ channel dysfunction and mechanical overstretch.

It was also observed that the Δ%C at the maximum $K^+$ dosage was unaffected by overstretch, but the sub-maximal levels of contraction were decreased in the test group exposed to the $1.3*\lambda_{IV}$ fast overstretch. At higher extracellular $K^+$ concentrations, the contractile behavior of vascular SMCs is primarily induced by the action of voltage sensitive calcium channels (VSCCs). These VSCCs have an opening probability that is a continuous function of membrane potential, rather than having a set membrane potential opening threshold (Smirnov and Aaronson, 1992). This function of opening probability would dictate the level of contraction observed at sub-maximal levels, while both VSCC behavior as well as the structural integrity of the contractile mechanisms in the SMCs would dictate the maximal level of contraction. The fact that the sub-maximal contractile behavior was affected by overstretch, while the maximal Δ%C was not, suggests that axial overstretch alters the specifics of the opening probability function for these VSCCs without necessarily damaging the underlying contractile structures, such as the myosin actin complexes.

Overstretch of cerebral arteries has been shown previously to result in an increase in mechanical compliance, also known as softening (Bell et al., 2015). While that previous study only investigated the effect of axial overstretch on the axial passive mechanical properties, the helical nature of collagen fibers in MCAs suggests that axially induced microstructural damage could also affect the circumferential direction. The confirmation of this hypothesis is currently an active area of research in our lab. The

concept of axial overstretch affecting circumferential behavior is further supported by the observed decrease in sub-maximal contractile response in the current study; which is attributed to altered contractile behavior in helically oriented SMCs. One aspect of mechanical softening is that greater applied forces lead to proportionately higher stretch levels. While it is possible that the observed changes in sub-maximal contraction could be due to mechanical softening, the use of the low luminal pressure (50 mmHg) minimizes the contribution of any potential circumferential softening in the results of the current study.

As noted above, the observed decrease in %C at sub-maximal levels appears to be contrary to the vasospasm commonly observed following TBI (Compton and Teddy, 1987; Kramer et al., 2013; Martin et al., 1992; Martin et al., 1997). Short-term cerebral vasospasm lasting less than 20 minutes has been produced experimentally by mechanically stretching connective tissue attached to cerebral arteries, but not when stretch was applied to the vessel itself (Arutiunov et al., 1974). Further, mechanical stretch applied directly to isolated femoral arteries has led to vasospasm, but this was even shorter in duration, lasting 2 minutes or less (Boock, 1991). However, longer term effects have been observed in cultured SMCs exposed to rapid mechanical stretch, lasting at least 24 hours (Alford et al., 2011). Additionally, we are not aware of any studies linking clinical post-TBI vasospasm to specific regions of significant deformation, but it is not clear that the question has ever been addressed. Rather, clinically observed vasospasm post-TBI is most often attributed to exposure to extravascular blood products (Martin et al., 1992; Zubkov et al., 2000). However, vasospasm has been observed post-TBI in the absence of hemorrhage, suggesting a second underlying cause (Martin et al.,

1992; Zubkov et al., 2000). Either way, the results of the current study indicate that mechanical damage alone, when present, is not likely the major cause of pathological post-TBI vasoconstriction.

The goal of the present study was to investigate the effect of mechanical overstretch on SMC function using isosmotic elevated extracellular $K^+$ concentrations. Following TBI, there is frequently an increase in extracellular $K^+$ in the brain released by neurons (Golding et al., 2000; Katayama et al., 1990; Nilsson et al., 1993; Takahashi et al., 1981), potentially returning to normal within an hour (Nilsson et al., 1993). This TBI-related increase in extracellular $K^+$ is hyperosmotic. It has been shown previously that the observed dilation and contraction evoked by hyperosmotic $K^+$ increases are endothelium dependent, whereas isosmotic $K^+$ increases lead to endothelium-independent dilation and contraction (Golding et al., 2000). Therefore, isosmotic $K^+$ doses were used in the present study, rather than the clinically observed hyperosmotic $K^+$ increase, in order to prevent any potential mechanically-induced endothelial damage from corrupting the evaluation of SMC function.

It should be noted that while the MCA was used here to determine the effect of mechanical overstretch on SMC function, pial arteries would typically experience larger deformations than the MCA during a head impact due to the interaction of the brain with the interior of the skull (Goldsmith and Monson, 2005). However, displacements of the MCA on the order of 2-3 mm have been observed via high speed cineflourography during primate closed head impact studies (Shatsky et al., 1974). Also, large cerebral arteries such as the MCA provide approximately 45-50% of the overall resistance in the cerebral circulation in rats (Harper et al., 1984), and evaluation of flow in the MCA via

transcranial Doppler ultrasound (Panerai, 1998) or near-infrared spectroscopy (Highton et al., 2015) are used clinically as noninvasive methods of monitoring cerebral autoregulation post-TBI. Use of the MCA in the present study is also helpful for comparison with other animal models of TBI autoregulatory dysfunction where the MCA is commonly characterized (Bell et al., 2013; Bukoski et al., 1997; Golding et al., 1998a; Golding et al., 1998b; Golding et al., 2000; Mathew et al., 1999).

In the current study, the internal pressure for the mounted samples was 6.65 kPa (50 mmHg). While this pressure is below the mean arterial pressure of 80 mmHg previously measured in rats (Barry et al., 1982), it is still within the pressure range of autoregulation for these vessels (Golding et al., 1998b). Further, since the myogenic response of vascular smooth muscle results in greater baseline contraction at higher pressures (Bayliss, 1902; Golding et al., 1998b), the lower pressure of 50 mmHg allows for a larger range of observable contraction upon application of elevated extracellular $K^+$. This lower pressure is also similar to that used in previous TBI studies of 90 cm H2O (or ≈ 66 mmHg) (Toklu et al., 2015) and 60 mmHg (Golding et al., 1999b). Additionally, preliminary tests in the current study confirmed that a higher pressure of 10.5 kPa (80 mmHg) produced higher levels of basal %C without changing the maximal level of %C. Therefore, the higher pressure did not allow as wide of a range on %C over which to observe stretch related changes. As this smaller range would make subtle changes in post-overstretch contraction more difficult to detect, the lower pressure level (6.65 kPa or 50 mmHg) was selected for testing.

The reported experiments show that axial overstretch changes the contractile behavior of primarily circumferentially oriented vascular SMCs, independent of the

altered chemical environment in the injured brain. While these observed differences are small, when combined with the mechanical softening that follows overstretch (Bell et al., 2015), especially at higher physiological pressures, these changes could contribute to second impact syndrome (Cantu and Gean, 2010; Laskowski et al., 2015) as well as play a role in potential treatments for autoregulatory dysfunction. Ongoing studies in our lab are seeking to better define the effects of axial overstretch on the biaxial mechanical properties and underlying microstructure of cerebral blood vessels. Additionally, the hypothesis suggested above that the observed change in sub-maximal contraction is due to alteration in the opening probability function of VSCCs should be confirmed. Finally, these mechanically-induced changes to the contractile behavior of SMCs emphasize the need to consider the interplay between mechanical and chemical insults to the cerebral vasculature associated with TBI.

## 3.6 References

Alford, P.W., Dabiri, B.E., Goss, J.A., Hemphill, M.A., Brigham, M.D., Parker, K.K., 2011. Blast-induced phenotypic switching in cerebral vasospasm. Proceedings of the National Academy of Sciences of the United States of America 108, 12705-12710.

Armstead, W.M., 1999. Endothelin-1 contributes to normocapnic hyperoxic pial artery vasoconstriction. Brain Research 842, 252-255.

Arutiunov, A.I., Baron, M.A., Majorova, N.A., 1974. The role of mechanical factors in the pathogenesis of short-term and prolonged spasm of the cerebral arteries. Journal of Neurosurgery 40, 459-472.

Barry, D.I., Strandgaard, S., Graham, D.I., Braendstrup, O., Svendsen, U.G., Vorstrup, S., Hemmingsen, R., Bolwig, T.G., 1982. Cerebral blood flow in rats with renal and spontaneous hypertension: resetting of the lower limit of autoregulation. Journal of Cerebral Blood Flow and Metabolism 2, 347-353.

Bastide, M., Bordet, R., Pu, Q., Robin, E., Puisieux, F., Dupuis, B., 1999. Relationship between inward rectifier potassium current impairment and brain injury after cerebral ischemia/reperfusion. Journal of Cerebral Blood Flow and Metabolism 19, 1309-1315.

Bayliss, W.M., 1902. On the local reactions of the arterial wall to changes of internal pressure. Journal of Physiology 28, 220-231.

Bell, E.D., Kunjir, R.S., Monson, K.L., 2013. Biaxial and failure properties of passive rat middle cerebral arteries. Journal of Biomechanics 46, 91-96.

Bell, E.D., Sullivan, J.W., Monson, K.L., 2015. Subfailure overstretch induces persistent changes in the passive mechanical response of cerebral arteries. Frontiers in Bioengineering and Biotechnology 3.

Boock, R.J., 1991. Vascular Response to Mechanical Deformations. University of Pennsylvania, Philadelphia.

Bramlett, H.M., Dietrich, W.D., Green, E.J., 1999. Secondary hypoxia following moderate fluid percussion brain injury in rats exacerbates sensorimotor and cognitive deficits. Journal of Neurotrauma 16, 1035-1047.

Bukoski, R.D., Wang, S.N., Bian, K., DeWitt, D.S., 1997. Traumatic brain injury does not alter cerebral artery contractility. American Journal of Physiology 272, H1406-1411.

Cantu, R.C., Gean, A.D., 2010. Second-impact syndrome and a small subdural hematoma: an uncommon catastrophic result of repetitive head injury with a characteristic imaging appearance. Journal of Neurotrauma 27, 1557-1564.

CDC, 2013. CDC grand rounds: reducing severe traumatic brain injury in the United States. MMWR: Morbidity and Mortality Weekly Report 62, 549-552.

Cherian, L., Robertson, C.S., Goodman, J.C., 1996. Secondary insults increase injury after controlled cortical impact in rats. Journal of Neurotrauma 13, 371-383.

Chesnut, R.M., Marshall, S.B., Piek, J., Blunt, B.A., Klauber, M.R., Marshall, L.F., 1993. Early and late systemic hypotension as a frequent and fundamental source of cerebral ischemia following severe brain injury in the Traumatic Coma Data Bank. Acta Neurochirurgica Supplement 59, 121-125.

Compton, J.S., Teddy, P.J., 1987. Cerebral arterial vasospasm following severe head injury: a transcranial doppler study. Brirish Journal of Neurosurgery 1, 435-439.

Coronado, V.G., Xu, L., Basavaraju, S.V., McGuire, L.C., Wald, M.M., Faul, M.D., Guzman, B.R., Hemphill, J.D., 2011. Surveillance for traumatic brain injury-related deaths--United States, 1997-2007. MMWR: Morbidity and Mortality Weekly Report, Surveillance Summaries 60, 1-32.

Czosnyka, M., Smielewski, P., Kirkpatrick, P., Menon, D.K., Pickard, J.D., 1996. Monitoring of cerebral autoregulation in head-injured patients. Stroke 27, 1829-1834.

Davis, M.J., 1993. Myogenic response gradient in an arteriolar network. American Journal of Physiology 264, H2168-2179.

DeWitt, D.S., Prough, D.S., 2003. Traumatic cerebral vascular injury: the effects of concussive brain injury on the cerebral vasculature. Journal of Neurotrauma 20, 795-825.

Donato, A.J., Lesniewski, L.A., Delp, M.D., 2007. Ageing and exercise training alter adrenergic vasomotor responses of rat skeletal muscle arterioles. Journal of Physiology 579, 115-125.

Ellison, M.D., Erb, D.E., Kontos, H.A., Povlishock, J.T., 1989. Recovery of impaired endothelium-dependent relaxation after fluid-percussion brain injury in cats. Stroke 20, 911-917.

Finney, D.J., 1976. Radioligand assay. Biometrics 32, 721-740.

Golding, E.M., 2002. Sequelae following traumatic brain injury: the cerebrovascular perspective. Brain Research Reviews 38, 377-388.

Golding, E.M., Contant, C.F., Jr., Robertson, C.S., Bryan, R.M., Jr., 1998a. Temporal effect of severe controlled cortical impact injury in the rat on the myogenic response of the middle cerebral artery. Journal of Neurotrauma 15, 973-984.

Golding, E.M., Robertson, C.S., Bryan, R.M., Jr., 1998b. Comparison of the myogenic response in rat cerebral arteries of different calibers. Brain Research 785, 293-298.

Golding, E.M., Robertson, C.S., Bryan, R.M., Jr., 1999a. The consequences of traumatic brain injury on cerebral blood flow and autoregulation: a review. Clinical and Experimental Hypertension 21, 299-332.

Golding, E.M., Steenberg, M.L., Contant, C.F., Jr., Krishnappa, I., Robertson, C.S., Bryan, R.M., Jr., 1999b. Cerebrovascular reactivity to $CO_2$ and hypotension after mild cortical impact injury. American Journal of Physiology 277, H1457-1466.

Golding, E.M., Steenberg, M.L., Johnson, T.D., Bryan, R.M., Jr., 2000. The effects of potassium on the rat middle cerebral artery. Brain Research 880, 159-166.

Goldsmith, W., Monson, K.L., 2005. The state of head injury biomechanics: past, present, and future part 2: physical experimentation. Critical Reviews in Biomedical Engineering 33, 105-207.

Hamel, E., 2006. Perivascular nerves and the regulation of cerebrovascular tone. Journal of Applied Physiology 100, 1059-1064.

Harper, S.L., Bohlen, H.G., Rubin, M.J., 1984. Arterial and microvascular contributions to cerebral cortical autoregulation in rats. American Journal of Physiology 246, H17-24.

Highton, D., Ghosh, A., Tachtsidis, I., Panovska-Griffiths, J., Elwell, C.E., Smith, M., 2015. Monitoring cerebral autoregulation after brain injury: multimodal assessment of cerebral slow-wave oscillations using near-infrared spectroscopy. Anesthesia and Analgesia 121, 198-205.

Hogestatt, E.D., Andersson, K.E., 1984. Mechanisms behind the biphasic contractile response to potassium depolarization in isolated rat cerebral arteries. Journal of Pharmacology and Experimental Therapeutics 228, 187-195.

Jiang, X., Kopp-Schneider, A., 2014. Summarizing EC50 estimates from multiple dose-response experiments: a comparison of a meta-analysis strategy to a mixed-effects model approach. Biometrical Journal 56, 493-512.

Johnson, P.C., 1986. Autoregulation of blood flow. Circulation Research 59, 483-495.

Johnson, T.D., Marrelli, S.P., Steenberg, M.L., Childres, W.F., Bryan, R.M., Jr., 1998. Inward rectifier potassium channels in the rat middle cerebral artery. American Journal of Physiology 274, R541-547.

Katayama, Y., Becker, D.P., Tamura, T., Hovda, D.A., 1990. Massive increases in extracellular potassium and the indiscriminate release of glutamate following concussive brain injury. Journal of Neurosurgery 73, 889-900.

Kontos, H.A., Raper, A.J., Patterson, J.L., 1977. Analysis of vasoactivity of local pH, $PCO_2$ and bicarbonate on pial vessels. Stroke 8, 358-360.

Kontos, H.A., Wei, E.P., 1992. Endothelium-dependent responses after experimental brain injury. Journal of Neurotrauma 9, 349-354.

Kramer, D.R., Winer, J.L., Pease, B.A., Amar, A.P., Mack, W.J., 2013. Cerebral vasospasm in traumatic brain injury. Neurology Research International, 415813.

Laskowski, R.A., Creed, J.A., Raghupathi, R., 2015. Pathophysiology of mild TBI: implications for altered signaling pathways, in: Kobeissy, F.H.P. (Ed.), Brain Neurotrauma: Molecular, Neuropsychological, and Rehabilitation Aspects, Boca Raton (FL).

Lassen, N.A., 1974. Control of cerebral circulation in health and disease. Circulation Research 34, 749-760.

Maas, A.I., Stocchetti, N., Bullock, R., 2008. Moderate and severe traumatic brain injury in adults. Lancet Neurology 7, 728-741.

Marrelli, S.P., Johnson, T.D., Khorovets, A., Childres, W.F., Bryan, R.M., Jr., 1998. Altered function of inward rectifier potassium channels in cerebrovascular smooth muscle after ischemia/reperfusion. Stroke 29, 1469-1474.

Martin, N.A., Doberstein, C., Zane, C., Caron, M.J., Thomas, K., Becker, D.P., 1992. Posttraumatic cerebral arterial spasm: transcranial Doppler ultrasound, cerebral blood flow, and angiographic findings. Journal of Neurosurgery 77, 575-583.

Martin, N.A., Patwardhan, R.V., Alexander, M.J., Africk, C.Z., Lee, J.H., Shalmon, E., Hovda, D.A., Becker, D.P., 1997. Characterization of cerebral hemodynamic phases following severe head trauma: hypoperfusion, hyperemia, and vasospasm. Journal of Neurosurgery 87, 9-19.

Mathew, B.P., DeWitt, D.S., Bryan, R.M., Jr., Bukoski, R.D., Prough, D.S., 1999. Traumatic brain injury reduces myogenic responses in pressurized rodent middle cerebral arteries. Journal of Neurotrauma 16, 1177-1186.

Nilsson, P., Hillered, L., Olsson, Y., Sheardown, M.J., Hansen, A.J., 1993. Regional changes in interstitial $K^+$ and $Ca^{2+}$ levels following cortical compression contusion trauma in rats. Journal of Cerebral Blood Flow and Metabolism 13, 183-192.

Osol, G., Brekke, J.F., McElroy-Yaggy, K., Gokina, N.I., 2002. Myogenic tone, reactivity, and forced dilatation: a three-phase model of in vitro arterial myogenic behavior. American Journal of Physiology: Heart and Circulatory Physiology 283, H2260-2267.

Panerai, R.B., 1998. Assessment of cerebral pressure autoregulation in humans--a review of measurement methods. Physiological Measurement 19, 305-338.

Prat, R., Markiv, V., Dujovny, M., Misra, M., 1997. Evaluation of cerebral autoregulation following diffuse brain injury in rats. Neurological Research 19, 393-402.

Robertson, C.S., Contant, C.F., Gokaslan, Z.L., Narayan, R.K., Grossman, R.G., 1992. Cerebral blood flow, arteriovenous oxygen difference, and outcome in head injured patients. Journal of Neurology, Neurosurgery, and Psychiatry 55, 594-603.

Saunders, M.L., Miller, J.D., Stablein, D., Allen, G., 1979. The effects of graded experimental trauma on cerebral blood flow and responsiveness to $CO_2$. Journal of Neurosurgery 51, 18-26.

Seals, D.R., Jablonski, K.L., Donato, A.J., 2011. Aging and vascular endothelial function in humans. Clinical Science 120, 357-375.

Shatsky, S.A., Alter, W.A., E., E.D., Armbrustmacher, V.W., Earle, K.M., Clark, G., 1974. Traumatic distortions of the primate head and chest: correlation of biomechanical, radiological and pathological data. SAE Technical Paper 741186.

Smirnov, S.V., Aaronson, P.I., 1992. $Ca^{2+}$ currents in single myocytes from human mesenteric arteries: evidence for a physiological role of L-type channels. Journal of Physiology 457, 455-475.

Takahashi, H., Manaka, S., Sano, K., 1981. Changes in extracellular potassium concentration in cortex and brain stem during the acute phase of experimental closed head injury. Journal of Neurosurgery 55, 708-717.

Talman, W.T., Nitschke Dragon, D., 2007. Neuronal nitric oxide mediates cerebral vasodilatation during acute hypertension. Brain Research 1139, 126-132.

Toklu, H.Z., Muller-Delp, J., Yang, Z., Oktay, S., Sakarya, Y., Strang, K., Ghosh, P., Delp, M.D., Scarpace, P.J., Wang, K.K., Tumer, N., 2015. The functional and structural changes in the basilar artery due to overpressure blast injury. Journal of Cerebral Blood Flow and Metabolism 35, 1950-6.

Udomphorn, Y., Armstead, W.M., Vavilala, M.S., 2008. Cerebral blood flow and autoregulation after pediatric traumatic brain injury. Pediatric Neurology 38, 225-234.

Ursino, M., 1994. Regulation of the circulation of the brain, in: Bevan, R.D., Bevan, J.A. (Eds.), The Human Brain Circulation: Functional Changes in Disease. Humana Press, Totowa, NJ, pp. 291-318.

Zubkov, A.Y., Lewis, A.I., Raila, F.A., Zhang, J., Parent, A.D., 2000. Risk factors for the development of post-traumatic cerebral vasospasm. Surgical Neurology 53, 126-130.

# CHAPTER 4

# SUBFAILURE OVERSTRETCH INDUCES PERSISTENT CHANGES IN THE PASSIVE MECHANICAL RESPONSE OF CEREBRAL ARTERIES

Reprinted from first publication in: Frontiers in Bioengineering and Biotechnology 3 (2015). Subfailure overstretch induces persistent changes in the passive mechanical response of cerebral arteries. Bell, E. D., Sullivan, J. W., Monson, K. L., 

frontiers in
BIOENGINEERING AND BIOTECHNOLOGY

ORIGINAL RESEARCH ARTICLE
published: 28 January 2015
doi: 10.3389/fbioe.2015.00002

# Subfailure overstretch induces persistent changes in the passive mechanical response of cerebral arteries

***E. David Bell*[1,2], *Jacob W. Sullivan*[2] *and Kenneth L. Monson*[1,2]***

[1] *Department of Bioengineering, University of Utah, Salt Lake City, UT, USA*
[2] *Laboratory of Head Injury and Vessel Biomechanics, Department of Mechanical Engineering, University of Utah, Salt Lake City, UT, USA*

***Edited by:***
*Linxia Gu, University of Nebraska-Lincoln, USA*

***Reviewed by:***
*Gerald A. Meininger, University of Missouri, USA*
*Zhe Sun, University of Missouri, USA*

****Correspondence:***
*Kenneth L. Monson, Laboratory of Head Injury and Vessel Biomechanics, Department of Mechanical Engineering, University of Utah, 50 S. Central Campus Drive, MEB 2110, Salt Lake City, UT 84112, USA*
*e-mail: ken.monson@utah.edu*

Cerebral blood vessels are critical in maintaining the health of the brain, but their function can be disrupted by traumatic brain injury (TBI). Even in cases without hemorrhage, vessels are deformed with the surrounding brain tissue. This subfailure deformation could result in altered mechanical behavior. This study investigates the effect of overstretch on the passive behavior of isolated middle cerebral arteries (MCAs), with the hypothesis that axial stretch beyond the *in vivo* length alters this response. Twenty nine MCA sections from 11 ewes were tested. Vessels were subjected to a baseline test consisting of an axial stretch from a buckled state to 1.05* *in vivo* stretch ($\lambda_{IV}$) while pressurized at 13.3 kPa. Specimens were then subjected to a target level of axial overstretch between 1.05*$\lambda_{IV}$ ($\lambda_z = 1.15$) and 1.52*$\lambda_{IV}$ ($\lambda_z = 1.63$). Following overstretch, baseline tests were repeated immediately and then every 10 min, for 60 min, to investigate viscoelastic recovery. Injury was defined as an unrecoverable change in the passive mechanical response following overstretch. Finally, pressurized MCAs were pulled axially to failure. Post-overstretch response exhibited softening such that stress values at a given level of stretch were lower after injury. The observed softening also generally resulted in increased non-linearity of the stress-stretch curve, with toe region slope decreasing and large deformation slope increasing. There was no detectable change in reference configuration or failure values. As hypothesized, the magnitude of these alterations increased with overstretch severity, but only once overstretch exceeded 1.2*$\lambda_{IV}$ ($p < 0.001$). These changes were persistent over 60 min. These changes may have significant implications in repeated TBI events and in increased susceptibility to stroke post-TBI.

**Keywords: traumatic brain injury, stroke, sheep cerebral arteries, arterial softening, tissue damage**

## INTRODUCTION

In the United States, in 2009, there were an estimated 2.4 million cases of traumatic brain injury (TBI) (CDC, 2013). Annual estimates of death from TBI and stroke are 53,000 (Coronado et al., 2011) and 130,000 (Go et al., 2014), respectively, with corresponding treatment costs of 76.5 (CDC, 2013) and 36.5 (Go et al., 2014) billion dollars. Cerebral hemorrhage is a common outcome of TBI, but blood vessels that are not deformed enough to rupture and bleed may also be damaged. Such damage may progress to pathological conditions, including stroke (Chen et al., 2011; Hills et al., 2012; Burke et al., 2013) that significantly increase overall morbidity and mortality following TBI (CDC, 2013). A more complete understanding of vessel response to supra-physiological, subfailure deformations is needed to better define the progression of TBI.

The mechanical properties of cerebral vessels that experience large deformations may be altered. Blood vessels from other areas in the body have been shown to experience strain softening, a reduction in stress at a given level of strain, following overstretch in both the circumferential and axial directions (Holzapfel and Gasser, 2007; Alastrue et al., 2008; Horný et al., 2010; Peña et al., 2010; Maher et al., 2012a). The extent of softening following overstretch has been shown to be dependent on location within the arterial tree, possibly due to regional variations in the amounts of collagen and elastin (Maher et al., 2012b). Softening has also been observed in several other soft tissues, including ligament (Pollock et al., 2000; Quinn et al., 2007), tendon (Duenwald et al., 2009; Duenwald-Kuehl et al., 2012), and intestine (Gregersen et al., 1998). Several constitutive models have been proposed to predict softening behavior in blood vessels (Peña et al., 2010; Maher et al., 2012a; Weisbecker et al., 2012). Despite the potential value of these models, it has been noted that more experimental data are needed for these models to be useful for many regions of the vascular tree (Peña et al., 2010; Weisbecker et al., 2012).

Little has been done to explore softening in cerebral vessels. Accordingly, our objective was to characterize this phenomenon in cerebral arteries at various levels of overstretch relevant to TBI. Because these vessels commonly rupture and bleed with trauma, it is clear that they may experience deformations ranging from the physiological state to ultimate failure. While the detailed loading conditions they experience are yet undefined, the vessels are expected to align themselves with deformations imposed on the surrounding brain tissue. Therefore,

alterations of cerebral artery mechanical properties resulting from a large range of axial overstretch values were explored. We hypothesized that even small levels of overstretch would alter vessel response but that the magnitude of the imposed changes would increase with extent of overstretch. Changes in properties were also evaluated over time following overstretch to differentiate persistent changes from temporary viscoelastic alterations.

## MATERIALS AND METHODS

### SAMPLE ACQUISITION AND PREPARATION

A total of 29 middle cerebral artery (MCA) sections were dissected from 11 adult ewes. All procedures met requirements established by the Institutional Animal Care and Use Committee at the University of Utah. Eight of the animals were pregnant Columbia-Rambouillet ewes, and the remaining three (Columbia ewes) were obtained from a local slaughterhouse. Pregnant ewes were euthanized via an overdose of Beuthanasia (MWI Veterinary Supply, Boise, ID, USA), and the brain was immediately removed from the skull and placed in 5°C Hanks buffered saline solution (HBSS; KCl 5.37, $KH_2PO_4$ 0.44, NaCl 136.9, $Na_2HPO_4$ 0.34, D-Glucose 5.55, $NaHCO_3$ 4.17; concentrations in mM) for transport back to the lab. Slaughterhouse ewes were euthanized via a humane stunner applied to the occipital lobe (not in the vicinity of the MCA tested), and the head was placed on ice for transport back to the lab where the brain was immediately removed and placed in 5°C HBSS until testing. Brains from slaughterhouse animals were removed from the skull within 2 h of death. As in previous studies (Bell et al., 2013), branches were ligated, vessels were secured to stainless steel needles attached to the testing apparatus, and black glass beads were spread over the adventitia to be used as fiducial markers (GL-0760, size 25–53 μm, MO-SCI Specialty Products, Rolla, MO, USA). Lack of calcium in HBSS ensured a passive response. All samples were tested within 48 h of death (Humphrey, 1995; Stemper et al., 2007; Amin et al., 2011; Weisbecker et al., 2013).

### EXPERIMENTAL APPARATUS AND METHODOLOGY

The mechanical testing apparatus was similar to that described previously (Bell et al., 2013). Briefly, the displacement of the needles on which the MCAs were mounted was controlled using a vertical custom linear stage (Parker Automation, Cleveland, OH, USA). Vessels were perfused with HBSS, and luminal pressure was controlled through a syringe attached to a computer-controlled linear actuator (D-A0.25-AB-HT17075-4-P, Ultra Motion, Cutchongue, NY, USA). Axial load and pressure were measured with an inline 250 g capacity load cell (Model 31 Low, Honeywell, Golden Valley, MN, USA) and pressure transducers (26PCDFM67G, Honeywell, Golden Valley, MN, USA) corresponding to the vessel inlet and outlet, respectively. Actuator positions were given by digital encoders (resolution 1.0 μm). The specimen was bathed in HBSS during testing, and its deformations were monitored with a digital video camera (PL-A641, Pixelink, Ottawa, ON, Canada) attached to a zoom lens (VZM 450i, Edmund Optics, Barrington, NJ, USA). Test control and data acquisition were performed with a custom LabVIEW program (National Instruments, Austin, TX, USA).

Following mounting of the MCA, it was preconditioned by oscillating the luminal pressure (6.7–20 kPa; 50–150 mmHg) for five cycles while length was held constant. Preconditioning tests were repeated at gradually increasing lengths until the *in vivo* length was identified (Van Loon et al., 1977). A final preconditioning test was conducted at a stretch level of 1.05 times the *in vivo* length. Each MCA was then subjected to an unpressurized axial stretch test to determine its unloaded length.

Following preconditioning, a five step protocol was conducted. *Step 1:* undamaged, baseline response was defined through a quasi-static, axial stretch test to ~$1.05^*\lambda_{IV}$. *Step 2:* vessels were subjected to a single quasi-static, axial overstretch to one of six target levels ranging from $1.05^*\lambda_{IV}$ (control vessels) to $1.5^*\lambda_{IV}$. Overstretch values were chosen to explore the full range of vessel axial stretch possible during TBI. Each overstretch group included 4–6 specimens. *Step 3:* to investigate any viscoelastic recovery in the sample after overstretch, each vessel was subjected to a baseline response test (Step 1) immediately following overstretch and then every 10 min for 60 min. *Step 4:* following the final repeated baseline test, an unpressurized axial stretch test to the previous maximum overstretch level was conducted to determine any changes in the unpressurized stress-stretch response. *Step 5:* finally, the vessel was axially stretched to failure. Luminal pressure was maintained at 13.3 kPa throughout the procedure, except during Step 4 as described.

### DATA ANALYSIS

Data collected during experiments were processed as previously described (Bell et al., 2013). Interpolation was used to produce one-to-one correspondence between current diameter ($d_e$) measurements obtained from video at 3 Hz and other data collected at 100 Hz. Reference diameter ($D_e$) and cross sectional area ($A$) were measured from unloaded vessel cross-sections cut from the end of each sample. Reference inner diameter ($D_i$) was computed from these values. Current inner diameter ($d_i$) during tests was calculated by assuming incompressibility (Eq. 1).

$$d_i = \sqrt{d_e^2 - 4A/(\pi\lambda_z)} \tag{1}$$

Axial stretch ($\lambda_z$) was determined separately using actuator displacements and adventitial marker displacements, with reference length $L$ taken at the unloaded configuration in both cases. Subsequent analysis showed that axial stretch values obtained from marker positions were highly variable, particularly during tests with high overstretch levels (see Discussion). As a result, reported axial stretch values are based on actuator position only.

Vessels were assumed to be homogeneous circular cylinders, with mid-wall stretch defined by Eqs 2 and 3

$$\lambda_\theta = \left(\frac{d_i + d_e}{D_i + D_e}\right) \tag{2}$$

$$\lambda_z = \left(\frac{l}{L}\right) \tag{3}$$

where subscripts θ and $z$ refer to the local cylindrical coordinates in the circumferential and axial directions, respectively. Enforcing

equilibrium in the two directions results in the mean Cauchy stresses defined in Eqs 4 and 5

$$T_\theta = p_i\left(\frac{d_i}{d_e - d_i}\right) \quad (4)$$

$$T_z = \frac{\lambda_z}{A}\left(F_z + \frac{\pi}{4}p_i d_i^2\right) \quad (5)$$

where $F_z$ represents the experimental axial force, and $p_i$ is the luminal pressure. Residual stresses were not considered.

To quantify the effect of overstretch, five parameters derived from the pre- and post-damage stress-stretch curves were compared: *in vivo* stiffness, tare load stretch, baseline stretch, strain energy, and failure values. *In vivo* stiffness was calculated as the slope of the curve at *in vivo* stretch in pressurized axial stretch tests (Monson et al., 2008; Bell et al., 2013). Tare load stretch was defined as the stretch value associated with an axial load of 0.0005 N, a force value consistently outside the noise range of the load cell, intended to help identify possible changes in reference length. Additionally, baseline stress was defined as the axial stress level corresponding to $1.03^*\lambda_{IV}$ in the pre-overstretch baseline test (**Figure 1A**). The corresponding stretch level was defined as the baseline stretch and was quantified in both the overstretch test ($\lambda_{Z1}$) and the post-overstretch failure test ($\lambda_{Z2}$) since both always included the baseline stress level (**Figure 1B**). The initial measurement of baseline stress was taken at $1.03^*\lambda_{IV}$ rather than the maximum applied stretch ($1.05^*\lambda_{IV}$) in order to avoid any artifacts in the data caused by deceleration of the actuator near the peak stretch level. The percent change in axial stretch for both the tare load stretch and the baseline stretch was calculated using (Eq. 6).

$$\%\Delta\lambda_z = 100 * \frac{\lambda_2 - \lambda_1}{\lambda_1} \quad (6)$$

where $\lambda_1$ and $\lambda_2$ are the relevant pre- and post-damage stretch values. Similar to work by others (Maher et al., 2012b), softening was also quantified using percent change in strain energy (%ΔU) (Eq. 7), where $A_1$ and $A_2$ are the areas under the curve to the overstretch level before and after damage, respectively, except in the case of repeated baseline tests where the maximum stretch was $1.05^*\lambda_{IV}$.

$$\%\Delta U = 100 * \frac{A_1 - A_2}{A_1} \quad (7)$$

One way ANOVA, followed by a two-tailed *t*-test with a Bonferroni correction, was used to determine the significance of differences between groups, with $p < 0.05$ indicating statistical significance for ANOVA. *Post hoc* tests between groups required a *p*-value below 0.00625 for significance. Additionally, data acquired from the pregnant and slaughter house ewes were compared using analysis of covariance (ANCOVA) to determine if there was any statistical difference between the groups.

## RESULTS

Twenty nine arteries were successfully tested. Mean (±SD) unloaded length and outer diameter of these specimens were 3.63 (±0.58) and 0.98 (±0.09) mm, respectively. Mean axial *in vivo* stretch was 1.12 (±0.04). The undamaged axial response of the arteries was qualitatively similar to what we have previously reported for other cerebral arteries (**Figure 1A**) (Monson et al., 2008; Bell et al., 2013). Post-overstretch response exhibited softening such that stress values at a given level of stretch were lower after injury (**Figure 2**). The observed softening also generally resulted in increased non-linearity of the stress-stretch curve, with toe region slope decreasing and large deformation slope increasing. There was no detectable change in reference configuration or failure values. As hypothesized, the magnitude of change increased with overstretch severity.

*In vivo* axial stiffness was shown to decrease with overstretch (**Figure 3**). However, this change in stiffness was non-linear, with less difference between adjacent groups with higher overstretch. Mean pre-overstretch *in vivo* stiffness was 0.65 (±0.13) MPa. *In vivo* stiffnesses from the control (non-overstretched) and $1.1^*\lambda_{IV}$ overstretch groups were not significantly different from the pre-damage value (**Table 1**). However, the measure was significantly reduced following each of the higher overstretch levels,

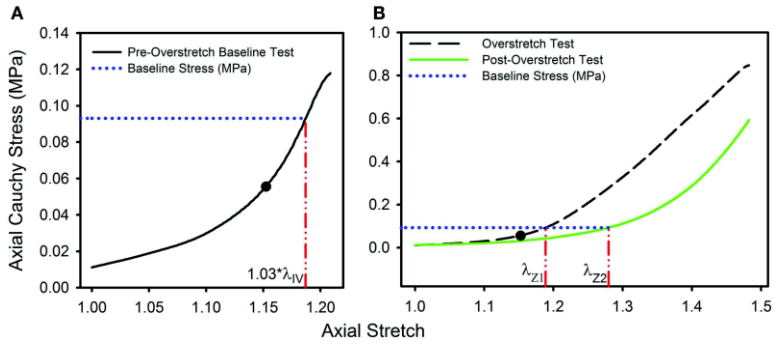


**FIGURE 1 | Data from a representative sample showing the definitions of (A) the baseline stress from the initial pre-overstretch baseline test (at $1.03^*\lambda_{IV}$) and (B) the baseline stretch levels $\lambda_{z1}$ (from the overstretch test; $\lambda_z$ max = $1.3^*\lambda_{IV}$) and $\lambda_{z2}$ (from the post-overstretch failure test; cropped data shown) corresponding to the baseline stress.** (●) indicates the undamaged *in vivo* stress-stretch state.

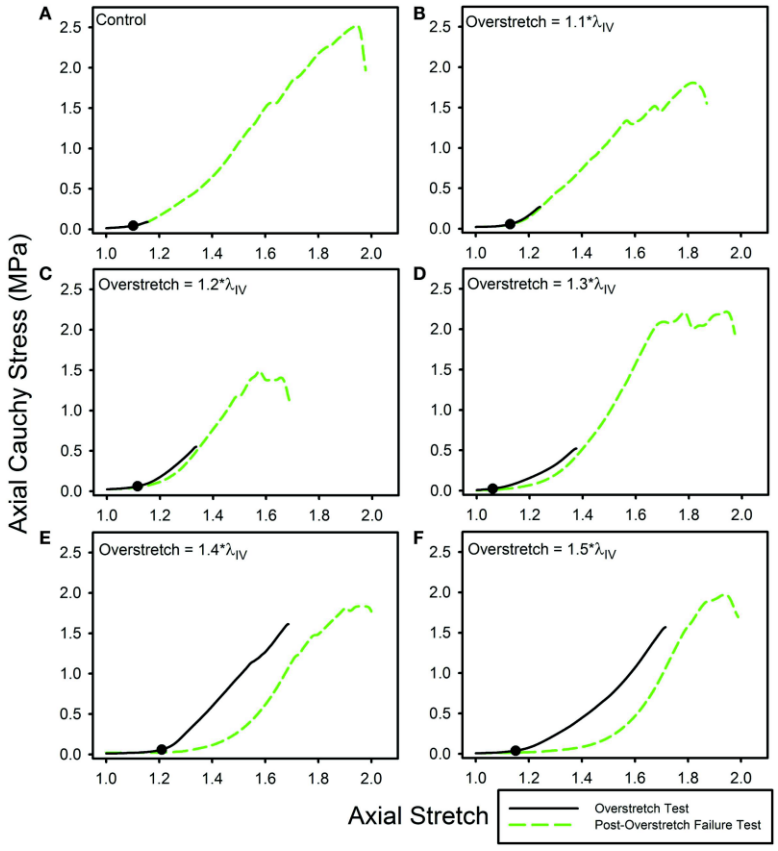


**FIGURE 2 | Data from representative samples showing axial stress-stretch responses for overstretch tests and post-overstretch failure tests for the (A) control vessels, (B) 1.1*$\lambda_{IV}$ overstretch group, (C) 1.2*$\lambda_{IV}$ overstretch group, (D) 1.3*$\lambda_{IV}$ overstretch group, (E) 1.4*$\lambda_{IV}$ overstretch group, and (F) 1.5*$\lambda_{IV}$ overstretch group.** Note: there is increased softening as the overstretch applied increases. (●) indicates the undamaged *in vivo* stress-stretch state.

with reductions of 40 and 80% following overstretches of 1.2 and 1.5, respectively. None of the large overstretch groups was found to be different from the adjacent group at a lower stretch level. However, the 1.3*$\lambda_{IV}$ ($p < 0.001$) and 1.4*$\lambda_{IV}$ ($p = 0.0058$) groups were statistically different from the overstretch group two levels lower. The 1.5*$\lambda_{IV}$ group was not significantly different from the 1.3*$\lambda_{IV}$ group ($p = 0.16$).

The tare load stretch was also affected by overstretch, but only once a threshold was surpassed, as shown in **Figure 4**. Mean tare load stretch in undamaged vessels was $\lambda_z = 1.01$ ($\pm 0.03$) (**Table 1**). Stretch values were not statistically different from this value in overstretch groups below 1.3*$\lambda_{IV}$ (note that this measure was not explored in controls other than undamaged specimens). Tare load stretch in the 1.4*$\lambda_{IV}$ and 1.5*$\lambda_{IV}$ groups was significantly increased relative to the pre-overstretch mean, but the two groups were not statistically different from each other ($p = 0.59$). Also, the 1.4*$\lambda_{IV}$ ($p = 0.003$) group was the only group statistically different from the adjacent group subjected to a lower overstretch.

As illustrated in **Figure 5**, the baseline stretch increased with overstretch. Measurements from the 1.1*$\lambda_{IV}$ group were not significantly different from controls, but each of the higher overstretch groups demonstrated significance (**Table 1**). The 1.2*$\lambda_{IV}$, 1.3*$\lambda_{IV}$, and 1.4*$\lambda_{IV}$ groups were all significantly different from their adjacent lower group ($p < 0.001$). Statistical analysis also showed a difference between the 1.4*$\lambda_{IV}$ and 1.5*$\lambda_{IV}$ groups ($p < 0.0001$), but there was concern about the higher variance in the 1.5*$\lambda_{IV}$ group, despite the baseline stretch data, as a whole, passing the Levene's test for the equality of variances for the groups ($p = 0.09 > 0.05$). Subsequently, a basic two-tailed *t*-test was conducted solely between the 1.4*$\lambda_{IV}$ and 1.5*$\lambda_{IV}$ groups resulting in $p = 0.11$, suggesting that the groups were not statistically different. Accordingly, the more conservative of these two statistical results was used in this case, leading to the conclusion

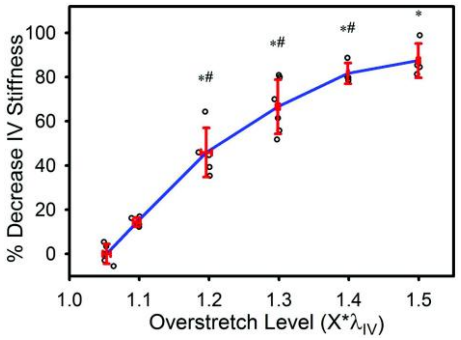


**FIGURE 3 | Percent decrease in axial *in vivo* stiffness following overstretch.** Red error bars indicate SD for each group. Blue line connects group means to clarify trends. (o) indicates individual data points. (*) indicates statistical difference from pre-overstretch values. (#) indicates statistical difference from the group subjected to an overstretch two levels lower.

that this particular difference was not significant. Finally, the baseline stretch measured from the overstretch tests (prior to reaching peak overstretch) was not statistically different from the initial baseline measurement ($p = 0.95$, $n = 28$).

The strain energy was also affected by overstretch, with increasing levels of overstretch leading to larger reductions in strain energy, similar to the pattern of change observed with *in vivo* stiffness. As shown in **Figure 6**, the percent decrease, relative to the control group, was not significantly different in the $1.1^*\lambda_{IV}$ group but was significant for all higher overstretch levels (**Table 1**). Further, the overstretch groups $1.2^*\lambda_{IV}$ ($p = 0.001$) and $1.3^*\lambda_{IV}$ ($p = 0.012$) were different from the adjacent lower overstretch group. However, once overstretch exceeded $1.3^*\lambda_{IV}$, differences between adjacent groups were no longer significant, similar to the pattern observed with *in vivo* stiffness. It should be noted (**Figure 6**) that there is a particular data point in the control group that is far lower than all the others, indicating a physically unreasonable increase in strain energy in the post-injury (sham) axial stretch test. Due to small axial forces at low stretch levels, the luminal pressure has a relatively large influence on the total axial stress (Eq. 5). Thus, it is likely that this unexpected data point is due to a slight variation in luminal pressure between the first and second stretch tests used to calculate %ΔU. This effect from pressure, and subsequent larger deviation in the control data, could also be the reason for the lack of significance in the differences between the control and $1.1^*\lambda_{IV}$ overstretch groups.

Ultimate stress and stretch values were not significantly affected by the level of imposed overstretch (**Figure 7**). Only those samples which failed within the midsection were used to quantify the failure properties. Control ($n = 4$) ultimate failure stress and stretch were 3.44 (±0.94) MPa and $1.61^*\lambda_{IV}$ ($\pm 0.15^*\lambda_{IV}$) (or $\lambda_z = 1.73 \pm 0.21$), respectively. Ultimate stress showed a tendency to decrease with overstretch, but the trend was not statistically significant.

**Table 1 | Statistical summary for *in vivo* stiffness (IV stiffness), tare load stretch, baseline stretch, and percent change in strain energy (%ΔU) following various levels of overstretch, including mean ± SD, number of samples, and *p*-value for comparison between overstretched and undamaged groups.**

| | Undamaged | Overstretch level | | | | | |
|---|---|---|---|---|---|---|---|
| | | Control | 1.1 | 1.2 | 1.3 | 1.4 | 1.5 |
| IV stiffness (MPa) | 0.65 ± 0.13 ($n = 29$) | 0.70 ± 0.17 ($n = 5$, $p = 0.42$) | 0.57 ± 0.12 ($n = 5$, $p = 0.09$) | 0.36 ± 0.07 ($n = 5$, ***p < 0.001***) | 0.18 ± 0.06 ($n = 6$, ***p < 0.001***) | 0.13 ± 0.03 ($n = 4$, ***p < 0.001***) | 0.07 ± 0.05 ($n = 4$, ***p < 0.001***) |
| Tare load stretch | 1.01 ± 0.03 ($n = 23$) | No data | 1.03 ± 0.02 ($n = 6$, $p = 0.17$) | 1.01 ± 0.02 ($n = 4$, $p = 0.90$) | 1.05 ± 0.04 ($n = 6$, $p = 0.02$) | 1.11 ± 0.04 ($n = 4$, ***p < 0.001***) | 1.12 ± 0.02 ($n = 4$, ***p < 0.001***) |
| Baseline stretch ($\lambda_z$) | 1.03 ± 0.001 ($n = 28$) | 1.03 ± 0.005 ($n = 5$, $p = 0.86$) | 1.04 ± 0.001 ($n = 5$, $p = 0.88$) | 1.06 ± 0.006 ($n = 4$, ***p < 0.001***) | 1.11 ± 0.02 ($n = 6$, ***p < 0.001***) | 1.15 ± 0.007 ($n = 4$, ***p < 0.001***) | 1.18 ± 0.03 ($n = 4$, ***p < 0.001***) |
| %ΔU | N/A | −1.19 ± 10.5 ($n = 5$) | 11.12 ± 1.84 ($n = 5$, $p = 0.01$) | 32.88 ± 6.03 ($n = 4$, ***p < 0.001***) | 49.26 ± 8.63 ($n = 6$, ***p < 0.001***) | 56.55 ± 3.14 ($n = 4$, ***p < 0.001***) | 59.72 ± 6.71 ($n = 4$, ***p < 0.001***) |

*Significant p-values are bolded.*

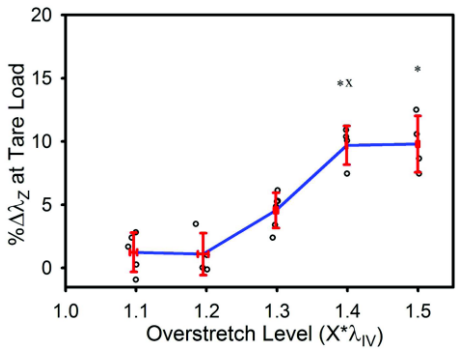


**FIGURE 4 | Percent increase in tare load stretch following overstretch.** Red error bars indicate SD for each group. Blue line connects group means to clarify trends. (o) indicates individual data points. (*) indicates statistical difference from pre-overstretch values. (x) indicates statistical difference from the adjacent group subjected to a lower overstretch level.

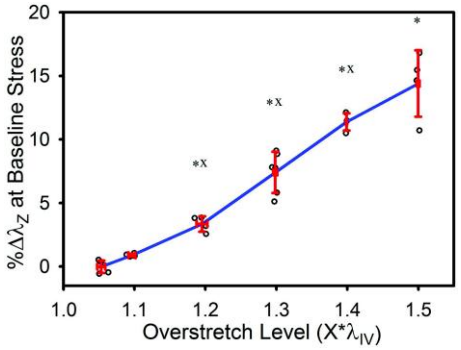


**FIGURE 5 | Percent increase in axial stretch, as measured at the baseline stress level, following overstretch.** Red error bars indicate SD for each group. Blue line connects group means to clarify trends. (o) indicates individual data points. (*) indicates statistical difference from the pre-overstretch mean baseline stretch. (x) indicates statistical difference from the adjacent group subjected to a lower overstretch level.

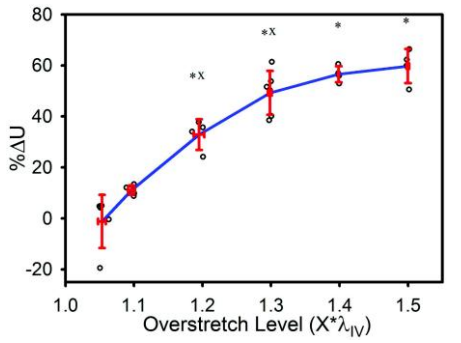


**FIGURE 6 | Percent decrease in strain energy under the axial stress-stretch curves, as calculated from initial overstretch test data, and post-overstretch failure test data (data truncated to stop at the previous overstretch level).** Red error bars indicate SD for each group. Blue line connects group means to clarify trends. (o) indicates individual data points. (*) indicates statistical difference from the control (non-overstretched) group. (x) indicates statistical difference from the adjacent group subjected to a lower overstretch level.

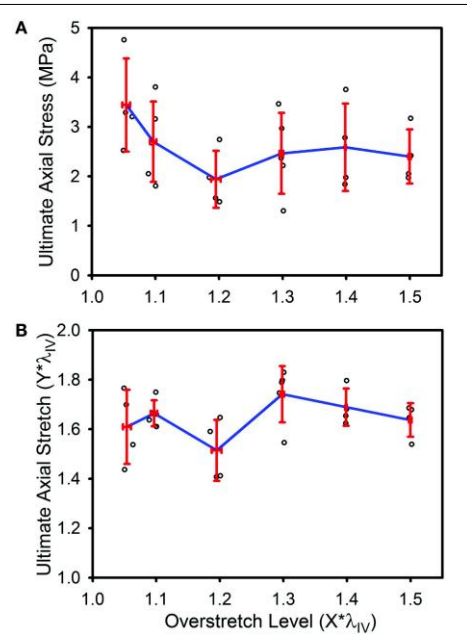


**FIGURE 7 | Ultimate stress (A) and stretch (B) for the various overstretch groups, as measured from the final pressurized axial stretch test (pulled to failure).** Red error bars indicate SD for each group. Blue line connects group means to clarify trends. (o) indicates individual data points.

The observed changes appear to be enduring, rather than passively recoverable due to viscoelasticity (**Figure 8A**). In order to measure any time dependence in the observed changes, the strain energy from the repeated baseline tests was calculated and compared to that of the pre-overstretch baseline test (**Figure 8B**). While the magnitude of the %ΔU following overstretch increased as the imposed overstretch increased, it did not change significantly over the 60 min it was measured. Preliminary tests extended this time frame up to 6 h without a change in the result.

In order to determine if there was any effect in the data imposed by either the source of the tissue or the time from death, ANCOVA tests were conducted on the change of baseline stretch following overstretch, as this was the most sensitive metric taken. Accordingly, it was determined that the data acquired from the two tissue sources (pregnant ewes vs. slaughter house ewes) were not significantly different ($p = 0.498$). Also, data sets were divided into bins defined by how long after death the vessels were tested

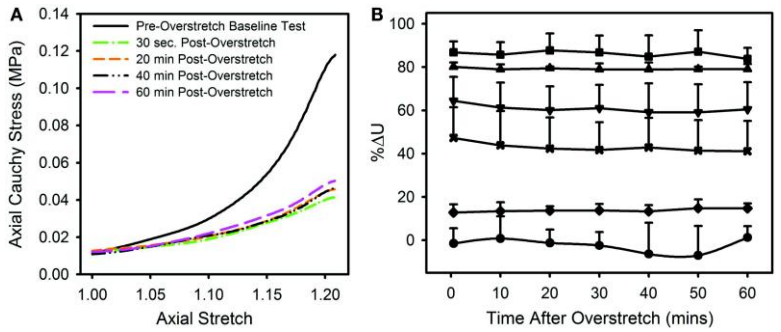


**FIGURE 8 | (A)** Data from a representative sample showing the axial stress-stretch curve for the pre-overstretch baseline test, as well as four of the seven post-overstretch baseline tests which were repeated every 10 min for 60 min after overstretch. **(B)** Means and SD for the various test groups and how these values evolved over time. Note, there was no significant recovery of strain energy following overstretch at any of the tested overstretch levels. [Symbols: (● Control Group, $n=5$), (♦ 1.1*$\lambda_{IV}$ Group, $n=5$) (x 1.2*$\lambda_{IV}$ Group, $n=5$), (▼1.3*$\lambda_{IV}$ Group, $n=6$), (▲ 1.4*$\lambda_{IV}$ Group, $n=4$), (■ 1.5*$\lambda_{IV}$ Group, $n=4$)].

(<8, 8–22, 25–44 h after death). These bins also roughly coincide with differing amounts of time the samples were refrigerated. This comparison also showed no significant effect in the data ($p=0.313$).

## DISCUSSION

The present study aimed to characterize stretch-induced softening in cerebral arteries. Results show that axial overstretches increased the amount of stretch required to obtain a target level of stress. Overstretch also reduced strain energy and *in vivo* stiffness. These effects were only significant above a certain threshold of overstretch. There was no recovery of properties over a 60-min period. These changes may have important implications in repeated TBI events and in increased susceptibility to stroke post-TBI (Chen et al., 2011; Hills et al., 2012; Burke et al., 2013).

In order to see how overstretch would alter the mechanical behavior of cerebral arteries at physiological levels, both *in vivo* stiffness and baseline stretch were determined. The *in vivo* stiffness quantifies how the physiological stiffness of the vessel would change following overstretch, assuming the surrounding brain tissue returned to a similar configuration after injury. This stiffness value was significantly affected by overstretches above 1.2*$\lambda_{IV}$, with a decrease in stiffness of over 40% at 1.2*$\lambda_{IV}$. The baseline stretch allows estimation of vessel length under similar loading after an injury. Given the observed decrease in stiffness, it is not surprising that baseline stretch was also significantly affected by overstretch, starting at the same threshold (1.2*$\lambda_{IV}$). These two metrics together show that the mechanical behavior of the lower end of the mechanical response is dramatically altered by even mild levels of overstretch. Since it has been shown that a higher stiffness in arteries is associated with improved stability (Cyron et al., 2014), it is reasonable to theorize that the inverse would also be true. Thus, these observed low end mechanical changes could cause the cerebral vessels to be more susceptible to subsequent pathologies, including stroke and aneurysm.

The mean tare load stretch prior to injury coincided with ~1% axial strain, or $\lambda_z=1.01$ (±0.03). As a result, the percent change in tare load stretch used here is comparable to metrics referred to in previous studies as either permanent set (Peña et al., 2010; Peña, 2011) or residual inelastic strain (Alastrue et al., 2008; Maher et al., 2012a,b; Weisbecker et al., 2012). In the current study, increased levels of overstretch resulted in an increase in the tare load stretch, similar to a previous arterial softening study by Maher et al. (2012b). However, as the goal of Maher et al. was to quantify differences between different arteries, they did not report statistical differences between loading levels applied to the same artery type. In the present study, the change in tare load stretch did not become significant until overstretch exceeded ~1.3*$\lambda_{IV}$ to 1.4*$\lambda_{IV}$. The change in tare load stretch then ceased to significantly change beyond the 1.4*$\lambda_{IV}$ overstretch level. In contrast, Maher et al. (2012b) observed a linear increase in residual inelastic strain up to the highest tested overstretch, corresponding to $\lambda_z=1.6$ (or ≈1.45*$\lambda_{IV}$) in this study. While this level of overstretch was lower than the highest level investigated here, the magnitude of change in tare load stretch at 1.4*$\lambda_{IV}$ for the cerebral arteries falls between the magnitudes of inelastic residual strain measured in carotid and femoral arteries reported by Maher et al. (2012b). This is consistent with their conclusions that this effect would be increased in more muscular arteries. This change in tare load stretch may indicate a change in the unloaded reference configuration or may just be a result of a reduction of slope in the stress-stretch curve between the reference and tare load configurations.

Strain energy was significantly affected by overstretch. The metric %ΔU quantifies the progression of damage averaged over the entire overstretch range. Interestingly, the magnitude of %ΔU ceases to significantly change once the overstretch level exceeds 1.3*$\lambda_{IV}$. Thus, it is possible that some aspect of microstructural damage is mostly complete by this overstretch level. A previous study of arterial softening investigated a similar parameter, referred to as "% stress softening" (Maher et al., 2012b), where the upper limit of the area quantified was a common axial force rather than a common level of stretch. This difference likely describes why Maher et al. (2012b) did not observe any significant change in strain energy with overstretch, while we did. We limited the

analysis of strain energy to the region bounded by the previously applied overstretch level since subsequent loading clearly showed additional damage prior to reaching the previous peak load. This damage behavior was observed in the form of temporary drops in axial stress as the stretch continued to increase toward ultimate failure, as seen in the failure curve of (**Figure 2E**).

It is interesting to note that significant changes were seen in the *in vivo* stiffness, baseline stretch, and strain energy as low as the $1.2^*\lambda_{IV}$ level. The range at which these various measurements of damage are significantly altered coincides well with a previous study of microstructural damage in rabbit aorta, which showed that repeated strains corresponding to 1.3 times *in situ* length resulted in a significant increase in microstructural damage relative to their control group (Austin et al., 2010).

The observed decreasing level of change in the various metrics at higher overstretch levels has not been previously reported in experiments, and the cause for it is not entirely clear. However, it is interesting to note that this phenomenon appears to be predicted by a constitutive damage model that includes both continuous and discontinuous softening (Peña et al., 2009). In this model, the inclusion of continuous damage resulted in an overall "damage" parameter having a decreased change at higher levels of stretch. The parameter did not have such a decreasing change when only considering discontinuous damage. This is due to the fact that the contribution from continuous damage in their model could reach a saturation point associated with a certain stretch level, where any additional damage at higher stretches would have increasing levels of discontinuous damage but a constant contribution from continuous damage. As the data in the current study does not show roll-off in the measured changes until overstretch levels approach failure, the application of such a damage model to these data would require a continuous damage saturation parameter that would ensure this contribution would level off near, yet prior to, ultimate failure. Comparison to models like this could lend insight into microstructural changes responsible for the softening phenomena observed here.

Interestingly, ultimate failure values were not significantly affected by overstretch. While the literature is lacking in comparable data for arteries following overstretch, these results are similar to what has been observed in ligaments (Panjabi et al., 1996). Panjabi et al. investigated failure values in undamaged and overstretched samples. They showed that the axial force and displacement, as well as the "energy to failure," were unchanged after an overstretch to 80% of failure (approximately corresponding to the $1.3^*\lambda_{IV}$ stretch level in this study). While the current study did not measure strain energy to failure, it is suspected, based on the softening observed at the lower end of the mechanical response that strain energy to failure would be reduced following overstretch in the ewe MCAs. However, it is perhaps less surprising that the failure properties would be unchanged provided there was no gross damage applied to the sample beforehand. The ultimate stress and stretch in a fibrous biological tissue would be associated with the highest values that can be sustained when all the fibers are maximally aligned in the direction of stretch. Any stretch beyond the point where fibers actually begin to fail on a large scale would naturally support less stress, thus occurring after the point where the ultimate stress was measured. Accordingly, it is logical to suspect that the overstretch-induced changes in this study are primarily due to rearrangement of the microstructural components rather than large-scale ruptures in the fibrous components, but additional analysis is needed to relate damage and microstructural change.

We did not observe any significant recovery of mechanical properties over the hour between overstretch and failure tests. Previous studies of viscoelastic recovery in tendons and ligaments show significant recovery in as little as 100 s (Duenwald et al., 2009, 2010). Maher et al. (2012a) discussed preliminary data investigating viscoelastic recovery in porcine arteries over a period of 1–2 h, without observing significant recovery. They suggested that a much longer period of time could be needed for recovery. While this is certainly possible, our preliminary studies showed no quantifiable recovery for 6 h post-overstretch.

Arterial softening has been shown to be dependent on location in the vascular tree (Maher et al., 2012b), but this is the first study known to quantify this effect in cerebral arteries. These location-specific differences are theorized to be due to variations in the proportions and arrangement of collagen and elastin fibers making up the arterial microstructure (Peña et al., 2010; Maher et al., 2012b; Weisbecker et al., 2013). The structure of cerebral arteries is different from other muscular arteries, as is evidenced by the lack of an external elastic lamina (Lee, 1995). Previously, Maher et al. (2012b) tested several non-cerebral arteries with varying proportions of collagen and elastin in the vessel wall. As mentioned briefly above, they subsequently concluded that overstretch of more muscular arteries results in greater inelastic strains. Their results agree well with the measurement of tare load axial stretch in this study.

Given the significance of location in the vascular tree, it should be noted that the present study was conducted on sheep MCA, though TBI-induced deformations are likely more relevant in smaller vessels. Previous work from our lab has shown that the microstructure and mechanical properties of human MCA and pial arteries are very similar (Monson et al., 2005). As a consequence, it seems reasonable to expect similar softening patterns for the two vessels. Use of the MCA here is also helpful for comparison with different animal models of both TBI and stroke where the MCA characterization is common (Högestätt et al., 1983; Coulson et al., 2002, 2004; González et al., 2005; Bell et al., 2013). Trauma-induced softening is likely also important in smaller arteries and arterioles, as well as in veins, venules, and perhaps even capillaries, but findings from this study are not expected to translate directly to these various vessel types due to significant microstructural differences.

As noted in the Section "Materials and Methods," black glass beads were placed on the adventitial surface in order to track local strain. However, the stretch values measured from markers were often inconsistent with observed overall vessel motion. For example, when samples were overstretched to relatively high overstretch levels, it was common to see a decrease in marker-derived axial stretch well before the overall overstretch was concluded. Based on this observation, it is likely that local sites of damage did not correspond with marker placement in a way that allowed reliable measurement of strains corresponding to that damage. During testing at high overstretch values, local sites of damage were observed to occur unpredictably at various locations throughout

the specimen. Measurements from markers could not then be expected to yield consistent measurements of deformation. As a result, average stretch values were calculated from actuator displacement in order to provide a more consistent basis for analysis between specimens.

There are some potential limitations to the current study. First, while the human system is of primary interest to our group, these tests were conducted in sheep cerebral vessels. However, overstretch-induced softening behavior has been observed in human systemic arteries (Weisbecker et al., 2012, 2013). Also, preliminary testing in human cerebral arteries has confirmed the presence of softening behavior in these vessels, though a detailed characterization has not been performed (Monson, 2001). So while the data in the current study are not directly translatable to human tissue, it does provide a greater understanding of the progression of softening in cerebral vessels associated with overstretch.

Second, while the majority of the sheep MCAs were obtained from pregnant ewes, some were acquired from non-pregnant ewes through a local slaughterhouse. It has been shown (Griendling et al., 1985) that arteries close to the fetus during pregnancy can have altered mechanical properties. However, this same study showed that arteries further away, such as the carotid arteries, do not have any pregnancy-induced changes in the mechanical properties. It was reasoned for this study that since the MCA is further along the arterial tree than the carotid arteries, it would be similarly unaffected by pregnancy. As reported, statistical testing showed no difference between the two groups.

The third limitation has to do with the quasi-static rate used in the present study. Deformations associated with TBI take place at a high rate. This quasi-static loading rate was chosen in order to enable comparison to pre-damage mechanical behavior (Monson et al., 2008; Bell et al., 2013). Further, the quasi-static loading rate allowed for more precise control of the levels of overstretch applied to samples in this study. Mechanical properties of cerebral vessels have been shown to be relatively insensitive to loading rates ranging from 0.001 to 50 $s^{-1}$ (Chalupnik, 1971) and 0.01 to 524 $s^{-1}$ (Monson et al., 2003). However, the possibility exists that the progression of softening may be altered at higher loading rates. This should be explored further.

The final limitation is related to the fact that specimens were stored at 5°C prior to testing. The duration of this refrigerated storage ranged from a few hours to as much as 40 h. It has been observed that refrigeration of tissue prior to testing can potentially alter material properties (Stemper et al., 2007; Chow and Zhang, 2011). However, refrigeration of arterial tissue samples prior to testing is a common practice (Humphrey, 1995; Amin et al., 2011; Maher et al., 2012b) and has been determined by other studies to have little effect on both the active and passive properties of arteries, with up to 48 h of storage at 5°C (Herlihy and Murphy, 1973; Cox, 1978; Dobrin, 1984). While Stemper et al. (2007) showed that subfailure stresses and the ultimate failure stress can be lower following refrigeration than in fresh tissue samples, subfailure strains, and ultimate failure strains were not significantly different between fresh and refrigerated tissues in their study. As all of our samples were similarly refrigerated, if there was any refrigeration-induced effect on the failure properties, it would be expected to have been similar for all samples, thus, not changing the relationship of the failure properties between overstretch groups. Finally, as mentioned above, no statistical difference was found for refrigeration time.

Overall, results demonstrate that sheep cerebral arteries experience a persistent change in properties as a result of isolated overstretch. It is currently unknown whether similar changes occur *in vivo*, but it is known that the brain and its supporting vasculature are deformed during trauma. While TBI is complex, including a number of factors that could promote blood vessel dysfunction, changes in vessel mechanical properties would likely play an important role in any acute, and potentially chronic, vessel impairment. Further work is needed to more fully characterize changes induced by overstretch. In particular, this study focused on changes in axial behavior, but alterations to circumferential response are surely also important physiologically and should be explored. However, even without direct study of circumferential changes, multiaxial considerations suggest that the observed increase in axial laxity will lead to a less stiff response circumferentially. At least in an isolated vessel, these changes could lead to disturbances in blood pressure and flow due to both buckling and circumferential expansion. It is not yet clear how forces from surrounding tissue may influence this, especially in an injured brain, but changes to vessel properties are likely an important consideration in the progression of TBI.

Because vessels likely do not experience axial stretch alone during head trauma, additional work is also needed to define the influence of circumferential overstretch on properties in both directions. While this information is expected to lead to a better understanding of TBI, it may be even more useful in improving surgical interventions. Finally, the vasculature is not passive, with both active regulation of its circumference (through smooth muscle cell contraction) and remodeling of the wall to adapt to both physiological and mechanical changes. Future investigation of how these active processes are affected by, or how they impose an effect upon, softening would also be beneficial.

## ACKNOWLEDGMENTS

The authors gratefully acknowledge Kurt Albertine and Mar Janna Dahl for their help with tissue acquisition. This work was partially supported by a grant from the Primary Children's Medical Center Foundation (PCMCF-ISA-KM-01-2012-02).

## REFERENCES

Alastrue, V., Pena, E., Martinez, M. A., and Doblare, M. (2008). Experimental study and constitutive modelling of the passive mechanical properties of the ovine infrarenal vena cava tissue. *J. Biomech.* 41, 3038–3045. doi:10.1016/j.jbiomech.2008.07.008

Amin, M., Kunkel, A. G., Le, V. P., and Wagenseil, J. E. (2011). Effect of storage duration on the mechanical behavior of mouse carotid artery. *J. Biomech. Eng.* 133, 071007. doi:10.1115/1.4004415

Austin, N., Difrancesco, L. M., and Herzog, W. (2010). Microstructural damage in arterial tissue exposed to repeated tensile strains. *J. Manipulative Physiol. Ther.* 33, 14–19. doi:10.1016/j.jmpt.2009.11.006

Bell, E. D., Kunjir, R. S., and Monson, K. L. (2013). Biaxial and failure properties of passive rat middle cerebral arteries. *J. Biomech.* 46, 91–96. doi:10.1016/j.jbiomech.2012.10.015

Burke, J. F., Stulc, J. L., Skolarus, L. E., Sears, E. D., Zahuranec, D. B., and Morgenstern, L. B. (2013). Traumatic brain injury may be an independent risk factor for stroke. *Neurology* 81, 33–39. doi:10.1212/WNL.0b013e318297eecf

CDC. (2013). CDC grand rounds: reducing severe traumatic brain injury in the United States. *MMWR Morb. Mortal. Wkly. Rep.* 62, 549–552.

Chalupnik, J. D. D. C. H. M. H. C. (1971). *Material Properties of Cerebral Blood Vessels.* Seattle, WA: Department of Mechanical Engineering, University of Washington.

Chen, Y. H., Kang, J. H., and Lin, H. C. (2011). Patients with traumatic brain injury: population-based study suggests increased risk of stroke. *Stroke* 42, 2733–2739. doi:10.1161/STROKEAHA.111.620112

Chow, M. J., and Zhang, Y. (2011). Changes in the mechanical and biochemical properties of aortic tissue due to cold storage. *J. Surg. Res.* 171, 434–442. doi:10.1016/j.jss.2010.04.007

Coronado, V. G., Xu, L., Basavaraju, S. V., Mcguire, L. C., Wald, M. M., Faul, M. D., et al. (2011). Surveillance for traumatic brain injury-related deaths – United States, 1997–2007. *MMWR Surveill. Summ.* 60, 1–32.

Coulson, R. J., Chesler, N. C., Vitullo, L., and Cipolla, M. J. (2002). Effects of ischemia and myogenic activity on active and passive mechanical properties of rat cerebral arteries. *Am. J. Physiol. Heart Circ. Physiol.* 283, H2268–2275. doi:10.1152/ajpheart.00542.2002

Coulson, R. J., Cipolla, M. J., Vitullo, L., and Chesler, N. C. (2004). Mechanical properties of rat middle cerebral arteries with and without myogenic tone. *J. Biomech. Eng.* 126, 76–81. doi:10.1115/1.1645525

Cox, R. H. (1978). Passive mechanics and connective tissue composition of canine arteries. *Am. J. Physiol.* 234, H533–H541.

Cyron, C. J., Wilson, J. S., and Humphrey, J. D. (2014). Mechanobiological stability: a new paradigm to understand the enlargement of aneurysms? *J. R. Soc. Interface* 11:20140680. doi:10.1098/rsif.2014.0680

Dobrin, P. B. (1984). Mechanical behavior of vascular smooth muscle in cylindrical segments of arteries in vitro. *Ann. Biomed. Eng.* 12, 497–510. doi:10.1007/BF02363919

Duenwald, S. E., Vanderby, R. Jr., and Lakes, R. S. (2009). Viscoelastic relaxation and recovery of tendon. *Ann. Biomed. Eng.* 37, 1131–1140. doi:10.1007/s10439-009-9687-0

Duenwald, S. E., Vanderby, R. Jr., and Lakes, R. S. (2010). Stress relaxation and recovery in tendon and ligament: experiment and modeling. *Biorheology* 47, 1–14. doi:10.3233/BIR-2010-0559

Duenwald-Kuehl, S., Kondratko, J., Lakes, R. S., and Vanderby, R. Jr. (2012). Damage mechanics of porcine flexor tendon: mechanical evaluation and modeling. *Ann. Biomed. Eng.* 40, 1692–1707. doi:10.1007/s10439-012-0538-z

Go, A. S., Mozaffarian, D., Roger, V. L., Benjamin, E. J., Berry, J. D., Blaha, M. J., et al. (2014). Heart disease and stroke statistics – 2014 update: a report from the American Heart Association. *Circulation* 129, e28–e292. doi:10.1161/01.cir.0000441139.02102.80

González, J. M., Briones, A. M., Starcher, B., Conde, M. V., Somoza, B., Daly, C., et al. (2005). Influence of elastin on rat small artery mechanical properties. *Exp. Physiol.* 90, 463–468. doi:10.1113/expphysiol.2005.030056

Gregersen, H., Emery, J. L., and Mcculloch, A. D. (1998). History-dependent mechanical behavior of guinea-pig small intestine. *Ann. Biomed. Eng.* 26, 850–858. doi:10.1114/1.109

Griendling, K. K., Fuller, E. O., and Cox, R. H. (1985). Pregnancy-induced changes in sheep uterine and carotid arteries. *Am. J. Physiol.* 248, H658–H665.

Herlihy, J. T., and Murphy, R. A. (1973). Length-tension relationship of smooth muscle of the hog carotid artery. *Circ. Res.* 33, 275–283. doi:10.1161/01.RES.33.3.275

Hills, N. K., Johnston, S. C., Sidney, S., Zielinski, B. A., and Fullerton, H. J. (2012). Recent trauma and acute infection as risk factors for childhood arterial ischemic stroke. *Ann. Neurol.* 72, 850–858. doi:10.1002/ana.23688

Högestätt, E. D., Andersson, K. E., and Edvinsson, L. (1983). Mechanical properties of rat cerebral arteries as studied by a sensitive device for recording of mechanical activity in isolated small blood vessels. *Acta Physiol. Scand.* 117, 49–61. doi:10.1111/j.1748-1716.1983.tb07178.x

Holzapfel, G. A., and Gasser, T. C. (2007). Computational stress-deformation analysis of arterial walls including high-pressure response. *Int. J. Cardiol.* 116, 78–85. doi:10.1016/j.ijcard.2006.03.033

Horný, L., Gultova, E., Chlup, H., Sedlácek, R., Kronek, J., Veselý, J., et al. (2010). *Mullins Effect in an Aorta and Limiting Extensibility Evolution.* Prague: Czech Technical University in Prague.

Humphrey, J. D. (1995). Mechanics of the arterial wall: review and directions. *Crit. Rev. Biomed. Eng.* 23, 1–162.

Lee, R. M. (1995). Morphology of cerebral arteries. *Pharmacol. Ther.* 66, 149–173. doi:10.1016/0163-7258(94)00071-A

Maher, E., Creane, A., Lally, C., and Kelly, D. J. (2012a). An anisotropic inelastic constitutive model to describe stress softening and permanent deformation in arterial tissue. *J. Mech. Behav. Biomed. Mater.* 12, 9–19. doi:10.1016/j.jmbbm.2012.03.001

Maher, E., Early, M., Creane, A., Lally, C., and Kelly, D. J. (2012b). Site specific inelasticity of arterial tissue. *J. Biomech.* 45, 1393–1399. doi:10.1016/j.jbiomech.2012.02.026

Monson, K. L., Barbaro, N. M., and Manley, G. T. (2008). Biaxial response of passive human cerebral arteries. *Ann. Biomed. Eng.* 36, 2028–2041. doi:10.1007/s10439-008-9578-9

Monson, K. L., Goldsmith, W., Barbaro, N. M., and Manley, G. T. (2003). Axial mechanical properties of fresh human cerebral blood vessels. *J. Biomech. Eng.* 125, 288–294. doi:10.1115/1.1554412

Monson, K. L., Goldsmith, W., Barbaro, N. M., and Manley, G. T. (2005). Significance of source and size in the mechanical response of human cerebral blood vessels. *J. Biomech.* 38, 737–744. doi:10.1016/j.jbiomech.2004.05.004

Monson, K. L. V. (2001). *Mechanical and Failure Properties of Human Cerebral Blood Vessels.* Berkeley: University of California.

Panjabi, M. M., Yoldas, E., Oxland, T. R., and Crisco, J. J. III (1996). Subfailure injury of the rabbit anterior cruciate ligament. *J. Orthop. Res.* 14, 216–222. doi:10.1002/jor.1100140208

Peña, E. (2011). Prediction of the softening and damage effects with permanent set in fibrous biological materials. *J. Mech. Phys. Solids* 59, 1808–1822. doi:10.1016/j.jmps.2011.05.013

Peña, E., Alastrue, V., Laborda, A., Martinez, M. A., and Doblare, M. (2010). A constitutive formulation of vascular tissue mechanics including viscoelasticity and softening behaviour. *J. Biomech.* 43, 984–989. doi:10.1016/j.jbiomech.2009.10.046

Peña, E., Peña, J. A., and Doblaré, M. (2009). On the Mullins effect and hysteresis of fibered biological materials: a comparison between continuous and discontinuous damage models. *Int. J. Solids Struct.* 46, 1727–1735. doi:10.1016/j.ijsolstr.2008.12.015

Pollock, R. G., Wang, V. M., Bucchieri, J. S., Cohen, N. P., Huang, C. Y., Pawluk, R. J., et al. (2000). Effects of repetitive subfailure strains on the mechanical behavior of the inferior glenohumeral ligament. *J. Shoulder Elbow Surg.* 9, 427–435. doi:10.1067/mse.2000.108388

Quinn, K. P., Lee, K. E., Ahaghotu, C. C., and Winkelstein, B. A. (2007). Structural changes in the cervical facet capsular ligament: potential contributions to pain following subfailure loading. *Stapp Car Crash J.* 51, 169–187. Available from: http://repository.upenn.edu/be_papers/105/

Stemper, B. D., Yoganandan, N., Stineman, M. R., Gennarelli, T. A., Baisden, J. L., and Pintar, F. A. (2007). Mechanics of fresh, refrigerated, and frozen arterial tissue. *J. Surg. Res.* 139, 236–242. doi:10.1016/j.jss.2006.09.001

Van Loon, P., Klip, W., and Bradley, E. L. (1977). Length-force and volume-pressure relationships of arteries. *Biorheology* 14, 181–201.

Weisbecker, H., Pierce, D. M., Regitnig, P., and Holzapfel, G. A. (2012). Layer-specific damage experiments and modeling of human thoracic and abdominal aortas with non-atherosclerotic intimal thickening. *J. Mech. Behav. Biomed. Mater.* 12, 93–106. doi:10.1016/j.jmbbm.2012.03.012

Weisbecker, H., Viertler, C., Pierce, D. M., and Holzapfel, G. A. (2013). The role of elastin and collagen in the softening behavior of the human thoracic aortic media. *J. Biomech.* 46, 1859–1865. doi:10.1016/j.jbiomech.2013.04.025

**Conflict of Interest Statement:** The authors declare that the research was conducted in the absence of any commercial or financial relationships that could be construed as a potential conflict of interest.

*Received: 15 October 2014; accepted: 05 January 2015; published online: 28 January 2015.*

*Citation: Bell ED, Sullivan JW and Monson KL (2015) Subfailure overstretch induces persistent changes in the passive mechanical response of cerebral arteries. Front. Bioeng. Biotechnol. 3:2. doi: 10.3389/fbioe.2015.00002*

*This article was submitted to Biomechanics, a section of the journal Frontiers in Bioengineering and Biotechnology.*

# CHAPTER 5

# CONCLUSION

## 5.1 Take Away Summary

The work contained in this dissertation investigated the effect mechanical stretch at physiological and supraphysiological levels has on the cerebrovasculature as pertaining to traumatic brain injury (TBI). The findings herein are relevant to a variety of applications. They provide an improved understanding of cerebral artery mechanical properties, and the relationship between such data acquired from animal and human cerebral arteries. In addition, these data could lead to improvement of computational models of TBI, as well improved interpretation and planning for studies of cerebrovascular dysfunction. Finally, these studies provide insight into the potential role of subfailure cerebrovascular damage in disease states associated with TBI, such as second impact syndrome and stroke. Discussions of the specific conclusions taken from this dissertation within each of these areas, along with their associated applicability and the resulting outstanding questions, are here provided.

### *5.1.1 Cerebral artery mechanical properties*

When applying measured mechanical behavior of animal tissue to the human case, whether at physiological or supraphysiological levels of loading, it is important to

keep in mind the intrinsic differences between species. While scaling of mechanical and failure properties according to the relative brain masses of the two species in question are often used to translate animal tissue data to the human case (Holbourn, 1943; Ljung, 1975; Rafaels et al., 2012), it is best if these assumptions are confirmed experimentally. For example, it is normally assumed that the threshold of TBI-related impact loading a subject can endure before injury occurs increases with the mass of the brain (Holbourn, 1943; Ljung, 1975). In general, this is a logical assumption when one considers that a larger brain would have more inertia and thus it would require a larger impact force to produce the same relative motion between the brain and the skull, stretching bridging veins. However, when one wishes to use interpolated animal data in a computational model of human head injury in order to calculate local strains, these brain mass-based scaling assumptions do not provide an accurate estimate of local tissue mechanical response. The work in this dissertation showed that rat middle cerebral arteries (MCAs) have a similar level of anisotropy to human cerebral vessels at physiological loading levels (Chapter 2). However, rat MCAs are less stiff in both the axial and circumferential directions. Additionally, while rat MCAs failed at a lower ultimate stress, the failure stretch was significantly higher than for human cerebral arteries. In contrast, while sheep MCAs also fail at a seemingly higher level of axially stretch, the ultimate stress is comparable to that of human cerebral arteries. Therefore, these results show that scaling based on species brain mass does not provide an accurate estimate of cerebrovascular mechanical properties. These data emphasize the need to define the similarities and differences of mechanical properties of tissues from animal models and humans. Specifically, the similarity of the failure stresses for sheep and human cerebral vessels

highlights the fact that the biaxial mechanical properties for sheep cerebral vessels have not yet been defined in order to allow for comparison of physiological level loading between these two species.

This dissertation also shows that axial mechanical overstretch leads to strain softening of cerebral arteries, as measured in sheep (Chapter 4). When these data are considered in light of the fact that both rat and sheep MCAs fail at a higher axial stretch than humans, it would logically follow that human cerebral vessels could experience strain softening, and associated subfailure damage, following a mechanical stretch below the threshold measured in sheep. One area where these results are particularly relevant is the ongoing efforts to map the strain field within a living brain during a TBI event. Recently, gated magnetic resonance imaging (MRI) has been used in an attempt to measure these strains (Bayly et al., 2006). However, since gated MRI is unable to scan the entire brain with sufficient speed, this method requires the loading to be repeated several times to get a complete strain map. Controlled cortical impacts of perinatal rats were imaged during either 64 or 128 repeated impacts on any given animal. Unfortunately, this method completely ignores the potential for strain softening of the tissues due to repeated deformation. In addition to the strain softening behavior observed in this dissertation, it has also been observed previously that repeated loading on living brain tissue has a preconditioning like effect (Gefen and Margulies, 2004). This could be due to softening of the associated cerebral arteries, but also may indicate the potential for strain softening of neuronal tissue itself, and should be studied further. Another area where cerebrovascular strain softening could be a factor is the clinical practice of using balloon angioplasty to restore blood flow for cerebral arteries in vasospasm following

TBI (Miley et al., 2011). If the arterial wall is indeed more compliant circumferentially following injury (Converse and Monson, 2014), the normally accepted balloon inflation parameters may lead to accidental vessel rupture, and do more damage than good.

### *5.1.2 Computational models of TBI*

This work provides data that have the potential to improve the accuracy and functionality of computational models of TBI. Specifically, as mentioned above, herein is provided a more complete characterization of biaxial passive mechanical and failure properties for cerebral vessels as well as a better understanding of how cerebral arteries in rats, in particular, compare to those of humans. This improved understanding also includes strain threshold information relative to subfailure mechanical damage and autoregulatory dysfunction. Here are two examples of how this more complete understanding of these properties could improve computational models. First, accident reconstruction computational models could better calculate the strain experienced by cerebral vessels during a given injury, and subsequently determine if this strain level was high enough to possibly lead to subfailure autoregulatory dysfunction or strain softening. This analysis could be utilized for the guidance of clinical treatments, or be incorporated into a legal argument should the TBI event be related to a court case. Second, TBI models being utilized to prevent injury, using a defined threshold for subfailure cerebrovascular damage, can be used more effectively in the development of superior protective equipment such as helmets or automotive airbags.

In conjunction with computational models, this dissertation also provides needed data for strain energy functions representing cerebrovascular behavior. The strain

thresholds for alteration of smooth muscle cell (SMC) contractility (Chapter 3) and alteration of passive mechanical properties via strain softening (Chapter 4) better informs strain energy functions, such as the those from Baek et al., which seeks to represent active mechanical behavior (Baek et al., 2007a) as well as the subsequent tissue remodeling (Baek et al., 2007b). These strain energy functions, as well as the data in this dissertation, emphasize the current lack of experimental data defining strain thresholds leading to endothelial dysfunction or other layer specific damage within the wall of cerebral arteries. Determination of these thresholds should be the subject of further study.

### *5.1.3 Investigation of cerebrovascular dysfunction*

Mechanical stretch above a certain threshold leads to both alteration of SMC contractility and strain softening, as discussed above. Similar to the argument made for strain softening above, since rat and sheep cerebral arteries fail at a higher stretch than humans, it is possible that SMC contractility is altered at a lower stretch level in humans than was measured in rats. It is also possible that overstretch induced strain softening and altered SMC contractility are related. This possibility is supported by the fact that SMC contractility depends on the stiffness of the extracellular matrix (Steucke et al., 2015). This leads to the question, if autoregulation can be impaired by a change in the underlying mechanical properties, how can this be corrected clinically? One potential method is proposed in the next section in relation to stroke prevention.

In regard to the observations in this dissertation that mechanical overstretch above a threshold resulted in alteration of SMC contraction, it is believed that the results from the study in Chapter 3 are not due solely to potential circumferential strain softening, but

rather alteration in the contractility of the SMCs themselves. This is based on the fact the study in Chapter 3 was done at a low internal pressure which would minimize the effect of circumferential strain softening on the results. This conclusion is further supported by the fact that the baseline, dilated, and maximum levels of contraction were not statistically affected by overstretch. However, at higher physiological pressures, strain softening could play a larger role in the SMC response post-TBI. Therefore, the potential for mechanically-induced alteration of SMC function should be taken into account when conducting studies of cerebrovascular autoregulation that involve contractile agents. A good practical example of this is a study by Toklu et al. (Toklu et al., 2015) which showed increased contraction to endothelin-1 (ET-1) following blast TBI. They confirmed this was not a result of changes in the intrinsic SMC contractility by also measuring the unchanging contraction evoked by exposure to elevated extracellular $K^+$.

The helical orientation of collagen and SMCs in cerebral arteries suggest that axial overstretch could lead to softening of the cerebral vessels in both the axial and circumferential directions. Considering additional preliminary data from our lab which supports the idea that axial overstretch leads to circumferential softening (Converse and Monson, 2014), strain softening alone could be an aggravating factor in the proper function of autoregulatory mechanisms post-TBI. This should be taken into account in future studies investigating the active function of vessels from TBI animal models. For example, consider a hypothetical study of autoregulatory dysfunction following TBI where an injury is imposed on the intact animal and vessels are then removed for in vitro testing. This hypothetical study uses the fully dilated diameter of the removed vessel at 100 mmHg internal pressure for the reference diameter in quantifying the myogenic

response at the same pressure. However, unknown to the investigator, this vessel has undergone circumferential strain softening during the applied injury. Prior to the injury, this vessel had a fully dilated diameter of 150 μm and would have produced a myogenic contraction resulting in a diameter of 100 μm under an internal pressure of 100 mmHg (a 33% contraction). However, what the investigator observes is a fully dilated diameter of 190 μm which changes to 125 μm when 100 mmHg internal pressure is applied (a 34% contraction). The investigator therefore concludes that the applied injury did not produce any significant effect to the autoregulation. While it may be true that the myogenic response specifically was not affected by the injury, this study produces a false conclusion that the vessel itself was not affected. In reality, the diameter of the artery is increased by 25% relative to what it should be under those conditions. This hypothetical scenario would result in elevated arterial pressures being propagated to smaller arterioles downstream, potentially leading to secondary hemorrhage or vasogenic edema (Faraci and Heistad, 1990; Tsubokawa and Katayama, 1998). Therefore, the false impression given by the study that the vessel is unaffected would ignore a potentially treatable mechanism of injury. Many TBI animal studies of cerebrovascular autoregulation use the assumption that vessels tested from the injured brain have comparable baseline parameters to samples taken from uninjured brains (Bukoski et al., 1997; Golding et al., 1998; Golding et al., 1999; Mathew et al., 1999; Toklu et al., 2015). While it is not always possible to measure pre-injury baseline properties of a particular vessel, such as with a closed head impact animal model, some consideration should be made for these potential changes due to strain softening in the analysis of the collected data.

The data in this dissertation showing cerebrovascular SMC function is affected by

mechanical overstretch also lend support to the concept that TBI induced injury to the cerebrovasculature is a combination of mechanical and chemical effects (DeWitt and Prough, 2003), rather than just resulting from post-TBI chemical insults as has also been proposed (Golding et al., 1999). The previous studies of autoregulatory dysfunction cited near the end of the previous paragraph do not all agree. Some show TBI-induced dysfunction of various pathways (Golding et al., 1998; Mathew et al., 1999; Toklu et al., 2015) while others do not (Bukoski et al., 1997; Golding et al., 1999). These seemingly contradictory results have been attributed to the effect the altered chemical environment in the post-TBI brain has on cerebrovascular function (DeWitt and Prough, 2003; Golding et al., 1999). While the altered chemical milieu in the injured brain can certainly affect cerebrovascular function, the potential contribution of mechanically-induced changes in SMC function should not be ignored, and future studies should be planned accordingly.

### *5.1.4 Cerebrovascular damage in post-TBI disease states*

Stretch-induced strain softening and autoregulatory dysfunction could play a role in second impact syndrome. Second impact syndrome refers to the situation where a head injury is sustained before the symptoms from a previous head injury have yet to be fully resolved. A minor injury during this vulnerable period combines with lingering cerebrovascular autoregulatory dysfunction to subsequently produce significant brain damage, resulting in a mortality rate of up to 50% (Cantu and Gean, 2010; Laskowski et al., 2015). Considering the mechanical contribution of pressurized cerebral vessels within to the brain, a reduction in the stiffness of these vessels due to a previous injury could

make the brain susceptible to minor impacts producing much larger strains then they otherwise would. Additionally, mechanically-induced autoregulatory dysfunction could persist after the chemical environment in the brain returned to normal as it would require biological remodeling of the vessel wall to be corrected.

Subfailure mechanical damage, measured in this dissertation as strain softening, could also play a role in stroke following TBI. It has been shown that a person is significantly more susceptible to stroke following a TBI event, even 5 years later (Burke et al., 2013; Chen et al., 2011; Hills et al., 2012). It is possible that this increased susceptibility could be due to altered mechanical properties of cerebral arteries. For example, greater circumferential stretch in response to physiological pressures would lead to increased arterial pressure in smaller downstream arteries and thus potentially lead to rupture of smaller vessels. Additionally, it should be noted that axial failure properties did show a decreasing trend following overstretch in vitro, but this was not found to be significant (Chapter 4). However, it is possible that the observed increase in subfailure passive mechanical compliance combined with natural repair mechanisms, such as matrix metalloproteinase (MMP) upregulation following injury (Asahi et al., 2001; Chase and Newby, 2003) could result in further altered mechanical properties (Monson et al., 2011), potentially resulting in decreased failure properties over time. These potentially decreased failure properties would make a subject more likely to have vascular failure (stroke) at a later time.

This leads to the question of how such TBI-induced subfailure mechanical damage to the cerebrovasculature could be treated. Methods of surgical intervention have been developed for other cerebrovascular problems, such as aneurysm coils (Rezek et al.,

2013) or the use of balloon angioplasty for reopening cerebral arteries that are constricted due to vasospasm (Miley et al., 2011). However, a major roadblock with the development of surgical interventions to treat strain softened cerebral arteries is the clinical identification of such arteries in order to treat them. One possible method of treatment is pharmaceutical rather than surgical, and may remove this need to clinically identify sites of vascular strain softening prior to treatment. Preliminary data from our lab indicates that strain softening is associated with the presence of unwound collagen fibrils (Converse and Monson, 2014) which can be labeled preferentially by collagen mimetic peptides (CMPs) (Li et al., 2012; Walther, 2015). If a pharmaceutical agent that either promotes collagen deposition or reduces collagen degradation (Akbik et al., 2014; Banerjee et al., 2015) was to be bound to CMP rather than the fluorophores used in our preliminary studies, it could lead to improved mechanical properties in these softened vessels and reduce the subsequent risk of stroke and second impact syndrome.

## 5.2 Looking Forward

In addition to the outstanding questions mentioned above, there are several questions still to be answered regarding cerebrovascular mechanics under both physiological and supraphysiological loading. These questions are separated here into two categories for discussion, based on the relevant loading level. Some potential methods for addressing these questions are also proposed. Following the discussion of supraphysiological loading, a broader question pertaining to the deformation of the cerebrovasculature during head injury is also discussed.

*5.2.1 Cerebrovascular mechanics under physiological loading*

Properly accounting for residual strain is important to correctly analyzing the mechanical behavior of cerebral arteries. To do this, the zero stress state, rather than the zero load state, should be utilized as the reference configuration (Chuong and Fung, 1986). All three studies in this dissertation used the zero load state as the reference. Specifically, residual strain in the circumferential direction was ignored. This was done due to two different problems associated with the measurement of the circumferential residual strain opening angle, which would need to be overcome. First, for smaller vessels, such as rat MCAs, the force attracting the sample to the bottom of the dissection dish seemed to be stronger than the forces within the tissue which would cause a radially sliced cross section to spring open. The result was that the cut cross section would not open as it should, but rather would remain in whatever configuration it was in when it touched the bottom. It is unknown if this was due to van der Waals forces between the sample and the dish or some other attractive force, but measurement of opening angle was attempted using dissection dishes where the bottom was polystyrene, glass, or silicone without improvement of the result. The second hurdle for properly accounting for circumferential residual strain is that the opening angle of larger vessels varies dramatically along the length of a given sample (Monson et al., 2008). A way to account for this variation along the length of a sample would need to be developed. In addition to circumferential residual strains, it should also be determined if cerebral vessels also exhibit any other types of residual strain observed in some peripheral arteries. For example, as discussed in the introductory chapter, coronary arteries have been shown to exhibit residual shear strain (Wang and Gleason, 2014), while the levels of

circumferential and axial residual strains in aorta differ greatly from layer to layer within the vessel wall (Holzapfel et al., 2007).

In addition to layer-specific residual strain, the mechanical response of the individual layers of cerebral arteries should be accounted for (Holzapfel et al., 2000), especially during injury. When using larger cerebral arteries, such as from sheep or human, it would be possible to physically separate these layers for traditional mechanical testing in order to define the layer-specific mechanical properties. Additionally, the strength of the connection between adjacent layers could be measured when they are separated, which would be useful as boundary conditions for through wall stress analysis. However, this physical separation for layer-specific mechanical characterization would be prohibitively difficult with smaller arteries such as rat MCAs due to the small scale and subsequent fragility of the individual layers. For these small vessels, perhaps layer-specific mechanical differences could be inferred from measured layer-specific strains. Marker tracking could be employed to track the strains in the adventitial and the intimal layers. Markers of one type or color could be attached to the adventitia while other markers could be perfused through the sample in order for them to adhere to the endothelial cells. These measured strains could then be used in a finite element model of the mounted vessel in order to calculate the through wall stresses and strains.

The effect of tethering by adjacent connective tissues in vivo on the vessel response, both active and passive, is another poorly understood consideration. It has been shown in cerebral arteries that the passive circumferential response is altered when such tethering is in place (Steelman et al., 2010). Specifically, the artery circumference becomes elliptical rather than circular at pressures above and below physiological levels.

Such an elliptical diameter could result in further decreased blood flow at sub-physiological pressures, compounding any autoregulatory problems. Additionally, mechanical interaction of the associated connective tissues can also affect the active response. This is illustrated by the presence of vasospasm following mechanical stretch applied to associated connective tissue, but not when applied to the cerebral arteries themselves (Arutiunov et al., 1974). It has also been noted previously (Zhang et al., 2002) that there is a current lack of sufficient data describing the mechanical interaction between cerebral vessels and the nervous tissue of the brain. One possible way to determine these properties is to excise a piece of cortex (to simplify the geometry) and apply subdamage level deformations to a pial artery still attached to the surface. During this deformation, the surface strains on both the vessel and the surrounding brain tissue would be tracked via strain markers. Next, the vessel in question would be dissected and the isolated biaxial mechanical properties determined. These vessel-specific properties, along with the combined surface strains, could be incorporated into a finite element model of the excised cortical section. The boundary conditions between the vessel and surrounding brain tissue would then be iteratively optimized in order to find a best fit between the surface strains calculated by the model and those measured experimentally.

The relative mechanical contribution of active SMCs between animal and human cerebral arteries is also poorly understood. As discussed at some length in the introductory chapter, the mechanical contribution of active SMCs is an important factor in the mechanical behavior of cerebral arteries. Various methods to measure this contribution have been described previously (Coulson et al., 2004; Wagner and Humphrey, 2011) utilizing SMC tone generated by either the myogenic response or

pharmacological agents. However, the relative mechanical contribution of SMC tone between species has not been previously investigated. Building on the work in this dissertation, comparing the biaxial passive mechanical properties of rat MCA and human pial arteries (Bell et al., 2013), such comparison studies could be done which also incorporate active SMC tone.

*5.2.2 Cerebrovascular mechanics under supraphysiological loading*

Active SMCs could potentially affect the failure properties of cerebral arteries, in addition to the mechanical response to physiological level loading discussed in the previous section. In contrast to subfailure contributions of SMC tone, a complete investigation of this contribution to failure properties should incorporate both myogenic tone and chemically induced SMC tone. This is because the active state of cerebral arteries is different for an initial traumatic event than for repeated impacts shortly thereafter. In order to measure how SMC tone affects failure properties related to an initial traumatic event, a protocol that utilizes myogenic tone would be more representative of the level of SMC tone under physiological conditions prior to injury. On the other hand, investigation of SMC tone effect on the failure properties relative to a repeated injury event may be better accomplished with pharmacologically-induced contraction. These elevated levels of chemically-induced SMC tone would be more indicative of the state of cerebral vessels shortly after an initial injury due to the elevated levels of several contractile agents present in the brain post-TBI, such as ET-1 and extracellular $K^+$.

Layer-specific deformation and damage from supraphysiological subfailure level

loading is another important topic for further investigation. As mentioned previously, preliminary data from our lab show that subfailure loading can cause layer-specific ruptures (Converse and Monson, 2014) as well as layer-specific alteration and/or damage to collagen (Walther, 2015). This microstructural rearrangement or damage is likely related to the strain softening observed in Chapter 4 (Bell et al., 2015). In order to more fully understand the consequences of overstretch on specific layers of cerebral arteries, it would be ideal to measure the layer-specific deformation during an overstretch in real time. Similar to the physiological loading discussion above, the attachment of different strain markers to the adventitia and luminal surfaces would enable quantification of the inner and outer layers. However, deformations to the media would still not be directly measured. While not in real time, multiphoton confocal microscopy can be used to preferentially image collagen and elastin through the depth of the vessel wall (Zoumi et al., 2004). Through wall deformation could be measured in this microstructural imaging. The vessel testing system developed for the study in Chapter 3 has the capability of being mounted to the stage of a confocal microscope. While this capability was not used in that study, it could be implemented in order to image the fiber geometry through the vessel wall while under various static loading levels. Such a protocol could also be used to image the through wall microstructure before and after overstretch to detect damage. The biggest hurdle to such an effort would be the observed alteration in tare load length following overstretch in Chapter 4, making it challenging to confirm subsequent scans are imaging the same tissue region in the sample in order to compare the scans.

A better understanding of vessel branch mechanics and how they may affect failure and subfailure behavior of cerebral vessels is also needed. The geometry of vessel branch

points suggests that these areas would experience stress concentrations during deformation. Additionally, unpublished human vessel data from our lab indicates that failure is more likely to occur at branch points than in unbranched regions during isolated vessel tests. The role of branch mechanics in failure should be further investigated by both observation of sites of failure during axial testing as well as tests which directly apply tension to branches to measure the failure stress associated with separation of branches from the main vessel.

While the development of strain energy functions to describe arterial mechanical behavior, as described in the introduction chapter, has made good progress in recent years, there is still no microstructurally-based strain energy function that is applicable to both physiological and injury level loading. One group has proposed a strain energy function using separate fiber families to represent the different microstructural components, the parameters for which can be changed to account for fiber degradation (Zeinali-Davarani et al., 2013). A function such as this is a good step in the right direction, but the value of corresponding function parameters related to microstructural reorganization or damage due to mechanical insult have yet to be determined. Additionally, a strain energy function accounting for damage should account for the properties intrinsic to specific layers of the vessel so as to account for layer-specific failure as well. One limiting factor to typical strain energy functions is the commonly used psuedoelasticity assumption (Humphrey et al., 1990). This typically results in only using data where vessel loading is increasing to determine the function parameters. For example, in Chapter 2 (Bell et al., 2013), data from the circumferential inflation tests, but not the axial stretch tests, were used to determine the reported function parameters. This

was because axial test data were very poorly represented by the function due to the circumferential stretch decreased during increasing axial stretch. Since it has been previously argued that the primary mode of loading to cerebral vessels during impact TBI is axial stretch (Goldsmith, 2001; Monson et al., 2003), any strain energy function meant to represent such responses would ideally be able to overcome this weakness. One solution for this would be the development of a piecewise strain energy function which uses one set of parameters when the stretch is increasing, and another set when the stretch is decreasing. Unfortunately, since both types of deformations can happen simultaneously along different axes as just explained, the complexity of such a function could potentially require prohibitively high computational power in order to utilize it in computational models of TBI.

There are also additional questions related to stretch-induced autoregulatory dysfunction that have yet to be investigated. First of all, in Chapter 3, discussion of the results led to the hypothesis that the observed change in SMC function was due to altered function in voltage sensitive calcium channels in the membrane of the SMCs. This hypothesis could be indirectly tested by repeating the tests conducted in Chapter 3 while using a blocking agent for voltage sensitive calcium channels, such as tamoxifen (Song et al., 1996). While this inhibitor also results in reduced extracellular $K^+$ evoked SMC contraction, if the level of SMC tone following the injurious level of overstretch is still reduced by a similar percentage to that in Chapter 3, relative to a tamoxifen-treated baseline test, than alteration of voltage sensitive calcium channel function as the cause would be proven incorrect. There are also other autoregulatory mechanisms which could be affected by mechanical overstretch. For example, since it has been observed that the

endothelium ruptures prior to failure in peripheral arteries (Vaishnav and Vossoughi, 1987), it is logical to assume that subfailure mechanical stretch could also lead to dysfunction of endothelial cell-mediated dilation. This could be tested using a protocol similar to that in Chapter 3 that measures the level of vasodilation evoked by the application of acetylcholine, an endothelial cell-dependant dilator, before and after overstretch.

The phenomenon of strain softening in cerebral arteries is still not fully understood. As discussed previously, any potential circumferential softening due to axial overstretch needs to be better defined, and this work is currently underway in our lab (Converse and Monson, 2014). Additionally, the question of rate dependence on overstretch-induced strain softening of cerebral arteries should be investigated. Failure properties of human cerebral vessels have been shown to be strain rate independent up to 500 $s^{-1}$ (Chalupnik, 1971; Monson et al., 2003). However, while the failure properties of the sheep MCAs in Chapter 4 (Bell et al., 2015) were also not affected by previous strain softening, the subfailure alteration to SMC function of rat vessels in Chapter 3 was strain rate dependent. These combined results suggest that while the failure properties of cerebral arteries may not be rate dependent, the subfailure strain softening might be. This can be investigated further using testing methods similar to those in Chapter 4, while incorporating varied strain rates.

The question of a potential correlation between strain softening and altered SMC function following overstretch should be further investigated. Ideally, tests should be conducted that incorporate measurement of circumferential strain softening as well as SMC function before and after overstretch. It would, of course, be best to conduct these

tests on human cerebral arteries. However, due to the low availability of viable human cerebral vessels, larger cerebral vessels from animals, like sheep, would be suitable. This would also allow for direct comparison of new results to data from Chapter 4 and current investigations into axial overstretch-induced circumferential softening which utilize sheep cerebral arteries (Converse and Monson, 2014). It is possible that the repeated baseline axial stretches applied in Chapter 4 may be detrimental to the viability of SMC function in an in vitro sample. Additionally, the current investigation of circumferential softening includes correlation of softening with microstructural damage following overstretch (Converse and Monson, 2014). As such, an investigation of potential correlations between overstretch-induced alteration of SMC function and strain softening could be accomplished by using imaging of microstructural damage as a measurement of softening, rather than repeated mechanical stretch tests. This future study should therefore avoid pulling samples to failure so the level of overstretch-induced microstructural damage can be measured. The basic structure of such a protocol would be to measure the SMC response of a vessel in vitro, apply an overstretch and then repeat the evaluation of SMC response again. Finally, the vessel would be carefully dismounted from the test system and the microstructural damage analyzed via staining with CMP and confocal microscopy (Li et al., 2012; Walther, 2015).

In order to better understand the long-term consequences of subfailure damage to cerebral blood vessels, the subsequent remodeling of damaged vessels should be studied. Such studies in vitro would require an organ culture system similar to one previously used to measure changes in arterial contraction due to hypertension over a seven day time period (Han and Ku, 2001). While the strain softening observed in Chapter 4 (Bell et al.,

2015) persisted for the 60 minutes of testing, and as long as 6 hours in preliminary data, an organ culture system could determine if such changes persisted over much longer time periods. In addition to just looking at how damaged vascular tissue remodels in a healthy chemical environment, the contents of such an organ culture bath could be altered to mirror specific aspects of the chemical environment present in the brain following TBI. For example, concentrations of ET-1 (Foley et al., 1994; Petrov, 2009; Petrov et al., 2002) and acetylcholine (Hayes et al., 1991; Lyeth and Hayes, 1992) in the brain are increased following TBI. By exposing subfailure overstretched vessels to elevated concentrations of specific compounds in the organ culture, the effect those specific compounds have on the vessel remodeling process could be established. Such studies would provide a better understanding of what the specific targets for clinical intervention should be in order to ensure proper healing of the cerebral vasculature after injury. Additionally, it has been shown that the levels of matrix metalloproteinase (MMP-2 and MMP-9), which degrade collagen, are significantly elevated in isolated peripheral veins following a sustained axial overstretch (Meng et al., 1999). The levels of MMP that develop in an acutely overstretched cerebral artery should be investigated, along with the effects these compounds have on the remodeling of injured vessels. Methods to investigate the specific effects MMP degradation of vascular extracellular matrix has on the properties of cerebral arteries have been proposed by our lab, but are not yet published.

*5.2.3 Traumatic deformation of cerebrovasculature*

One major outstanding issue on the subject of mechanical injury to cerebrovascular during impact TBI is the fact that the actual deformation experienced by the cerebrovasculature during an impact event is poorly understood. Without this information, any attempt to determine injury strain thresholds is still not going to be directly applicable for clinical applications or the development of protective equipment. One previous method to measure strain within the brain during an impact event utilized high-speed tracking of radio-opaque strain markers in cadaver heads (Hardy et al., 2001). Unfortunately, while this method does provide a general strain distribution during impact, the mechanical properties of living and cadaver brains are quite different (Gefen and Margulies, 2004). In addition to the mechanical differences due to the loss of vascular pressurization at death, which potentially could be overcome by repressurizing the cadaver brain (Alem et al., 1977; Stalnaker et al., 1977), the mechanical properties of brain tissue are significantly different only 24 hours after death as compared to immediately postmortem (Vappou et al., 2008). A more recent attempt to measure strains in the living brain during TBI utilized gated MRI during controlled cortical impact on rats (Bayly et al., 2006), as was discussed in the first section of this chapter. Again briefly, the limitations of the scanning speed for gated MRI made it incapable of scanning the entire brain fast enough to capture the event in real time with sufficient resolution. Accordingly, it was required that the cortical impact be repeated over one hundred times on some animals, ignoring any effects from repeated loading such as strain softening or preconditioning. A somewhat improved version of this MRI strain tracking has been used to track deformations within the brain during low-level head impacts on live human

volunteers (Knutsen et al., 2014), which required only scanning eight repeated impact events to capture the desired strain distribution. However, since this study was conducted on human volunteers, injury level loading could not be imposed. Also, if this method was used on animals where injury level impacts could be used, the need for repeated scans to capture the desired deformations still has the same pitfalls as the rat study just discussed. Therefore, there is a pressing need to develop a method by which high resolution, real-time strain distributions can be measured in a living brain during a single injury level loading event. It is possible that the strains on the cortical surface could at least be measured by tracking the pial vasculature itself. Two potential methods to do this are here proposed.

Deformations of the pial vasculature on the superior cortical surface could be visually tracked during an injurious impact event using an animal model where the top of the skull has been replaced with a transparent skull cap. Such a model has been used on rhesus monkeys in the past in order to measure rotation of the brain within the skull during TBI (Hirsch et al., 1970). Multiple high-speed cameras at differing viewing angles could be used to record the three-dimensional motion of the pial arteries during impact. Individual branch points could then be used as strain markers to calculate the resulting surface strains. While these measurements of strains on the cortical surface would not provide direct information about strains elsewhere in the brain, they could be used to better validate finite element head injury models capable of then better estimating subcortical strains.

Another possible method to track pial artery motion during head impact takes advantage of the fact that these vessels are innervated by perivascular nerves originating

outside the cranium. Therefore, tracking these nerves would indirectly track the deformation experience by the pial arteries. Since these perivascular nerves are present in all pial arteries at varying density, and since they are not present in subcortical arteries (Hamel, 2006; Handa et al., 1990), if a method could be developed to inject these nerves with a radio-opaque agent, strains over the entire cortical surface could be tracked in a living brain during impact using high-speed radiography (Lavrinovich et al., 2013). Several methods have been developed to preferentially label the length of a living optic nerve (Kanamori et al., 2010), and at least short segments of other nerve fibers (Kuwabara, 2012; Progatzky et al., 2013), but these are primarily fluorescent markers not visible to X-ray. One labeling method that may provide a basis for the development of this perivascular nerve staining utilizes infusion of gadolinium-labeled albumin into nerve fibers (Lonser et al., 1998). In sufficiently high concentrations, gadolinium is visible on X-ray and the infusion method in peripheral nerves described by Lonser et al. resulted in the gadolinium being distributed along the axonal fibers for long distances, contained within the epineurium. One additional complication would be the need to selectively label some perivascular nerves, but not all. Due to the high vascular density in the brain, staining all the perivascular nerves in this way would result in X-ray images that are just a cloud of indistinguishable signal. One way to avoid this is to only stain perivascular nerves in certain regions, like just the inferior surface of the left hemisphere. This would allow high rate radiographic deformation tracking on the surface of these selected structures during an impact. Impact strains in other regions would then be obtained from similar impacts to other animals (to avoid repeated impacts on a single animal). The combined results from tracking the various cortical surface regions

individually would produce a complete strain map over the surface of the living brain during an impact TBI event. Again, these surface strains could then be used to better validate finite element models of TBI which would then be used to calculate subcortical strains.

## 5.3 Final Thoughts

Traumatic brain injury is frequently referred to as a silent epidemic since many of the associated problems that result from it are not always visible via outwardly observable symptoms. While this dissertation has focused on the effect of mechanical stretch of the larger cerebral arteries associated with impact TBI, this is only one of many aspects of TBI worth investigating. Just a few examples of some additional important topics of investigation related to TBI are autoregulatory dysfunction in smaller arterioles, effects of blast TBI on cerebrovascular autoregulation, generation of diffuse axonal injury, concussion, chronic traumatic encephalopathy, as well as the resulting brain damage and impaired social functionality that often result from TBI. Another important area of research is TBI resulting from head acceleration without head impact, such as occurs in contact sports or during car accidents with whiplash. While the narrow focus of this dissertation is not intended any way to downplay the importance of these other aspects of TBI, in the end the important thing to remember is that injury to the cerebrovasculature can lead to additional injury or death of neural tissue in the brain. As such, it is this author's sincere hope that the work contained in this dissertation will be a meaningful addition to the utterly vast amount of knowledge still needed to fully understand TBI and adequately treat those who suffer from it.

## 5.4 References

Akbik, D., Ghadiri, M., Chrzanowski, W., Rohanizadeh, R., 2014. Curcumin as a wound healing agent. Life Sciences 116, 1-7.

Alem, N.M., Stalnaker, R.L., Melvin, J.W., 1997. Measurement of head impact response. In International IRCOBI: Conference on the Biomechanics of Impact. Berlin, Germany.

Arutiunov, A.I., Baron, M.A., Majorova, N.A., 1974. The role of mechanical factors in the pathogenesis of short-term and prolonged spasm of the cerebral arteries. Journal of Neurosurgery 40, 459-472.

Asahi, M., Wang, X., Mori, T., Sumii, T., Jung, J.C., Moskowitz, M.A., Fini, M.E., Lo, E.H., 2001. Effects of matrix metalloproteinase-9 gene knock-out on the proteolysis of blood-brain barrier and white matter components after cerebral ischemia. Journal of Neuroscience 21, 7724-7732.

Baek, S., Gleason, R.L., Rajagopal, K.R., Humphrey, J.D., 2007a. Theory of small on large: potential utility in computations of fluid-solid interactions in arteries. Computer Methods in Applied Mechanics and Engineering 196, 3070-3078.

Baek, S., Valentin, A., Humphrey, J.D., 2007b. Biochemomechanics of cerebral vasospasm and its resolution: II. Constitutive relations and model simulations. Annals of Biomedical Engineering 35, 1498-1509.

Banerjee, P., Suguna, L., Shanthi, C., 2015. Wound healing activity of a collagen-derived cryptic peptide. Amino Acids 47, 317-328.

Bayly, P.V., Black, E.E., Pedersen, R.C., Leister, E.P., Genin, G.M., 2006. In vivo imaging of rapid deformation and strain in an animal model of traumatic brain injury. Journal of Biomechanics 39, 1086-1095.

Bell, E.D., Kunjir, R.S., Monson, K.L., 2013. Biaxial and failure properties of passive rat middle cerebral arteries. Journal of Biomechanics 46, 91-96.

Bell, E.D., Sullivan, J.W., Monson, K.L., 2015. Subfailure overstretch induces persistent changes in the passive mechanical response of cerebral arteries. Frontiers in Bioengineering and Biotechnology 3.

Bukoski, R.D., Wang, S.N., Bian, K., DeWitt, D.S., 1997. Traumatic brain injury does not alter cerebral artery contractility. American Journal of Physiology 272, H1406-1411.

Burke, J.F., Stulc, J.L., Skolarus, L.E., Sears, E.D., Zahuranec, D.B., Morgenstern, L.B., 2013. Traumatic brain injury may be an independent risk factor for stroke. Neurology 81, 33-39.

Cantu, R.C., Gean, A.D., 2010. Second-impact syndrome and a small subdural hematoma: an uncommon catastrophic result of repetitive head injury with a characteristic imaging appearance. Journal of Neurotrauma 27, 1557-1564.

Chalupnik, J.D.D.C.H.M.H.C., 1971. Material properties of cerebral blood vessels. Department of Mechanical Engineering, University of Washington, Seattle, Wash.

Chase, A.J., Newby, A.C., 2003. Regulation of matrix metalloproteinase (matrixin) genes in blood vessels: a multi-step recruitment model for pathological remodelling. Journal of Vascular Research 40, 329-343.

Chen, Y.H., Kang, J.H., Lin, H.C., 2011. Patients with traumatic brain injury: population-based study suggests increased risk of stroke. Stroke 42, 2733-2739.

Chuong, C.J., Fung, Y.C., 1986. On residual stresses in arteries. Journal of Biomechanical Engineering 108, 189-192.

Converse, M., Monson, K.L., 2014. Alteration and failure of cerebral artery internal elastic lamina following mechanical insult, 7th World Congress of Biomechanics, Boston, MA.

Coulson, R.J., Cipolla, M.J., Vitullo, L., Chesler, N.C., 2004. Mechanical properties of rat middle cerebral arteries with and without myogenic tone. Journal of Biomechanical Engineering 126, 76-81.

DeWitt, D.S., Prough, D.S., 2003. Traumatic cerebral vascular injury: the effects of concussive brain injury on the cerebral vasculature. Journal of Neurotrauma 20, 795-825.

Faraci, F.M., Heistad, D.D., 1990. Regulation of large cerebral arteries and cerebral microvascular pressure. Circulation Research 66, 8-17.

Foley, P.L., Caner, H.H., Kassell, N.F., Lee, K.S., 1994. Reversal of subarachnoid hemorrhage-induced vasoconstriction with an endothelin receptor antagonist. Neurosurgery 34, 108-112; discussion 112-103.

Gefen, A., Margulies, S.S., 2004. Are in vivo and in situ brain tissues mechanically similar? Journal of Biomechanics 37, 1339-1352.

Golding, E.M., Contant, C.F., Jr., Robertson, C.S., Bryan, R.M., Jr., 1998. Temporal effect of severe controlled cortical impact injury in the rat on the myogenic response of the middle cerebral artery. Journal of Neurotrauma 15, 973-984.

Golding, E.M., Steenberg, M.L., Contant, C.F., Jr., Krishnappa, I., Robertson, C.S., Bryan, R.M., Jr., 1999. Cerebrovascular reactivity to $CO_2$ and hypotension after mild cortical impact injury. American Journal of Physiology 277, H1457-1466.

Goldsmith, W., 2001. The state of head injury biomechanics: past, present, and future: part 1. Critical Reviews in Biomedical Engineering 29, 441-600.

Hamel, E., 2006. Perivascular nerves and the regulation of cerebrovascular tone. Journal of Applied Physiology 100, 1059-1064.

Han, H.C., Ku, D.N., 2001. Contractile responses in arteries subjected to hypertensive pressure in seven-day organ culture. Annals of Biomedical Engineering 29, 467-475.

Handa, Y., Caner, H., Hayashi, M., Tamamaki, N., Nojyo, Y., 1990. The distribution pattern of the sympathetic nerve fibers to the cerebral arterial system in rat as revealed by anterograde labeling with WGA-HRP. Experimental Brain Research 82, 493-498.

Hardy, W.N., Foster, C.D., Mason, M.J., Yang, K.H., King, A.I., Tashman, S., 2001. Investigation of head injury mechanisms using neutral density technology and high-speed biplanar X-ray. Stapp Car Crash Journal 45, 337-368.

Hayes, R.L., Jenkings, L.W., Lyeth, B.G., 1991. Neuropharmacological mechanisms of traumatic brain injury: acetylcholine and excitatory amino acids. Journal of Neurotrauma 8, S173-S187.

Hills, N.K., Johnston, S.C., Sidney, S., Zielinski, B.A., Fullerton, H.J., 2012. Recent trauma and acute infection as risk factors for childhood arterial ischemic stroke. Annals of Neurology 72, 850-858.

Hirsch, A.E., Ommaya, A.K., Mahone, R.H., 1970. Tolerance of subhuman primate brain to cerebral concussion, in: Gurdjian, E.S., Lange, W.A., Patrick, L.M., Thomas, L.M. (Eds.), Impact Injury and Crash Protection. Charles C Thomas, Springfield, IL, pp. 352-371.

Holbourn, A.H.S., 1943. Mechanics of head injuries. The Lancet 242, 438-441.

Holzapfel, G., Gasser, T., Ogden, R., 2000. A new constitutive framework for arterial wall mechanics and a comparative study of material models. Journal of Elasticity 61, 1-48.

Holzapfel, G.A., Sommer, G., Auer, M., Regitnig, P., Ogden, R.W., 2007. Layer-specific 3D residual deformations of human aortas with non-atherosclerotic intimal thickening. Annals of Biomedical Engineering 35, 530-545.

Humphrey, J.D., Strumpf, R.K., Yin, F.C., 1990. Determination of a constitutive relation for passive myocardium: II. parameter estimation. Journal of Biomechanical Engineering 112, 340-346.

Kanamori, A., Catrinescu, M.M., Traistaru, M., Beaubien, R., Levin, L.A., 2010. In vivo imaging of retinal ganglion cell axons within the nerve fiber layer. Investigative Ophthalmology and Visual Science 51, 2011-2018.

Knutsen, A.K., Magrath, E., McEntee, J.E., Xing, F., Prince, J.L., Bayly, P.V., Butman, J.A., Pham, D.L., 2014. Improved measurement of brain deformation during mild head acceleration using a novel tagged MRI sequence. Journal of Biomechanics 47, 3475-3481.

Kuwabara, N., 2012. Neuroanatomical technique for studying long axonal projections in the central nervous system: combined axonal staining and pre-labeling in parasagittal gerbil brain slices. Biotechnic & Histochemistry : Official Publication of the Biological Stain Commission 87, 413-422.

Laskowski, R.A., Creed, J.A., Raghupathi, R., 2015. Pathophysiology of mild TBI: implications for altered signaling pathways, in: Kobeissy, F.H.P. (Ed.), Brain Neurotrauma: Molecular, Neuropsychological, and Rehabilitation Aspects, Boca Raton (FL).

Lavrinovich, I.V., Zharova, N.V., Petin, V.K., Ratakhin, N.A., Fedushchak, V.F., Shlyakhtun, S.V., Erfort, A.A., 2013. A compact pulsed X-ray source for high-speed radiography. Instruments and Experimental Techniques 56, 329-334.

Li, Y., Foss, C.A., Summerfield, D.D., Doyle, J.J., Torok, C.M., Dietz, H.C., Pomper, M.G., Yu, S.M., 2012. Targeting collagen strands by photo-triggered triple-helix hybridization. Proceedings of the National Academy of Sciences 109, 14767-14772.

Ljung, C., 1975. A model for brain deformation due to rotation of the skull. Journal of Biomechanics 8, 263-274.

Lonser, R.R., Weil, R.J., Morrison, P.F., Governale, L.S., Oldfield, E.H., 1998. Direct convective delivery of macromolecules to peripheral nerves. Journal of Neurosurgery 89, 610-615.

Lyeth, B.G., Hayes, R.L., 1992. Cholinergic and opioid mediation of traumatic brain injury. Journal of Neurotrauma 9 (Supplement 2), S463-474.

Mathew, B.P., DeWitt, D.S., Bryan, R.M., Jr., Bukoski, R.D., Prough, D.S., 1999. Traumatic brain injury reduces myogenic responses in pressurized rodent middle cerebral arteries. Journal of Neurotrauma 16, 1177-1186.

Meng, X., Mavromatis, K., Galis, Z.S., 1999. Mechanical stretching of human saphenous vein grafts induces expression and activation of matrix-degrading enzymes associated with vascular tissue injury and repair. Experimental and Molecular Pathology 66, 227-237.

Miley, J.T., Tariq, N., Souslian, F.G., Qureshi, N., Suri, M.F., Tummala, R.P., Vazquez, G., Qureshi, A.I., 2011. Comparison between angioplasty using compliant and noncompliant balloons for treatment of cerebral vasospasm associated with subarachnoid hemorrhage. Neurosurgery 69, 161-168; discussion 168.

Monson, K.L., Barbaro, N.M., Manley, G.T., 2008. Biaxial response of passive human cerebral arteries. Annals of Biomedical Engineering 36, 2028-2041.

Monson, K.L., Goldsmith, W., Barbaro, N.M., Manley, G.T., 2003. Axial mechanical properties of fresh human cerebral blood vessels. Journal of Biomechanical Engineering 125, 288-294.

Monson, K.L., Matsumoto, M.M., Young, W.L., Manley, G.T., Hashimoto, T., 2011. Abrupt increase in rat carotid blood flow induces rapid alteration of artery mechanical properties. Journal of the Mechanical Behavior of Biomedical Materials 4, 9-15.

Petrov, T., 2009. Amelioration of hypoperfusion after traumatic brain injury by in vivo endothelin-1 knockout. Canadian Journal of Physiology and Pharmacology 87, 379-386.

Petrov, T., Steiner, J., Braun, B., Rafols, J.A., 2002. Sources of endothelin-1 in hippocampus and cortex following traumatic brain injury. Neuroscience 115, 275-283.

Progatzky, F., Dallman, M.J., Lo Celso, C., 2013. From seeing to believing: labelling strategies for in vivo cell-tracking experiments. Interface Focus 3, 20130001.

Rafaels, K.A., Bass, C.R., Panzer, M.B., Salzar, R.S., Woods, W.A., Feldman, S.H., Walilko, T., Kent, R.W., Capehart, B.P., Foster, J.B., Derkunt, B., Toman, A., 2012. Brain injury risk from primary blast. The Journal of Trauma and Acute Care Surgery 73, 895-901.

Rezek, I., Mousan, G., Wang, Z., Murad, M.H., Kallmes, D.F., 2013. Coil type does not affect angiographic follow-up outcomes of cerebral aneurysm coiling: a systematic review and meta-analysis. American Journal of Neuradiology 34, 1769-1773.

Song, J., Standley, P.R., Zhang, F., Joshi, D., Gappy, S., Sowers, J.R., Ram, J.L., 1996. Tamoxifen (estrogen antagonist) inhibits voltage-gated calcium current and contractility in vascular smooth muscle from rats. Journal of Pharmacology and Experimental Therapeutics 277, 1444-1453.

Stalnaker, R.L., Melvin, J.W., Nusholtz, G.S., Alem, N.M., Benson, J.B., 1977. Head impact response. SAE Technical Paper 770921.

Steelman, S.M., Wu, Q., Wagner, H.P., Yeh, A.T., Humphrey, J.D., 2010. Perivascular tethering modulates the geometry and biomechanics of cerebral arterioles. Journal of Biomechanics 43, 2717-2721.

Steucke, K.E., Tracy, P.V., Hald, E.S., Hall, J.L., Alford, P.W., 2015. Vascular smooth muscle cell functional contractility depends on extracellular mechanical properties. Journal of Biomechanics 48, 3044-3051.

Toklu, H.Z., Muller-Delp, J., Yang, Z., Oktay, S., Sakarya, Y., Strang, K., Ghosh, P., Delp, M.D., Scarpace, P.J., Wang, K.K., Tumer, N., 2015. The functional and structural changes in the basilar artery due to overpressure blast injury. Journal of Cerebral Blood Flow and Metabolism 35, 1950-6.

Tsubokawa, T., Katayama, Y., 1998. Cerebral vasomotor reactivity in head-injured patients. Critical Reviews in Neurosurgery 8, 112-121.

Vaishnav, R.N., Vossoughi, J., 1987. Residual stress and strain in aortic segments. Journal of Biomechanics 20, 235-239.

Vappou, J., Breton, E., Choquet, P., Willinger, R., Constantinesco, A., 2008. Assessment of in vivo and post-mortem mechanical behavior of brain tissue using magnetic resonance elastography. Journal of Biomechanics 41, 2954-2959.

Wagner, H.P., Humphrey, J.D., 2011. Differential passive and active biaxial mechanical behaviors of muscular and elastic arteries: basilar versus common carotid. Journal of Biomechanical Engineering 133, 051009.

Walther, R.G., 2015. Collagen Mimetic Peptide as a Marker of Mechanical Damage in Cerebral Arteries. University of Utah.

Wang, R., Gleason, R.L., Jr., 2014. Residual shear deformations in the coronary artery. Journal of Biomechanical Engineering 136, 061004.

Zeinali-Davarani, S., Chow, M.J., Turcotte, R., Zhang, Y., 2013. Characterization of biaxial mechanical behavior of porcine aorta under gradual elastin degradation. Annals of Biomedical Engineering 41, 1528-1538.

Zhang, L., Bae, J., Hardy, W.N., Monson, K.L., Manley, G.T., Goldsmith, W., Yang, K.H., King, A.I., 2002. Computational study of the contribution of the vasculature on the dynamic response of the brain. Stapp Car Crash Journal 46, 145-164.

Zoumi, A., Lu, X., Kassab, G.S., Tromberg, B.J., 2004. Imaging coronary artery microstructure using second-harmonic and two-photon fluorescence microscopy. Biophysiology Journal 87, 2778-2786.